ABSTRACT

MILES, JASON ROBERT. Precise Tuning of Surface Properties by Degrafting Organosilanes for Evaluation of Interfacial Phenomena. (Under the direction of Dr. Jan Genzer).

The ability to modify physical and chemical characteristics of surfaces and interfaces is important to achieve desired wetting, adsorbing, releasing, and adhesive properties. Organosilanes are among the most commonly used materials for the modification of surface properties, with their ability to undergo a rapid condensation reaction with hydroxyl groups present on oxide surfaces. The increased use of composite materials and the decreased feature sizes present on devices requires a greater degree of control over the density and distribution of functional groups on the surface than was possible to achieve by the deposition of organosilanes. The primary goal of this Ph.D. dissertation is the development of a surface modification technique that allows for precise control over surface energy and chemistry along with the ability to impart multiple functionalities on the surface to control more complex interfacial phenomena.

We prepare silica surfaces functionalized with homogeneous silane SAMs by solution and vapor phase deposition approaches. The degrafting of silanes from these surfaces, using tetrabutylammonium fluoride (TBAF), allows for the precise tuning of the fractional coverage of silanes on the surface while maintaining a uniform surface coverage and regenerating surface hydroxyl groups. We can generate substrate-bound gradients of fractional coverage of silanes with tunable profiles over the desired length scale. We model the kinetic of TBAF degrafting by a series of first-order rate equations, with initial conditions that are dependent on the binding structure of the silanes at the surface. Mono-functional silanes exhibit a single exponential decay in their degrafting profiles as they can only form one bond with the surface. Tri-functional silanes exhibit a delay in degrafting as they form multiple surface and in-plane bonds, and the silanes connectivity to the surface must completely break before their removal from the surface.

By comparing the degrafting profiles of various silane SAMs to those predicted by the kinetic model, we probe the binding structure of the silane at the surface to gain insight into the stability of the SAM. Silane SAMs deposited from the vapor phase undergo faster degrafting than those deposited from a good solvent, indicating that the SAMs formed from vapor consist of more loosely packed arrays with less in-plane connectivity. Alkyl silanes deposit on surfaces in a mogul-like structure due to geometric constraints, leading to a large amount of in-plane condensation relative to the amount of condensation with surface hydroxyls. The mogul-like structures

accelerate the rate of degrafting. In comparison, fluorinated silanes have a larger van der Waals diameter that limits the amount of in-plane condensation and favors condensation with the surface. Silanes with short alkyl backbones or ones that exhibit favorable interactions of the functional group with the surface, lead to poor alignment and rapidly degraft due to their highly aggregated structures.

We use these silane functionalized surfaces to investigate the adsorption and covalent attachment of stimuli-responsive elastin-like polypeptides (ELPs) to silica surfaces. ELPs show significant adsorption onto surface energy gradients and the presence of a strong denaturant allowed for partial removal of the peptides, with more desorption occurring from the hydrophilic end of the gradient. We attempted the covalent attachment of ELPs to silane functionalized surfaces exhibiting anhydride and glycidyl ether functionalities. Attachment to anhydride functionalized surfaces resulted in similar surface morphology to that of physical adsorption. However, attachment to glycidyl ether functionalized surfaces resulted in distinct features present on the surface. Grafted homopolymer ELPs exhibited limited stimuli-responsive behavior when heated above their bulk transition temperature, ~29-35°C. The use of TBAF degrafting, to control the density of grafted ELPs and for minimizing physical adsorption, is promising for future studies involving the attachment of peptides to surfaces while maintaining their functionality.

Precise Tuning of Surface Properties by Degrafting Organosilanes for Evaluation of Interfacial Phenomena

by
Jason Robert Miles

A dissertation submitted to the Graduate Faculty of
North Carolina State University
in partial fulfillment of the
requirements for the degree of
Doctor of Philosophy

Chemical Engineering

Raleigh, North Carolina
2019

APPROVED BY:

Dr. Jan Genzer Committee Chair	Dr. Kirill Efimenko
Dr. Balaji Rao	Dr. Yaroslava Yingling

DEDICATION

To my family and friends, thank you for always pushing me to be a better person both professionally and personally.

BIOGRAPHY

Jason Robert Miles was born in Hagerstown, MD. He attended high school in Hedgesville, WV, and graduated in 2009. Jason attended West Virginia University in Morgantown, WV, where he received a Bachelor of Science in Chemical Engineering and a Biomedical Engineering certificate in 2014. During his undergraduate career he participated in the WVNano SURE program and worked as an undergraduate research assistant, under the direction of Dr. Charter Stinespring, from 2011 to 2014. His undergraduate research focused on the patterning of large-area graphene-on-insulator films for gas sensing applications.

Jason started his graduate studies at North Carolina State University in the fall of 2014. He joined the Genzer group in January 2015, working as a Research Triangle MRSEC fellow on the covalent attachment of stimuli-responsive peptides to oxide surfaces. As part of the MRSEC, he mentored two undergraduate students and participated in outreach opportunities in the research triangle area. During his time at NCSU, he was selected to participate in the DAAD RISE Professional program. As part of this program he traveled to Potsdam, Germany for three months as a visiting scholar, working in the lab of Dr. Hans Riegler to improve the dispersity of nanoparticles in polymer thin films. As part of his stay in Germany he had time to explore Berlin, Ludwigshafen, Heidelberg, and Marburg.

Upon returning to North Carolina, Jason's research focused on the tuning of surface properties by the manipulation of self-assembled monolayers. In the last year of his studies, he worked with the Eastman Chemical Company on a project involving the synthesis of high-performance copolyesters. During his free time, Jason occupied himself with running, cycling, and cooking. As he finishes his Ph.D., he looks forward to applying the broad knowledge he has gained over the years to aid in the development of functional materials.

ACKNOWLEDGMENTS

First, I would like to thank my undergraduate advisors for academics and research. Dr. Charter Stinespring, thank you for taking me on as an undergraduate research assistant and for trusting me to work alone in a laboratory with no other students. You fostered my interest in scientific research and supported me throughout the years. Dr. Joseph Shaeiwitz, thank you for always stressing the importance of mentorship and the ability to present information in a clear, precise, and accurate manner; also, for taking care of my leave of absence paperwork when I was unable to do so.

I would also like to thank my two undergraduate students, Spencer Schlenker and Patrick Delgado. Spencer, thank you for your hard work and persistence despite the difficulties with performing precise work with silanes during the summer; at least there were always times where you could dispense liters of water, one drop at a time, to take your mind off of the process. Patrick, thank you for your positive attitude and for working on a project that was new to both of us. The amount and quality of work you were able to do in a short time were phenomenal. You were both wonderful individuals to work with, and I wish you the best.

Thank you to all the people I have had the pleasure to work with during my time at NCSU. The Research Triangle MRSEC always provided me with useful feedback on my project and presented numerous opportunities to engage with the public. Dr. Hans Reigler for hosting me in his lab during my time in Germany and to the DAAD staff for their assistance during that time. The Eastman Chemical Company, for funding the last year of my studies and to the project leads and staff at the Eastman Innovation Center for their mentorship and assistance. To my advisor, Dr. Jan Genzer, and his research group for providing me with support, feedback, and motivation throughout my studies.

Most importantly, I would like to thank the friends that I have made since moving to Raleigh. To my roommates (Ryan Maloney, Seif Yusef, and Russell Schmitz), thank you for always being up for hosting a brunch and for engaging in nonsensical conversations to pass the time. Amber Hubbard, for always being up for whiskey and for listening to my rants. Jennifer Clark, for always being there despite the time you put into your work. Leah Granger, for always being a wonderful friend who is always looking to swing dance or to provide a terrible pun. Taylor Neumann, for his impeccable font and design choices. Ryan Dudek, for his insights into almost every topic of conversation and for putting up with me giving him a hard time since we met.

Minyung Song, for having the brightest personality and always being ready to get sushi instead of going for a run. Sahand Saberi, for always just being yourself. Emily Facchine, for being an incredible person all around and for always being down for everything. Dr. Ashton Lavoie Ph.D., for also being the worst, so I didn't always have to be. Emily Krzystowczyk, for her faith and friendship. Ria Cordier, for always being up for brunch and letting me watch Remy. It has been a blessing to get to know you all, and I would not have been able to do it without you.

TABLE OF CONTENTS

LIST OF TABLES

LIST OF FIGURES

Chapter 1: Introduction & Dissertation Scope

1.1 Introduction

Properties of materials surface often differ dramatically from those in bulk. Examples include chemical composition, density, modulus, molecular assembly, molecular mobility, and many others. Variations in surface properties can also be observed for solid materials as their crystal or chemical structures vary in the outermost layers. Traditional engineering problems often focus on the bulk material properties (i.e., modulus, toughness, strength, and conductivity) to determine the applicability and usefulness of materials; however, many modern applications require the use of micro or nanostructured materials where these interfacial layers have a considerable effect on the overall physical properties. Also, the use of composite materials or devices requires a deep knowledge of surface properties to be able to determine interactions with another material or the surrounding environment.

The ability to control the surface characteristics of a material is important to impart desirable functionality to increase the lifetime and effectiveness of the material. Commonly, surface modification focuses on the ability to modulate surface energy to control wetting, adsorbing, releasing, and adhesive properties. A wide variety of approaches have been employed for modification, depending on the material, but generally, consist of either a change in the physical nature of the surface (typically by varying roughness or by adding a thin coating of another material) or by a change in chemical structure through the addition of functional groups. While the physical surface modification is relatively easy to perform on a wide variety of surfaces, these methods typically lack selectivity and tunability. Chemical techniques rely on the covalent attachment of different functional groups to the surface by a reaction pathway and as such can target a desired surface property; however, they require detailed knowledge about and ability to perform the desired reactions without degrading or changing the structure of the bulk material.

Despite the thorough investigation of surface modification techniques for traditional wettability and adhesion applications, complex biological interactions require a deeper understanding of these processes. The biocompatibility and biointegration of materials depend on the surface properties, including roughness, modulus, and chemistry. The homogeneity and organization of these properties on the surface are crucial factors for cell viability and protein functionality, making the ability to pattern surfaces of increasing importance. An example of this would include the patterning of a passivating layer on the surface to limit the regions of biomolecule interaction. Herein, we briefly discuss several of the characterization techniques used to assess surface properties and commonly used methods to modify and pattern surfaces.

1.2 Surface Characterization Techniques

1.2.1 Secondary Ion Mass Spectroscopy

Secondary ion mass spectroscopy (SIMS) is a useful technique for determining the chemical nature of a surface. In this technique, a beam of primary atoms or ions (typically Ne, Ar, or Xe) sputters the material. When the primary atoms or ions hit the surface, the energy is dissipated by a series of collisions with the atoms of the material, resulting in the emission of secondary particles. A mass analyzer measures the emitted particles which ionize as part of this process. The source can be tuned to have a lateral resolution of ~1 x 1 μm and can raster the surface to investigate the distribution of chemical functionality. For static SIMS measurements, the primary particles penetrate the sample with a depth of ~10 nm, but the emitted secondary particles come from a maximum depth of ~1 nm, making this a highly surface-sensitive technique. Dynamic SIMS measurements are possible by increasing the ion current, resulting in a rapid sputtering of the surface and allowing for depth profiling to be performed. Interpretation of the spectra can prove difficult as they are a function of the emission and ionization mechanisms, which vary based on the material. Thus, to provide quantitative data, the sensitivity of each fragment must be defined for the material of interest. Additional complications arise when converting the sputtering time into measurement depth because the rate of sputtering depends on the local chemical composition. Despite this drawback, the qualitative data obtained from a SIMS spectrum has one of the highest sensitivities among surface spectroscopic techniques.[1]

1.2.2 X-ray Photoelectron Spectroscopy

X-ray photoelectron spectroscopy (XPS) operates by irradiating a sample with a monochromatic X-ray source. The source photons collide with core electrons in atoms present in the specimen, emitting those core electrons from the surface with a kinetic energy equal to the difference between the energy of the incident photon and the binding energy of the electron to its nucleus. The photoelectrons ejected from the surface vary in kinetic energy, according to their electronic level and the type of source atom. The unique electronic structure of each atom allows for quantitative elemental analysis of the surface. The photoelectron kinetic energy also depends on the chemical environment of the target atom. When chemically bound to another atom, some charge transfers to a more electronegative or from a less electronegative neighboring atom; consequently, the photoelectrons kinetic energy will be lower or higher, respectively. This chemical shift allows for a qualitative analysis of the chemical structure.[2]

While the X-rays have a relatively large penetration depth, the inelastic mean free path of the generated photoelectrons results in the emission of electrons originating from the top ~10 nm of the material. The sampling depth of XPS means that it is less surface sensitive than SIMS. However, non-destructive depth profiling is possible with the use of angular resolved XPS, with sampling angles of 15° to 90° allowing for variation in sampling depth from ~ 2 to 10 nm with a lateral resolution on the order of 10 µm x 10 µm.

1.2.3 Fourier-transform Infrared Spectroscopy

Fourier-transform infrared spectroscopy (FTIR) measures chemical properties by collecting an infrared absorption spectrum. When exposed to infrared radiation, a molecule selectively absorbs radiation at a specific wavelength. Absorption causes the vibrational energy level to change from the ground state to an excited state; the frequency of the adsorption is related to the vibrational energy gap. The absorption required of most organic compounds falls in the mid-infrared region (4000 – 200 cm^{-1}), allowing for the determination of structural information of the material. The ability of an FTIR to simultaneously measure all frequencies in this range allows for a greatly enhanced signal to noise ratio, compared to a dispersive instrument.

When operated with attenuated total reflectance (ATR) FTIR becomes a surface-sensitive technique. For this technique, a single crystal, with a refractive index greater than that of the surface, is placed in intimate contact with the surface to be examined. The IR radiation strikes one face of the crystal, undergoes one or multiple reflections at the crystal/sample interface, and the detector then measures the absorption. When the radiation contacts the surface, an evanescent wave is generated and penetrates a sample to a certain depth (typically 0.5 – 2 µm) which is a function of the refractive index of the materials, the wavelength, and the angle of incidence. The lower detection limit of FTIR-ATR is a few monolayers of material on a surface. The penetration depth of the evanescent wave can be decreased by increasing the angle of incidence or the refractive index of the crystal and can be further decreased by depositing a non-adsorbing thin film at the material interface. While this makes FTIR-ATR a more surface-sensitive technique, the lower detection limit rapidly increases and results in a much lower signal to noise ratio.

1.2.4 Spectroscopic Ellipsometry

Spectroscopic ellipsometry is an optical technique used to measure the thickness and optical properties of thin films. Source light is polarized, travels along the plane of incidence, reflects and refracts from any region in the material that exhibits different dielectric constant (related to the refractive index), and all signals then collectively pass through a second polarizer (analyzer) before reaching the detector. When the source light reflects from the surface, with its angle of reflection equal to the angle of incidence, a shift in polarization occurs due to differences in optical properties between the measurement medium, typically air, the material's surface, and the bulk material. The changes in amplitude of the s and p components of the polarized light, along with the phase shift, are used to determine the optical constants of the surface layers.

While ellipsometry is a powerful technique for determining the thickness of surface layers along with their optical properties, a difficulty arises during data analysis. A model analysis must be performed to convert the measured amplitude ratio and phase shift into desired physical properties. For most materials, this process involves the development of a multilayer model that considers the material and thin film properties, such as the refractive index, dielectric constant, and thickness. Confidence and accuracy of these models increase with the number of known variables in the model, the wavelengths measured, and with the ability to measure multiple angles to maximize the difference between the source and reflected light.[3] While ellipsometry has been traditionally used to measure thicknesses and composition profiles of smooth, homogeneous films on flat surfaces, the development of more advanced models allows for limited measurement of rough or porous surfaces and films with vertical gradients in composition.

1.2.5 Atomic Force Microscopy

Atomic force microscopy (AFM) is most commonly employed to measure the surface morphology on the nano and micrometer scale. Scanning of surfaces with AFM occurs by measuring the deflection of a cantilever, typically with a beam from a laser source reflected off the cantilever to a photodetector. For contact mode measurements, the cantilever is brought into contact with the sample and is bent upward until reaching a setpoint deflection. The force applied by the AFM tip on the sample is on the order of nN. Rasterization of topographical images results from vertical deflection of the cantilever; whereas, the lateral forces applied to the cantilever during scanning, resulting in torsion of the cantilever, provides information concerning the friction between the tip and the sample surface. Due to the constant contact of the AFM tip, surface modification and damage can occur when measuring softer materials or features. Dynamic AFM measurements overcome most of these problems, with the most common being tapping mode AFM.

The oscillation of the AFM cantilever at its resonance frequency with a piezo is the basis of tapping mode scanning. When engaged, the sample surface and tip come into intermittent contact, which results in shifts in the amplitude, phase, and resonant frequency of the oscillating cantilever. The generation of topography images typically results from the feedback mechanism of the AFM controlling the vertical position of the sample or tip to maintain a constant setpoint amplitude. Variations in the phase and resonant frequency are used to generate interaction maps of the surface, with phase images more commonly employed. Variations in chemical composition, adhesion, friction, viscoelasticity, and a myriad of other factors that affect the energy dissipation resulting from contact between the tip and sample surface cause shifts in the phase of the oscillation. The phase image also contains topographic information as the energy dissipation is a function of surface area (which is influenced by differences in slope on the sample surface), leading to ambiguity when interpreting contrast in these images and making this most suitable for use on flat surfaces or in conjunction with height images.[4]

1.2.6 Contact Angle

Contact angle measurements are the most common approach to measure the surface energy of a substrate. The basis of this measurement is the equilibrium balance at the three-phase boundary of the solid surface, the probing medium, and the surrounding medium (typically air).[5] The Young equation (*cf.* **Equation 1**) describes how interfacial tensions dictate the shape and angle of the drop on a surface,

$$\gamma_{sv} - \gamma_{sl} = \gamma_{lv} \cos \theta_Y \tag{1}$$

where γ_{ij} denotes the interfacial tension between two phases and θ denotes the equilibrium contact angle. Difficulty in determining the solid surface tension arises from the ability of drops to adopt a range of angles on most surfaces, known as contact angle hysteresis, and there has been much debate on which value gives the true surface energy. This hysteresis can be measured by three common approaches which include inclining the solid surface which distorts the drop shape as it begins to slide, by the addition and removal of the probing medium from the drop, and by the Wilhelmy plate technique.

While the contact angle hysteresis makes an absolute determination of the solid surface tension difficult, it allows for insight to be gained concerning the chemical and physical structure of a surface. Hysteresis caused by the non-ideality of real surfaces, arising from chemical and physical heterogeneity, can be characterized by either thermodynamic or kinetic hysteresis. Thermodynamic hysteresis typically results from two factors: surface roughness (including porous structures) and variations in surface chemistry. The Wenzel equation[6] is commonly used to describe wetting behavior on a rough surface:

$$\cos\theta_W = r\cos\theta_Y \tag{2}$$

where r denotes the roughness of the actual surface relative to an ideal geometric surface and is always greater than unity. The result of this relationship is that surface roughness enhances the wetting properties of the surface; the apparent contact angle will decrease with roughness if the Young contact angle is less than 90° and will increase for angles greater than 90°. This wetting behavior is referred to as the Wenzel state and is a result of the increased surface area of rough surfaces, typically observed with low aspect ratio features. When the aspect ratio of features on a rough surface increases, a transition is observed from the Wenzel state to the Cassie-Baxter state.[7] In the Cassie-Baxter state, the probing medium does not penetrate the surface features, and the contact angle is affected by regions with different compositions. The Cassie-Baxter equation[8] is used to describe wetting on two-component surfaces:

$$\cos\theta_C = \phi_1\cos\theta_1 + \phi_2\cos\theta_2 \tag{3}$$

where ϕ_i and θ_i are the fractional areal coverage and Young contact angle of component i, respectively. The Cassie-Baxter relationship describes the wetting behavior of these rough surfaces where one of the components is trapped air but also describes smooth, chemically heterogeneous surfaces. Kinetic hysteresis arises from time-dependent liquid-solid interactions that cause a modification of the surface or the probing medium and can be caused by the diffusion of the probing medium into the surface, rearrangement of surface groups to expose more favorable chemistry, and absorption of surface contaminants into the probing medium to name a few.[9]

1.3 Surface Modification Techniques

Surface modification techniques have been used to alter the original surface characteristic of metals, oxides, and polymers. These involve either subtractive physical or chemical modification of the surfaces, which can be further enhanced by additive methods, involving physical adsorption of or chemical reaction with active molecules or macromolecules that define the properties of the newly-created surfaces.

Subtractive physical modification of surfaces is accomplished by a wide variety of techniques ranging from the etching of surfaces, generating roughness, to highly controlled surface reactions. Each of these processes allows for tuning of one or more surface properties with varying degrees of control. It is important to use the right technique for the material and application of interest to generate a sufficiently functionalized and stable interface. Friction and adhesion properties, along with surface energy and wetting behavior, are dictated by variations in surface topography. Surface etching techniques allow for the generation of random surface roughness. Traditional machining techniques can result in large variations in roughness on a surface and allow for little control over the amplitude or distribution of features. For applications that require a greater degree of control, the preferred methods are typically wet chemical etching or dry etching.

Numerous subtractive chemical modification methods exist. Wet chemical etching of material surfaces relies on the reaction of the surface with an etching solution, typically strong acids or bases, and can result in isotropic or anisotropic removal of material depending on the crystallinity of the material and the reactivity of the etchant. Wet etching allows for selective etching of composite materials; however, resulting feature sizes are limited to greater than one micrometer, and it is difficult to achieve high aspect ratios due to diffusion limitations. Dry etching, or plasma etching, procedures involve the generating of a high energy plasma consisting of ionic and chemically reactive species that interact with surface species and result in their removal.[10] These processes involve chemical and physical etching mechanisms with relative strengths depending on the gasses used to generate the plasma and the processing conditions. Higher pressures and lower energies favor chemical etching mechanisms as a large amount of reactive radical species are generated. These radical species diffuse to the target material, react with surface species, and generate volatile products that leave the surface. While reactive plasma etching processes allow for selective removal of surface species, the diffusion limitations result in anisotropic etching. Decreasing the pressure of the vacuum system and increasing the energy allows for a higher concentration of ions in the plasma; the self-bias of the cathode behind the target material directs these ions toward the surface. Ion bombardment of the surface usually does not result in significant etching alone but causes damage, such as dangling bonds or dislocations, which makes the surface more reactive to the etchant radicals.[11] The directionality of the ion bombardment greatly improves the anisotropy of this process, allowing for nearly vertical etching at nanometer resolution. While these etching processes allow for variations in surface energy, based on roughness of the surface, they provide no control over the chemical nature of the surface and are best used in conjunction with other additive surface modification techniques to achieve the desired properties.

Additive physical techniques for surface modification rely on the adsorption of polymeric materials or small molecules due to attractive forces (*i.e.*, van der Waals forces, hydrophobic interactions, hydrogen bonding, and electrostatics). Commonly used techniques include the deposition of multilayers and the assembly of small molecules on surfaces. All methods depend on the interactions of suitable functionalization materials with the underlying surface, and the necessary strength and stability of these interactions depend on the needs of the final application. Polymeric films or multilayers are generally easy to deposit and provide robust surface coverage, but often do not feature strong interactions with the underlying surface and lack molecular control. Thin polymer films allow for improved chemical resistance and adhesive properties along with imparting chemical functionality and modulating physical properties, such as modulus, of a material's surface.

Solution-based approaches, such as dip coating and spin coating, are used for the deposition of thin films.[12] Dip coating involves the vertical immersion of the material into a bath of the dilute polymer solution, a short dwell period, the gradual removal of the material from the solution, and the entrained solution drying on the material's surface. The thickness of the resulting film depends on the withdraw rate, controlling the thickness of the entrained solution, and the drying rate. This technique coats all sides of the material immersed in the solution and works best on flat substrates but can be used on various geometries with some success. Due to the slow drying of the film, it is subject to ambient factors, such as variable airflow, which can result in non-uniform films. In spin coating, a small amount of dilute polymer solution is placed onto a flat substrate before or during rotation, and the centripetal force distributes the solution over the surface into a thin film. The resulting film thickness is a function of the viscosity and concentration of the solution and the spin speed. In contrast to dip coating, spin coating is only able to coat small, flat substrates and is less scalable; however, the faster drying times make it less sensitive to ambient conditions. It is important that the deposition solvent wets the surface and that the polymers surface tension is such that its spreading coefficient (*cf.* **Equation 4**) is greater than zero to prevent dewetting above the polymers T_g to form a stable and uniform polymer film.[13,14]

$$S = \gamma_{SG} - \gamma_{SL} - \gamma_{LG} \tag{4}$$

Another commonly used method for generating multilayer structures on surfaces is layer by layer (LbL) assembly that involves the alternating deposition of positive and negatively charged species onto a surface. The simplicity and applicability of various materials make LbL processes versatile surface modification techniques.[15] Stable multilayer films are typically assembled using polyelectrolytes and biomaterials, such as proteins, DNA, and polysaccharides, due availably of charges sites on their surfaces. These films can also comprise charged inorganic materials (i.e., nanoparticles, zeolites, and clays) which allow for finely tuned modification of surface properties, including but not limited to conductivity, modulus, and porosity.[16] The dynamic nature of the electrostatic interactions making up these films as well as the incorporation of various crosslinking agents also makes them good candidates for protective and anti-wear coatings.[17] However, LbL assembled films suffer from the same drawback as polymeric assemblies, the need for appropriate surface properties to ensure a robust surface-film interaction to prevent delamination.

Modification of surfaces with small molecules modulates surface properties with a higher degree of molecular control and can be applied as precursor layers to help improve the stability of polymeric or other multilayer films. Geometric constraints or attractive forces guide the self-assembly of small molecules on surfaces and can result in the formation of dense, highly ordered layers. Assembly can be accomplished by physical adsorption onto surfaces from solution or vapor phases, with their coverage and stability depending on deposition conditions and strength of interactions with the surface. Adsorbed small molecules can undergo significant desorption when exposed to mild conditions; however, some procedures have found extensive application due to their ease of use, self-assembly into uniform films, and relatively high stability.

The additive chemical modification involves chemisorption of small molecules or polymers onto activated substrates. Most notably, the absorption of thiols on noble metallic surfaces has been studied extensively in a myriad of applications. Thiols readily absorb onto metallic surfaces due to activation of the S-H bond of the thiol, and while the mechanism of this process is not completely understood, it may result from significant charge transfer from the metal surface to the sulfur.[18] This high degree of charge transfer results in a stable interaction between the metal and the thiol with dissociation energy of ~50 kcal/mol and is sometimes mistakenly referred to as a covalent interaction due to its strength.[19] While many fundamental studies use thiol SAMs, the stability of the layer is often not suitable for many applications as the structure can be disrupted by species with a more preferential absorption to the gold surface, weak mechanical forces, and can readily desorb at temperatures exceeding ~100 °C.[20,21] For these reasons it is often favored to modify surface chemistry by covalent interactions.

Covalent modification of surface properties relies on the knowledge and implementation of specific chemistries. The most stable covalent interactions often involve the formation of C-C[22,23] or Si-C[24,25] bonds, but processes for these modifications are only applicable to some materials and often have high energy barriers. A compromise between stability and ease of access involves the generation of an oxide surface on the material of interest, resulting in the formation of surface hydroxyl (-OH) functionalities. A wide variety of materials such as metal, glass, semiconductors, and polymers can undergo this initial functionalization; the hydroxyl surface functionality allows for the application of a wide range of chemistries for modification of surface properties including but not limited to the use of phosphonates, carboxylates, catechols, alkenes, and amines.[26] The most commonly used method for modifying these activated surfaces employs organosilanes.

Organosilanes typically have the chemical structure $RSiX_n(CH_3)_{3-n}$ where R is an alkyl backbone (often exhibiting a desired chemical functionality) and X is a leaving group that readily hydrolyzes. The hydrolyzed silanes can form SAMs on oxide surfaces due to initial hydrogen bonding with surface hydroxyls and alignment of the alkyl backbones due to van der Waals interactions; following the alignment of silanes on the surface, condensation occurs between the Si-OH groups to form Si-O-Si bonds. Monofunctional silanes with one hydrolyzable group can form highly reproducible SAMs on the surface; however, they provide relatively low coverage due to presence of the bulky methyl groups close to the silicon head-group. Trifunctional silanes have less steric hindrance, allowing them to pack more densely on the surface, and can form a siloxane network with neighboring silanes. This siloxane network can increase the overall stability of the SAM but may lead to the formation of aggregate and multilayer structures. Silane functionalization of materials is an important technique for many applications as silanes are commercially available with a wide variety of terminal functionalities and can be further modified to impart the desired surface chemistry. Examples of this include the use of amine functional silanes for biological applications[27–29] to promote protein adhesion and cell viability and the use of alkyl and fluorinated silanes to generate non-wetting and low friction surfaces.[30–33] Two main issues arise when using silanes for surface modification: deposition reproducibility and hydrolytic stability. Silane SAM's structure is highly dependent on the reaction conditions, with moisture content and solvent polarizability having a large impact.[34–38] The hydrolytic stability of the SAM depends heavily on the SAM structure and the underlying material, with some layers being almost completely removed from surfaces on the order of hours at neutral pH.[39] These drawbacks merit further investigation of the underlying silane structure and their stability as modern applications require resilient and highly tunable surfaces.

Of increasing interest is the modification of surfaces that allows for control of not only macroscopic interactions but also the density and spatial distribution of the functionalization on the nanoscale to further improve material performance. Methods for patterning silane SAMs consist of two overall approaches that depend on either the masking of the surface or the directed addition/removal of silanes. Traditionally, conventional photolithography techniques have allowed for pattern formation on the surface, before or after silane functionalization, allowing for the deposition or removal of the SAM in desired regions.[40–42] Equipment for photolithography is often cost-prohibitive and can run into resolution issues during patterning and development. Other masking techniques, such as macromolecule[43] and nanoparticle assemblies[44–47], have been used to pattern surfaces with silane SAMs but some spatial control is lost as resulting features are often random or periodic.

Selected positioning or removal of silanes from the surface allows for a direct method to pattern SAMs. Microcontact printing approaches use a patterned stamp loaded with a silane solution to transfer the pattern onto the material. While this allows for large areas to be patterned, the resolution is limited, and diffusion constraints complicate the process.[48,49] Dip pen lithography techniques are promising for the high-resolution patterning of surfaces as they transfer a small number of species from an AFM tip to the material.[50] However, these techniques have found little use for silane modification due to their rapid hydrolysis and self-condensation.[51] Mechanical surface patterning is a more promising AFM based technique for patterning of silane SAMs based on their removal from the surface.[52,53] AFM approaches to patterning allow for resolution on a nanometer scale but are very time consuming and are only able to pattern small areas of the surface.

Patterning techniques previously mentioned allow for the spatial control of surface chemistry but result in sharp boundaries and provide little control over the local density of functional groups. Traditionally, attempts to control the local density of silane SAMs have focused on limiting the exposure times of the material to the silane source and their extension to generating gradients in coverage on surfaces.[54–58] This approach does allow for varying the fractional coverage of the surface but results in a heterogeneous layer due to nucleation and growth of silane domains on the surface. Other approaches focus on the removal of silane species from the surface; this is most commonly achieved by UV irradiation to degrade the alkyl backbone.[59,60] While the UV based subtractive approach can vary the density of functional groups on the surface and can result in less sharp boundaries on the surface, by the use of waveguides or moving shutters, it often does not completely remove silanes from the surface and can have negative impacts on some surface chemistries.

1.4 Dissertation Scope

The primary goal of this Ph.D. dissertation is to demonstrate the importance of finely tuned surface modification to achieve robust and functional surfaces. Herein, we demonstrate a degrafting approach for the tuning of the silanes fractional coverage on oxide surfaces using tetrabutylammonium fluoride (TBAF). TBAF degrafting of organosilanes from the surface results in overall homogeneous coverage and allows for the formation of gradient surfaces with tunable profiles. We use this degrafting approach to elucidate the structure of the SAM to provide valuable information about the stability of the functionalization. Further, we demonstrate the importance of proper surface functionalization for the use in biological applications by investigating the covalent attachment of a stimuli-responsive polypeptide to a silane functionalized surface.

In Chapter 1, we describe the degrafting process of organosilanes from silica surfaces by TBAF. The degrafting process involves the formation of a homogeneous SAM on the surface, followed by a gradual degrafting during incubation in TBAF. The kinetic for this process depends on temperature, the concentration of TBAF, silane composition, and the structure of the bonding network of silanes at the surface. We demonstrate the ability of this procedure to generate reproducible fractional coverage gradients with highly tunable profiles.

In Chapter 2, we further the structure of silane SAMs on the surface by examining their degrafting kinetics. We observe that the degrafting of alky silanes with varying leaving groups (chloro *vs.* alkoxy) shows little difference when deposited from nonpolar solvents with low water content due to their ability to align on the surface by van der Waals forces. Differences arise, however, when deposited from the vapor phase under vacuum conditions as there is less condensation between silanes before surface attachment. Degrafting of silane-based polymerization initiators before and after the growth of polymer brushes shows the importance of diffusion barriers and bond tension on the stability of silane SAMs.

In Chapter 3, we study the adsorption and covalent attachment of elastin-like polypeptides (ELP) to silane functionalized silica. We employ gradients in surface energy to investigate the adsorption behavior of ELPs, with adsorption occurring on a wide range of surfaces. The adsorbed ELP layers are found to be more stable on hydrophobic surfaces. We attempt to attach ELPs covalently onto these surfaces using anhydride and epoxide chemistries. Following covalent attachment, the stimuli-responsive behavior of the ELP is tested to determine if the polypeptide was able to maintain its functionality.

1.5 References

(1) Vickerman, J. C.; Gilmore, I. S. *Surface Analysis – The Principal Techniques*; Vickerman, J. C., Gilmore, I. S., Eds.; John Wiley & Sons, Ltd: Chichester, UK, 2009.

(2) van der Heide, P. *X-Ray Photoelectron Spectroscopy: An Introduction to Principles and Practices*; John Wiley & Sons, Inc.: Hoboken, NJ, USA, 2011.

(3) Brunner, H.; Vallant, T.; Mayer, U.; Hoffmann, H. Formation of Ultrathin Films at the Solid-Liquid Interface Studied by in Situ Ellipsometry. *J. Colloid Interface Sci.* **1999**, *212*, 545–552.

(4) Magonov, S. N.; Whangbo, M. *Surface Analysis with STM and AFM*; Wiley, 1995.

(5) Young, T. III. An Essay on the Cohesion of Fluids. *Philos. Trans. R. Soc. London* **1805**, *95*, 65–87.

(6) Wenzel, R. N. Resistance of Solid Surfaces to Wetting by Water. *Ind. Eng. Chem.* **1936**, *28*, 988–994.

(7) Murakami, D.; Jinnai, H.; Takahara, A. Wetting Transition from the Cassie-Baxter State to the Wenzel State on Textured Polymer Surfaces. *Langmuir* **2014**, *30*, 2061–2067.

(8) Cassie, A. B. D.; Baxter, S. Wettability of Porous Surfaces. *Trans. Faraday Soc.* **1944**, *40*, 546–551.

(9) Kwok, D. Y.; Neumann, A. W. Contact Angle Measurement and Contact Angle Interpretation. *Adv. Colloid Interface Sci.* **1999**, *81*, 167–249.

(10) Cardinaud, C.; Peignon, M.-C.; Tessier, P.-Y. Plasma Etching: Principles, Mechanisms, Application to Micro- and Nano-Technologies. *Appl. Surf. Sci.* **2000**, *164*, 72–83.

(11) Cui, Z. *Nanofabrication: Principles, Capabilities and Limits: Second Edition*; Springer International Publishing: Cham, 2017.

(12) Scriven, L. E. Physics and Applications of Dip Coating and Spin Coating. *MRS Proc.* **1988**, *121*, 717.

(13) Qu, S.; Clarke, C. J.; Liu, Y.; Rafailovich, M. H.; Sokolov, J.; Phelan, K. C.; Krausch, G. Dewetting Dynamics at a Polymer−Polymer Interface. *Macromolecules* **1997**, *30*, 3640–3645.

(14) Ashley, K. M.; Raghavan, D.; Douglas, J. F.; Karim, A. Wetting-De Wetting Transition Line in Thin Polymer Films. *Langmuir* **2005**, *21*, 9518–9523.

(15) Ariga, K.; Hill, J. P.; Ji, Q. Layer-by-Layer Assembly as a Versatile Bottom-up Nanofabrication Technique for Exploratory Research and Realistic Application. *Phys. Chem. Chem. Phys.* **2007**, *9*, 2319.

(16) Srivastava, S.; Kotov, N. A. Composite Layer-by-Layer (LBL) Assembly with Inorganic Nanoparticles and Nanowires. *Acc. Chem. Res.* **2008**, *41*, 1831–1841.

(17) An, Q.; Huang, T.; Shi, F. Covalent Layer-by-Layer Films: Chemistry, Design, and Multidisciplinary Applications. *Chem. Soc. Rev.* **2018**, *47*, 5061–5098.

(18) Inkpen, M. S.; Liu, Z.; Li, H.; Campos, L. M.; Neaton, J. B.; Venkataraman, L. Non-Chemisorbed Gold–Sulfur Binding Prevails in Self-Assembled Monolayers. *Nat. Chem.* **2019**, *11*, 351–358.

(19) Nuzzo, R. G.; Zegarski, B. R.; Dubois, L. H. Fundamental Studies of the Chemisorption of Organosulfur Compounds on Gold(111). Implications for Molecular Self-Assembly on Gold Surfaces. *J. Am. Chem. Soc.* **1987**, *109*, 733–740.

(20) Chandekar, A.; Sengupta, S. K.; Whitten, J. E. Thermal Stability of Thiol and Silane Monolayers: A Comparative Study. *Appl. Surf. Sci.* **2010**, *256*, 2742–2749.

(21) Delamarche, E.; Michel, B.; Kang, H.; Gerber, C. H. Thermal Stability of Self-Assembled Monolayers. *Langmuir* **1994**, *10*, 4103–4108.

(22) Stavis, C.; Clare, T. L.; Butler, J. E.; Radadia, A. D.; Carr, R.; Zeng, H.; King, W. P.; Carlisle, J. a; Aksimentiev, A.; Bashir, R.; Hamers, R. J. Surface Functionalization of Thin-Film Diamond for Highly Stable and Selective Biological Interfaces. *Proc. Natl. Acad. Sci. U. S. A.* **2011**, *108*, 983–988.

(23) Hamers, R. J.; Yang, W.; Auciello, O.; Butler, J. E. DNA-Modified NCD Thin Films as Stable, Biologically Active Substrates. *Nat. Mater.* **2002**, *1*, 253–258.

(24) Li, Y.; Calder, S.; Yaffe, O.; Cahen, D.; Haick, H.; Kronik, L.; Zuilhof, H. Hybrids of Organic Molecules and Flat, Oxide-Free Silicon: High-Density Monolayers, Electronic Properties, and Functionalization. *Langmuir* **2012**, *28*, 9920–9929.

(25) Bhairamadgi, N. S.; Pujari, S. P.; Trovela, F. G.; Debrassi, A.; Khamis, A. A.; Alonso, J. M.; Al Zahrani, A. A.; Wennekes, T.; Al-Turaif, H. A.; Van Rijn, C.; Alhamed, Y. A.; Zuilhof, H. Hydrolytic and Thermal Stability of Organic Monolayers on Various Inorganic Substrates. *Langmuir* **2014**, *30*, 5829–5839.

(26) Pujari, S. P.; Scheres, L.; Marcelis, A. T. M.; Zuilhof, H. Covalent Surface Modification of Oxide Surfaces. *Angew. Chemie - Int. Ed.* **2014**, *53*, 6322–6356.

(27) Aissaoui, N.; Bergaoui, L.; Landoulsi, J.; Lambert, J.-F.; Boujday, S. Silane Layers on Silicon Surfaces: Mechanism of Interaction, Stability, and Influence on Protein Adsorption. *Langmuir* **2012**, *28*, 656–665.

(28) Awsiuk, K.; Budkowski, A.; Psarouli, A.; Petrou, P.; Bernasik, A.; Kakabakos, S.; Rysz, J.; Raptis, I. Protein Adsorption and Covalent Bonding to Silicon Nitride Surfaces Modified with Organo-Silanes: Comparison Using AFM, Angle-Resolved XPS and Multivariate ToF-SIMS Analysis. *Colloids Surfaces B Biointerfaces* **2013**, *110*, 217–224.

(29) Shircliff, R. a.; Stradins, P.; Moutinho, H.; Fennell, J.; Ghirardi, M. L.; Cowley, S. W.; Branz, H. M.; Martin, I. T. Angle-Resolved XPS Analysis and Characterization of Monolayer and Multilayer Silane Films for DNA Coupling to Silica. *Langmuir* **2013**, *29*, 4057–4067.

(30) Booth, B. D.; Vilt, S. G.; Lewis, J. B.; Rivera, J. L.; Buehler, E. A.; McCabe, C.; Jennings, G. K. Tribological Durability of Silane Monolayers on Silicon. *Langmuir* **2011**, *27*, 5909–5917.

(31) Bhushan, B.; Kasai, T.; Kulik, G.; Barbieri, L.; Hoffmann, P. AFM Study of Perfluoroalkylsilane and Alkylsilane Self-Assembled Monolayers for Anti-Stiction in MEMS/NEMS. *Ultramicroscopy* **2005**, *105*, 176–188.

(32) Depalma, V.; Tillman, N. Friction and Wear of Self-Assembled Trichlorosilane Monolayer Films on Silicon. *Langmuir* **1989**, *5*, 868–872.

(33) Khatri, O. P.; Devaprakasam, D.; Biswas, S. K. Frictional Responses of Octadecyltrichlorosilane (OTS) and 1H, 1H, 2H, 2H-Perfluorooctyltrichlorosilane (FOTS) Monolayers Self-Assembled on Aluminium over Six Orders of Contact Length Scale. *Tribol. Lett.* **2005**, *20*, 235–246.

(34) Duchet, J.; Chabert, B.; Chapel, J. P.; Gérard, J. F.; Chovelon, J. M.; Jaffrezic-Renault, N. Influence of the Deposition Process on the Structure of Grafted Alkylsilane Layers. *Langmuir* **1997**, *13*, 2271–2278.

(35) Bunker, B. C.; Carpick, R. W.; Assink, R. A.; Thomas, M. L.; Hankins, M. G.; Voigt, J. A.; Sipola, D.; De Boer, M. P.; Gulley, G. L. Impact of Solution Agglomeration on the Deposition of Self-Assembled Monolayers. *Langmuir* **2000**, *16*, 7742–7751.

(36) Desbief, S.; Patrone, L.; Goguenheim, D.; Guérin, D.; Vuillaume, D. Impact of Chain Length, Temperature, and Humidity on the Growth of Long Alkyltrichlorosilane Self-Assembled Monolayers. *Phys. Chem. Chem. Phys.* **2011**, *13*, 2870–2879.

(37) Onclin, S.; Ravoo, B. J.; Reinhoudt, D. N. Engineering Silicon Oxide Surfaces Using Self-Assembled Monolayers. *Angew. Chemie Int. Ed.* **2005**, *44*, 6282–6304.

(38) Kim, J.; Seidler, P.; Wan, L. S.; Fill, C. Formation, Structure, and Reactivity of Amino-Terminated Organic Films on Silicon Substrates. *J. Colloid Interface Sci.* **2009**, *329*, 114–119.

(39) Marcinko, S.; Fadeev, A. Y. Hydrolytic Stability of Organic Monolayers Supported on TiO2 and ZrO2. *Langmuir* **2004**, *20*, 2270–2273.

(40) Herzer, N.; Hoeppener, S.; Schubert, U. S. Fabrication of Patterned Silane Based Self-Assembled Monolayers by Photolithography and Surface Reactions on Silicon-Oxide Substrates. *Chem. Commun.* **2010**, *46*, 5634–5652.

(41) Mooney, J. F.; Hunt, A. J.; McIntosh, J. R.; Liberko, C. A.; Walba, D. M.; Rogers, C. T. Patterning of Functional Antibodies and Other Proteins by Photolithography of Silane Monolayers. *Proc. Natl. Acad. Sci.* **1996**, *93*, 12287–12291.

(42) Jonas, U.; Del Campo, A.; Krüger, C.; Glasser, G.; Boos, D. Colloidal Assemblies on Patterned Silane Layers. *Proc. Natl. Acad. Sci. U. S. A.* **2002**, *99*, 5034–5039.

(43) Surwade, S. P.; Zhou, F.; Li, Z.; Powell, A.; O'Donnell, C.; Liu, H. Nanoscale Patterning of Self-Assembled Monolayers Using DNA Nanostructure Templates. *Chem. Commun.* **2016**, *52*, 1677–1680.

(44) Lin, W. F.; Swartz, L. A.; Li, J. R.; Liu, Y.; Liu, G. Y. Particle Lithography Enables Fabrication of Multicomponent Nanostructures. *J. Phys. Chem. C* **2013**, *117*, 23279–23285.

(45) Li, J. R.; Garno, J. C. Elucidating the Role of Surface Hydrolysis in Preparing Organosilane Nanostructures via Particle Lithography. *Nano Lett.* **2008**, *8*, 1916–1922.

(46) Lusker, K. L.; Yu, J. J.; Garno, J. C. Particle Lithography with Vapor Deposition of Organosilanes: A Molecular Toolkit for Studying Confined Surface Reactions in Nanoscale Liquid Volumes. *Thin Solid Films* **2011**, *519*, 5223–5229.

(47) Cai, Y.; Ocko, B. M. Large-Scale Fabrication of Protein Nanoarrays Based on Nanosphere Lithography. *Langmuir* **2005**, *21*, 9274–9279.

(48) Yanker, D. M.; Maurer, J. A. Direct Printing of Trichlorosilanes on Glass for Selective Protein Adsorption and Cell Growth. *Mol. Biosyst.* **2008**, *4*, 502–504.

(49) Sathish, S.; Ricoult, S. G.; Toda-Peters, K.; Shen, A. Q. Microcontact Printing with Aminosilanes: Creating Biomolecule Micro- and Nanoarrays for Multiplexed Microfluidic Bioassays. *Analyst* **2017**, *142*, 1772–1781.

(50) Piner, R. D.; Zhu, J.; Xu, F.; Hong, S.; Mirkin, C. A. "Dip-Pen" Nanolithography. *Science.* **1999**, *283*, 661–663.

(51) Jung, H.; Kulkarni, R.; Collier, C. P. Dip-Pen Nanolithography of Reactive Alkoxysilanes on Glass. *J. Am. Chem. Soc.* **2003**, *125*, 12096–12097.

(52) Krämer, S.; Fuierer, R. R.; Gorman, C. B. Scanning Probe Lithography Using Self-Assembled Monolayers. *Chem. Rev.* **2003**, *103*, 4367–4418.

(53) Liu, G.-Y.; Xu, S.; Qian, Y. Nanofabrication of Self-Assembled Monolayers Using Scanning Probe Lithography. *Acc. Chem. Res.* **2000**, *33*, 457–466.

(54) Chaudhury, M. K.; Whitesides, G. M. How to Make Water Run Uphill. *Science.* **2013**, *20*, 38–59.

(55) Elwing, H.; Welin, S.; Askendal, A.; Nilsson, U.; Lundström, I. A Wettability Gradient Method for Studies of Macromolecular Interactions at the Liquid/Solid Interface. *J. Colloid Interface Sci.* **1987**, *119*, 203–210.

(56) Giri, D.; Li, Z.; Ashraf, K. M.; Collinson, M. M.; Higgins, D. A. Molecular Combing of λ-DNA Using Self-Propelled Water Droplets on Wettability Gradient Surfaces. *ACS Appl. Mater. Interfaces* **2016**, *8*, 24265–24272.

(57) Albert, J. N. L.; Kim, J. D.; Stafford, C. M.; Epps, T. H. Controlled Vapor Deposition Approach to Generating Substrate Surface Energy/Chemistry Gradients. *Rev. Sci. Instrum.* **2011**, *82*, 065103.

(58) Lee, J. H.; Hon, M. H.; Chung, Y. W.; Leu, I. C. Microcontact Printing of Organic Self-Assembled Monolayers for Patterned Growth of Well-Aligned Zno Nanorod Arrays and Their Field-Emission Properties. *J. Am. Ceram. Soc.* **2009**, *92*, 2192–2196.

(59) Roberson, S. V.; Fahey, A. J.; Sehgal, A.; Karim, A. Multifunctional ToF-SIMS: Combinatorial Mapping of Gradient Energy Substrates. *Appl. Surf. Sci.* **2002**, *200*, 150–164.

(60) Herzer, N.; Haensch, C.; Hoeppener, S.; Schubert, U. S. Orthogonal Functionalization of Silicon Substrates Using Self-Assembled Monolayers. *Langmuir* **2010**, *26*, 8358–8365.

Chapter 2: Design and Fabrication of Wettability Gradients with Tunable Profiles through Degrafting Organosilane Layers from Silica Surfaces by Tetrabutylammonium Fluoride

Miles, J.; Schlenker, S.; Ko, Y.; Patil, R.; Rao, B. M.; Genzer, J. Design and Fabrication of Wettability Gradients with Tunable Profiles through Degrafting Organosilane Layers from Silica Surfaces by Tetrabutylammonium Fluoride. *Langmuir* **2017**, *33*, 14556–14564.

2.1 Abstract

Surface-bound wettability gradients allow for a high-throughput approach to evaluate surface interactions for many biological and chemical processes. Here we describe the fabrication of surface wettability gradients on flat surfaces by a simple, two-step procedure that permits precise tuning of the gradient profile. This process involves the deposition of homogeneous silane SAMs followed by the formation of a surface coverage gradient through the selective removal of silanes from the substrate. Removal of silanes from the surface is achieved by using tetrabutylammonium fluoride which cleaves selectively the Si-O bonds at the headgroup of the silane. The kinetics of degrafting has been modeled by using a series of first order rate equations, based on the number of attachment points broken to remove a silane from the surface. Degrafting of mono-functional silanes exhibits a single exponential decay in surface coverage; however, there is a delay in degrafting of tri-functional silanes due to the presence of multiple attachment points. The effects of degrafting temperature and time are examined in detail and demonstrate the ability to reliably and precisely control the gradient profile on the surface. We observe a relatively homogenous coverage of silane (*i.e.* without the presence of islands or holes) throughout the degrafting process, providing a much more uniform surface when compared to additive approaches of gradient formation. Linear gradients were formed on the substrates to demonstrate the reproducibility and tuneability of this subtractive approach.

2.2 Introduction

The ability to tune the surface wettability by adjusting surface chemical composition is important in controlling wettability,[1,2] self-assembly,[3,4] adhesion,[5] protein adsorption, and cell growth and proliferation.[6–9] These applications require detailed understanding of the effects of surface chemistry. Therefore, rapid and efficient screening of a large parameter space is desirable. Surface-bound molecular gradients can provide this high-throughput approach on a single surface. A successful method for this application must involve a number density gradient, which is easy to prepare, should provide sufficient control over the profile of the gradient, and should allow for specific chemistries needed for applications.[3]

Traditionally surface wettability gradients have been fabricated by either gradual removal from or a gradual addition of a material to a substrate. Existing methods have been reviewed in the past.[10–12] Among the most popular methods is the deposition of self-assembled monolayers (SAMs) comprising thiols to gold (or other noble metal surfaces) or organosilanes to silica.[13–16] While the first system is very simple to implement and offers a large variety of thiols to work with, the relatively low stability of Au-S bond may limit utilization of such structures in practical applications.[17] Compared to thiols, organosilane SAMs offer much higher stability. Organosilanes ($RSiX_3$, R_2SiX_2, or R_3SiX, where R is an alkyl group and X is a leaving group, such as chloride, alkoxy, or hydride) form SAMs on hydroxyl functionalized surfaces due to their rapid formation of strong covalent linkages between the head group and the substrate.[18] The surface attachment occurs by the hydrolysis of the silane to form silanol groups and the subsequent condensation reaction with surface hydroxyls to form siloxane bonds. Monofunctional silanes form reproducibly consistent SAMs on the surface, but result in lower surface coverage due to steric hindrance around the siloxane head-group due to bulky methyl groups.[19] Trifunctional silanes pack more densely and result in more complete surface coverage as they have three hydrolysable groups, which can react with the surface and may also form intramolecular crosslinks among neighboring silanes molecules. One of the drawbacks of organosilanes with multiple reactive groups is that they can form multilayers and disordered structures.[20]

In the mid-1980s Elwing and coworkers developed several solution deposition methods that enable the formation of wettability gradients based on organosilane SAMs on flat surfaces.[21] This general strategy was later adopted by Chaudhury and Whitesides who extended it to a vapor based technique.[2] The vapor based method has been used frequently over the past few decades to control wetting behavior,[22] guide self-assembly processes,[3,23] tailor chemical properties,[14,24] and tune the grafting density of polymer brushes.[25,26] While these gradients are easy to achieve, they typically result in sigmoidal profiles whose steepness, typically on the order of a few millimeters to a few centimeters, is difficult to control since it depends on the environmental conditions during silane deposition (*i.e.*, temperature, humidity). Micro-contact printing and lithography techniques have also been employed to generate patterns in surface coverage for these applications on much greater length scales;[27,28] however, this approach results typically in relatively sharp boundaries on the surface with heterogeneous coverage.

To overcome the challenges associated with controlling the properties of silane-based SAM gradients, efforts have focused on selective removal of surface-bound species. One of the most commonly used approaches is to etch previously formed, homogeneous SAMs with an ultraviolet-ozone (UVO) treatment to remove the surface-bound silanes.[9,29,30] This method provides some control over the steepness of the gradient but it is limited by the resolution of the lithography mask and can result in degradation of other species on the surface, such as polymer brushes. It has been demonstrated previously that solutions of tetrabutylammonium fluoride (TBAF) can be employed to degraft polymer grafts, which have been covalently bound to surfaces via silane linkages.[26,31] TBAF reacts selectively with Si-O bonds at the head group of the silanes, thus cleaving them from the surface. The gradient profile formed by this method can be tuned to have the desired properties by adjusting the incubation time, temperature, and TBAF concentration. As TBAF is a relatively mild etching agent, the surface remains relatively smooth and generates hydroxyl functionalities which can later be used for backfilling to produce a two-component coating. We have evaluated the degrafting kinetics for various n-alkylchlorosilanes and have proposed a simple model to describe this process. The degrafting kinetics showed a dependence on the length of the alkyl chain and on the possible number of bonds to the surface. We also show that the morphology of the surface remains uniform throughout the degrafting process. The reproducibility of this approach and the ability to model the degrafting kinetics allows for the tuning of the surface wettability gradient profile over a desired length scale.

2.3 Experimental Section

All chemicals were purchased from Sigma-Aldrich and used without further purification unless otherwise specified. Deionized water was obtained using Millipore Elix 3. Silicon wafers (p-doped, orientation <100>) were purchased from Silicon Valley Microelectronics. The n-octyltrichlorosilane (OTCS), n-octyldimethylchlorosilane (ODMCS), n-propyltrichlorosilane (PTCS), and n-propyldimethylchlorosilane (PDMCS) were purchased from Gelest.

2.3.1 Silane Deposition

Monolayers of silanes were deposited on flat silicon substrates (45 mm x 30 mm). The substrates were cleaned by rinsing with toluene followed by sonication in toluene for 1 min. Subsequently the substrates were rinsed with methanol and acetone and dried under a stream of nitrogen gas. The silicon wafers were then placed in an ultraviolet-ozone (UVO, Model 42, Jelight Co.) chamber for 20 minutes to generate free hydroxyl (-OH) groups at the surface. The silane solutions were prepared by adding 150 μL of the desired silane to a solution consisting of 13.5 mL of hexanes (water content of 45 ppm) and 1.5 mL of carbon tetrachloride. UVO treated silicon wafers were placed in a glass jar containing the silane solutions, filled with nitrogen, and were sealed. Substrates were incubated in OTCS solutions for 5 hours, PTCS solutions for 30 minutes, and ODMCS and PDMCS solutions for 16 hours. After deposition was complete, the substrates were rinsed with hexanes and sonicated in chloroform for 30 seconds followed by rinsing with methanol and DI water before drying under a nitrogen stream. The substrates were divided into four segments (45 mm x 7.5 mm each) and rinsed with DI water prior to use in degrafting experiments.

2.3.2 Degrafting the Attached Silane Layer

Silane gradients were fabricated by progressively dipping silane functionalized substrates into a TBAF solution. Solutions of 0.1 M TBAF were made by adding 3 mL of 1 M TBAF in tetrahydrofuran (THF) and 30 mL of dimethylacetamide (DMA) to a glass jar. The solutions were heated to 60°C in an oil bath for at least 3 hours to evaporate the THF, ensuring a constant solution level during the degrafting process. The temperature of the solution was adjusted to 40, 45, 50, or 55°C prior to incubation of the silane functionalized substrates. Silane functionalized substrates were progressively dipped into the TBAF solution using a KSV NIMA Single Vessel Dip Coater. The substrates were dipped in 5 mm steps at a rate of 100 mm/min. After each 5 mm step the sample was held at that position to vary the degrafting time. For the kinetic studies, the degrafting times for each region on the substrate were 180, 120, 60, 30, 10, 5, 1, and 0.5 min.

2.3.3 Characterization

The thickness of the silane SAMs was determined using variable angle spectroscopic ellipsometry (VASE, J.A. Woollam Co.) at a 70° angle of incidence. The silane layer thickness was obtained by fitting the ellipsometry data using a 3-layer model with a 1 mm silicon layer, a 15 Å SiO_x layer, and a "Cauchy" layer with a refractive index of 1.45. Static water contact angle was measured using a contact angle goniometer (Model 100-00, Ramé Hart). All measurements were made using DIW using the probing liquid (3-5 μL in volume) deposited as drops from a syringe. For each WCA measurement the drop was lowered onto the substrate and the angle recorded within

5 seconds. The water contact angle measurements were performed under atmospheric conditions at 40-60% humidity. Advancing and receding contact angle measurements were measured by adding and removing water from the drop, contact angles were determined by when the base area first increased or decreased, respectively (Model 1000B, First Ten Angstroms). AFM measurements were performed on an Asylum Research MFP-3D AFM with an Asylum Research AC160TS-R3 cantilever. Topographical images were collected with a frame size of 2 μm^2 in AC mode.

2.4 Results and Discussion

2.4.1 Degrafting Model

As described earlier in the paper, the type of binding an organosilane molecule exhibits with the substrate depends strongly on the chemical nature of the headgroup chemistry. While mono-functional silanes attach to the substrate via a single Si-O bond, tri-functional silanes may, in principle, participate in the formation of 3 Si-O bonds. It is highly unlikely that all three Si-O bonds (if indeed formed) will attached to surface-bound –OH groups.[32] It is reasonable, however, to consider that tri-functional silanes may form a single Si-O bond with the substrate and up-to 2 Si-O bonds with neighboring silanes molecules; the latter will contribute to the formation of an in-plane -Si-O-Si- network whose existence has been confirmed previously.[33–35] Thus, for a single tri-functional organosilane, there may be, in principle, up to three different initial bonding states present, involving, one, two or three Si-O bonds.

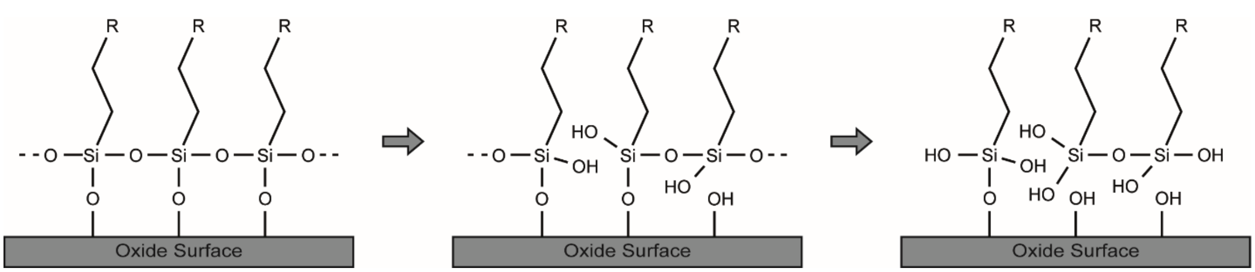

Figure 2-1. Idealized schematic of silane SAM structure during the degrafting process. From left to right shows the structure of silanes with three, two, or one bond.

The kinetics of degrafting can be roughly described by using a series of first order rate equations (*cf.* **Equations (1)-(3)**). These rate equations correspond to the cleaving of Si-O bonds at the surface with α, β and γ representing the fractions of species attached to the surface with one, two and three Si-O bonds respectively. The rate constants, k_i, characterize the rate of breaking a single bond from a species; the subscript denotes the number of bonds present for a species prior to the breaking.

$$\frac{d\gamma}{dt} = -k_3\gamma \tag{1}$$

$$\frac{d\beta}{dt} = k_3\gamma - k_2\beta \tag{2}$$

$$\frac{d\alpha}{dt} = k_2\beta - k_1\alpha \tag{3}$$

The model can be fit to experimental data by setting the fractional coverage of silanes equal to the summation of α, β and γ. This approach allows for the breaking of a single bond on the doubly or triply bound species without their removal from the surface; therefore, the fractional coverage only changes with the removal of the last covalent bond from the surface. It is important to note that this model does not account for the removal of multilayer/aggregate structures that can be formed by tri-functional silanes.

By assuming that a single rate constant can be used to describe the breakage of the Si-O bond regardless of its binding state (*i.e.*, the rate constant for breaking the Si-O bond for a species with one remaining bond is the same as that corresponding to breaking the Si-O bond for species with two or three remaining bonds), **Equations (1)-(3)** can be simplified to yield:

$$\gamma = \gamma_0 e^{-kt} \tag{4}$$

$$\beta = k\gamma_0 t e^{-kt} + \beta_0 e^{-kt} \tag{5}$$

$$\alpha = \tfrac{1}{2}k^2\gamma_0 t^2 e^{-kt} + k\beta_0 t e^{-kt} + \alpha_0 e^{-kt} \tag{6}$$

In **Equations (4)-(6)**, α_0, β_0, and γ_0 represent the initial fractions of the molecules containing one, two, and three Si-O bonds, respectively. For degrafting of monofunctional silanes the β and γ values can be set to zero as there should be no species on the surface with more than one Si-O bond.

2.4.2 Monte Carlo Simulation Model of Degrafting

We have performed a coarse-grained, two-dimensional Monte Carlo (MC) simulation for the degrafting of small molecules from a planar substrate. This highly simplified lattice model was conceived to validate the use of our degrafting model and to ensure that it can reproduce the initial binding configuration of molecules covalently attached to the surface. A one-dimensional model was used for the planar substrate with grid sites ($x \in [1,25]$, $y = 1$) representing binding domains on the surface; similarly, the bound species occupied grid sites ($x \in [1,25]$, $y = 2$). This simulation was performed for systems consisting of mono-, di-, and tri-functional species on the surface. An additional simulation was carried out with a mixture of mono-, di-, and tri-functional species on the surface with fractional coverages of 0.36, 0.32, and 0.32, respectively. The initial configuration for the simulation is depicted in **Figure 2-2** with each species being bound to the surface with at least one bond. For the di- and tri-functional species, the additional bonds were added as in-plane linkages between species in the network.

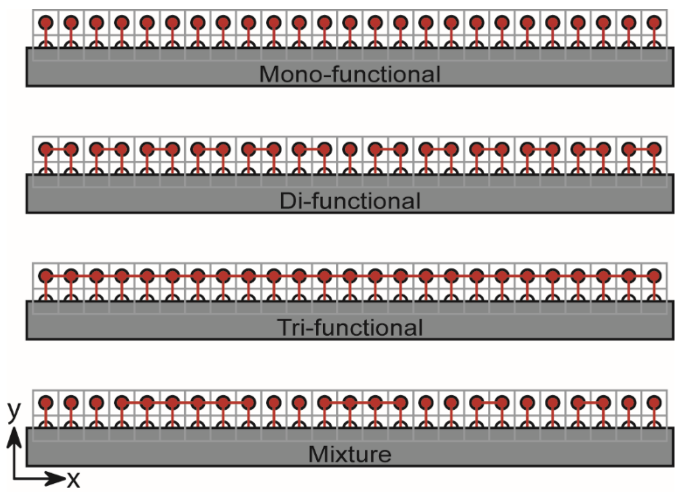

Figure 2-2. Schematic depicting the initial geometry and bond structure of mono, di, and trifunctional molecules covalently attached to a substrate. The grey squares denote the lattice sites in the simulation box.

For each MC step a bond is randomly selected from the existing set of bonds; if the bond exists, it can break with a certain probability (here set to p = 0.0675 to consistently achieve a fractional coverage of 0.10 after ~3000 Monte Carlo steps for all cases examined). All bonds in the system can break with an equal probability, thus representing the condition that only a single rate constant associated with breaking the bond is needed. If the bond breaks, the algorithm removes the bond from the existing set of bonds and updates the number of bonds attached to each species. This process continues until all bonds are broken. During the process, the total number of species with at least one bond remaining is monitored to calculate the fractional coverage. The MC procedure was repeated at least 25 times prior to the results being averaged and the standard deviation being calculated. We used Equations **(4)-(6)** to model the simulation data. Results from these simulations are shown in **Figure 2-3**.

The degrafting of mono-functional species is described well by a single exponential decay and is reflected well by the model fit with an α_0 value close to 1. A clear shoulder in the profiles of the di and tri-functional species can be seen and is reflected in the model fits with β_0 and γ_0 close to 1 in each case respectively. In the more complicated mixed system the model captures the trend well, but exhibits a slight deviation in the model fitting parameters. The model presented by **Equations (4)-(6)** appears to capture the essential details of the degrafting process, but it is important to note that the model and simulations are oversimplified and do not account for interconnectivity, *i.e.*, a species can still be included in the fractional coverage if in-plane bonds are still present but with no surface-species bonds.

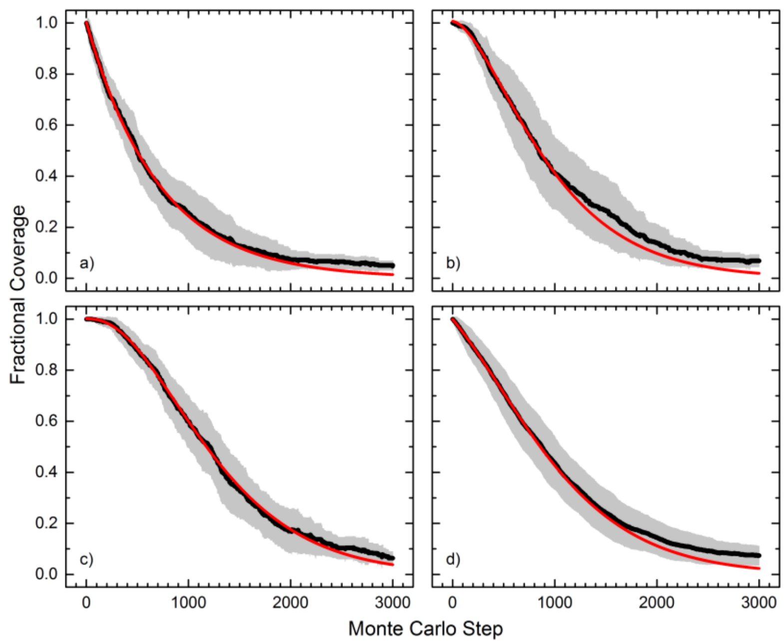

Figure 2-3. Fractional coverage of a) mono-, b) di-, c) tri-functional, and d) mixed molecules attached covalently to the surface as a function of the number of Monte Carlo (MC) steps. The black line and the grey shaded area denote the average and standard deviation from the MC simulation, respectively. The red lines are the best fits to Equations (4)-(6).

Table 2-1. Summary of the fitting parameters of the degrafting model for the Monte Carlo simulation of the degrafting process for mono-, di-, tri-functional, and mixed molecules.

Functionality	α_0	β_0	γ_0
Mono	0.996	0.004	0.000
Di	0.011	0.988	0.001
Tri	0.000	0.080	0.920
Mixed	0.227	0.321	0.453

2.4.3 Silane Degrafting

The four chlorosilanes investigated in our study differ in the length of the alkyl chain and the number of reactive chloride groups (*cf.* **Figure 2-4**). Alkyl chain lengths of 3 and 8 carbons were used for this study with mono and trifunctional binding domains. Deposition of these silanes was performed in a mixture of hexanes and carbon tetrachloride to limit the formation of aggregates and micelles in the bulk solution and to limit the incorporation of hexanes into the resulting film.

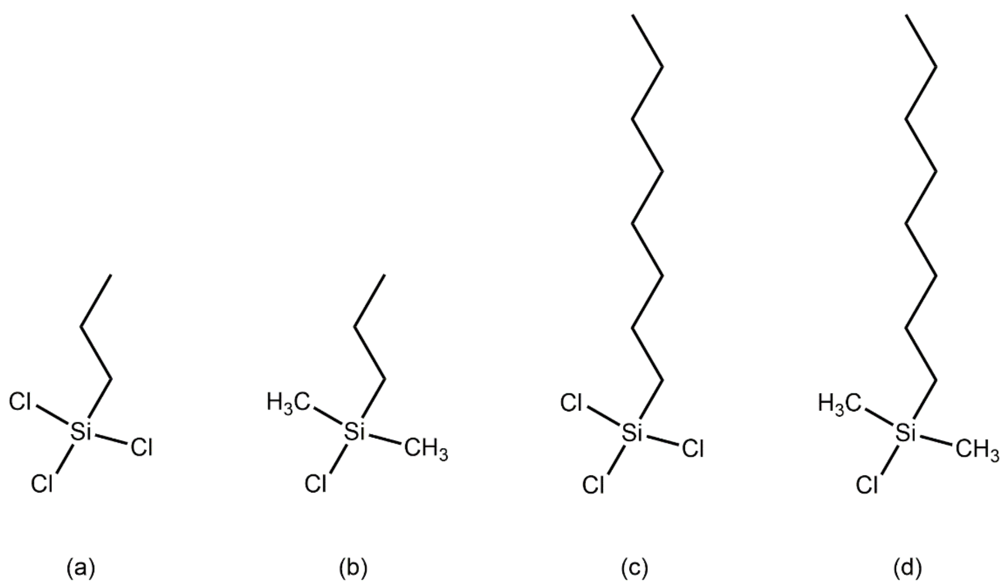

Figure 2-4. Self-assembled monolayers of a) n-propyltrichlorosilane (PTCS), b) n-propyldimethylchlorosilane (PDMCS), c) n-octyltrichlorosilane (OTCS), and d) n-octyldimethylchlorosilane (ODMCS) were deposited on UVO treated silicon substrates.

Table 2-2. Summary of the measured thicknesses, contact angles, and approximate roughness for the various silanes. See Figure 2-4 for abbreviations.

Silane	Thickness (nm)	Water contact angle (deg)	RMS Roughness (pm)
ODMCS	0.50 ± 0.08	98.5 ± 1.6	92.2
OTCS	1.32 ± 0.14	109.8 ± 1.2	47.3
PDMCS	0.51 ± 0.24	90.9 ± 2.3	119.4
PTCS	1.22 ± 0.21	98.0 ± 3.0	206.5

The resulting silane assembly was confirmed by contact angle analysis and ellipsometric thickness prior to their use in degrafting studies (*cf.* **Table 2-2**). For n-alkylchlorosilanes, a general increase in water contact angle with increasing chain length was observed; the reported values are consistent with previous experimental results.[9,36,37] The thickness values and corresponding contact angles obtained for the homogeneous silane films show relatively complete monolayer coverage for all silanes; however, some multilayer formation is observed for the PTCS layers. The lower thickness and water contact angle values for PDMCS and ODMCS is attributed to a lower density of silanes on the surface due to the bulky methyl groups. The approximate roughness of the silane SAMs further supports this observation as greater roughness is observed for monofunctional silanes except when compared to PTCS, which is most likely due to the presence of multilayers or aggregate structures (*cf.* **Figure A-1-1**). It should be noted that the measured ODMCS thickness is lower than expected; this is most likely due to thickness variations in the SiO_x layer prior to silane deposition.

Wettability gradients were formed on the surface by degrafting uniform silane SAMs in a 0.1 M TBAF solution. To generate gradient surfaces the silane coated substrates were lowered gradually in a vertical direction into the solution in a stepwise fashion. This method produced eight 5.0 mm x 7.5 mm regions on the surface that had been exposed to the TBAF solution for varying TBAF exposure times. The hydrophobicity of the substrate decreases along its length as the degrafting time increases (*cf.* **Figure 2-5**). The wettability profiles for the monofunctional silanes are similar and exhibit single exponential decays. The wettability profile for the degrafted OTCS substrate shows a sharp decrease initially followed by a significant shoulder, but remains more hydrophobic than the monofunctional silanes for all times studied. The wettability profile for the degrafted PTCS substrate shows a sharp decrease initially followed by a slight shoulder.

The fractional coverage of silane on the surface can be calculated using the Cassie-Baxter equation (**Equation (7)**),[38] where θ_1 is the contact angle of component 1 with the fractional coverage ϕ_1 and θ_2 is the contact angle of component 2 with fractional coverage ϕ_2. By setting one of these components to a bare silicon substrate we can determine the areal fractional coverage of a silane left after degrafting. The water contact angles corresponding to fully covered PDMCS, PTCS, ODMCS, OTCS, and a hydroxyl functionalized silicon wafer were selected as 93, 100, 100, 110, and 5 degrees, respectively. The 5 degree WCA of a hydroxyl functionalized silicon wafer was used as it has been shown that hydroxyl groups are regenerated with little fluorine contamination.[25]

$$cos\,\theta = \phi_1\,cos\,\theta_1 + \phi_2\,cos\,\theta_2 \tag{7}$$

The fractional coverage of silane on the substrate after degrafting shows similar trends to those seen in the wettability profiles (*cf.* **Figure 6**). The rate of degrafting increases with increasing degrafting temperature and results in a steeper coverage profile. Within three hours of incubation the PDMCS and PTCS substrates appear to be completely degrafted at the temperatures studied. However, the ODMCS and OTCS substrates degraft at significantly slower rates.

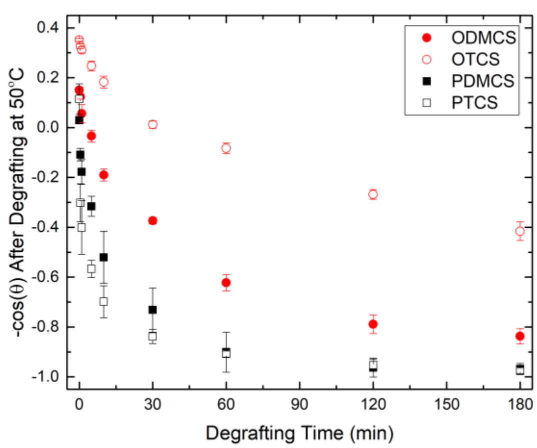

Figure 2-5. Wettability profiles generated by degrafting silane layers in 0.1 M TBAF in DMA at 50°C as a function of incubation time in TBAF solution.

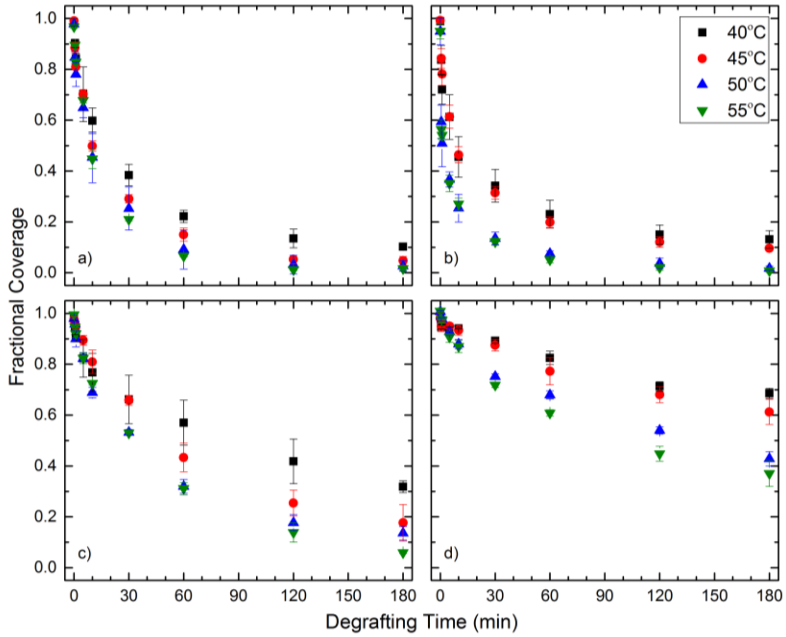

Figure 2-6. Fractional coverage profiles of a) PDMCS, b) PTCS, c) ODMCS, and d) OTCS from degrafting in 0.1 M TBAF in DMA as a function of temperature and incubation time.

Fitting the experimental data to Equations (4)-(6) produced the profiles plotted in **Figure 2-7**. The proposed model can capture the general trend of the TBAF degrafting, but is unable to account for the sharp decrease in coverage exhibited by the trichlorosilanes at short degrafting times. This sharp decrease may arise from inhomogeneities in the initial silane layer, such as the presence of multilayers or many silanes attached through in-plane linkages with few surface linkages. These situations could result in many silanes being removed from the surface with the occurrence of a few degrafting events.

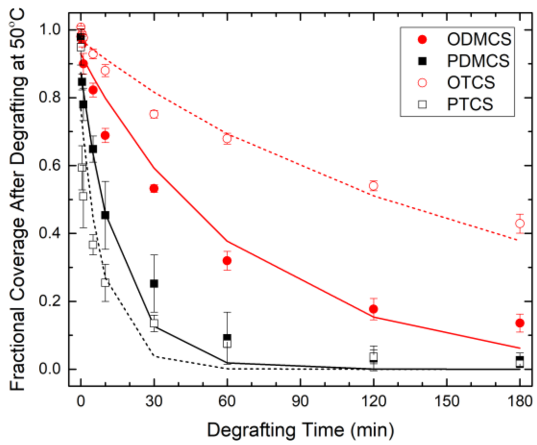

Figure 2-7. Fractional coverage profiles from degrafting in 0.1 M TBAF in DMA at 50°C as a function of incubation time. Solid and dashed lines show best fits to Equations (4)-(6) and represent mono- and tri-functional silanes, respectively.

Table 2-3. Summary of the rate constants (k in (min-1)) for the various silane degrafting processes.

Silane	**Degrafting temperature (°C)**			
	40	45	50	55
ODMCS	0.007	0.012	0.017	0.019
PDMCS	0.027	0.042	0.055	0.060
OTCS	0.004	0.005	0.009	0.010
PTCS	0.044	0.051	0.154	0.171

Table 2-3 lists the rate constants from the fitted model. Silanes with the same length alkyl chain exhibit similar rate constants with longer alkyl chains degrafting more slowly. Some variation from this trend is observed for degrafting of the PTCS layers at higher temperatures. This most likely arises from the fitting over accounting for the sharp decrease of fractional coverage of silanes on the substrate at short degrafting times, which leads to a much sharper profile.

2.4.4 Surface Morphology

Ellipsometric thickness measurements were taken on octylsilane monolayers after degrafting in a 0.1 M TBAF solution at 50°C. Measurements were taken at 25 minute degrafting intervals (*cf.* **Figure 2-8**). As degrafting time increased the thickness of the silane layer decreased, which is expected due to a decrease in surface coverage of the silane on the surface. After degrafting, a small increase in thickness is observed across the sample, resulting in a greater thickness than was initially measured for the silane SAM. Additional studies are needed to understand this phenomenon.

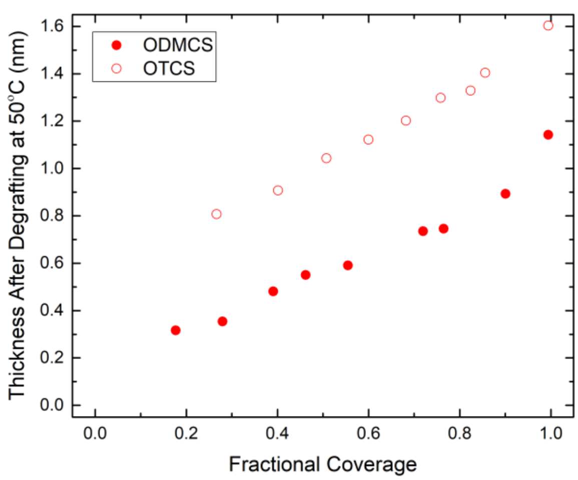

Figure 2-8. Ellipsometric thickness measurements of a silane monolayers after degrafting in a 0.1 M TBAF solution.

Figure 2-9 depicts AFM micrographs demonstrating morphology changes upon degrafting of an OTCS monolayer. An increase in roughness is observed at short degrafting times as OTCS molecules begin to be removed from the layer and this trend proceeds until approximately 50% coverage; after this point, the roughness decreases as the silane coverage on the surface continues to decrease (*cf.* **Figure 2-10**). It is important to note that the surfaces appear relatively homogeneous with no large holes or islands of silane apparent on the surface during degrafting.

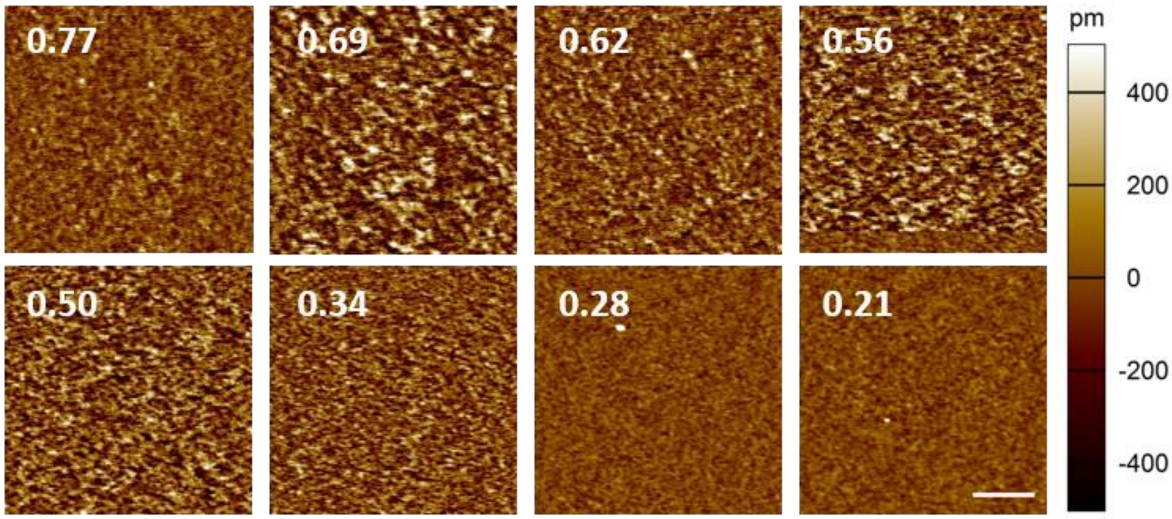

Figure 2-9. AFM micrographs of OTCS monolayer after degrafting in a 0.1 M TBAF solution at 50°C (500 nm scale bar). Inset numbers correspond to fractional coverage of OTCS after degrafting as calculated by the Cassie-Baxter equation.

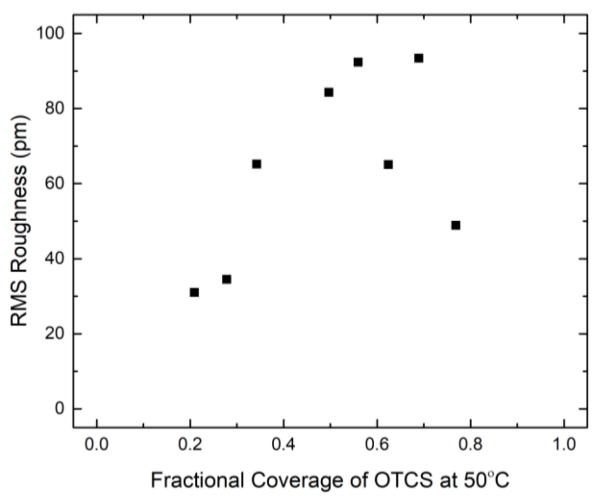

Figure 2-10. Fractional coverage and RMS roughness of an OTCS monolayer after degrafting in a 0.1 M TBAF solution at 50°C.

2.4.5 Linear Gradients

The parameters derived from fitting the model were used to generate linear gradients in fractional coverage for each of the silanes (**Figure 2-11**). The degrafting times were calculated to achieve a linear profile in fractional coverage, decreasing 10% coverage every 5 mm along the length of the surface. The resulting gradient profiles are within good agreement with the model. The most significant deviation is observed for the OTCS layers. This deviation is most likely the result of extrapolating the model to significantly longer degrafting studies than were performed for the kinetic analysis.

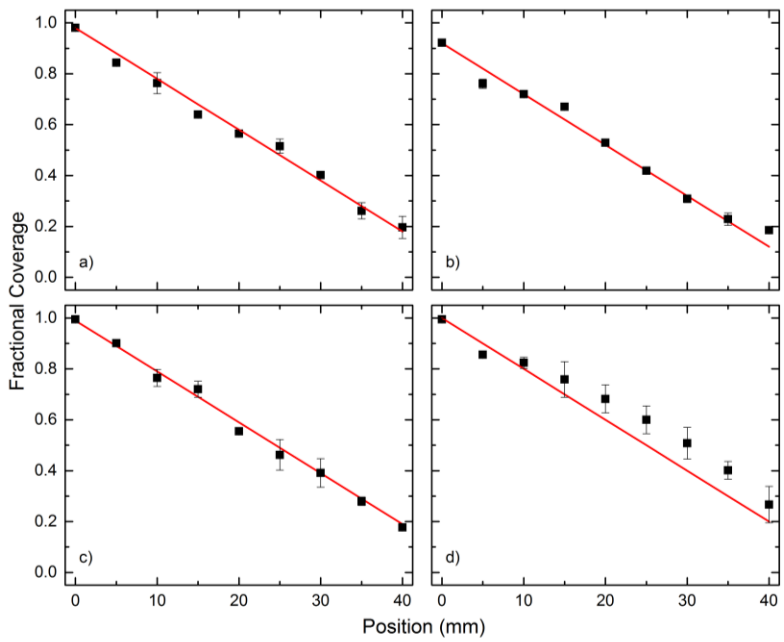

Figure 2-11. Linear fractional coverage gradients in a) PDMCS, b) PTCS, c) ODMCS, and d) OTCS. Solid red line represents target fractional coverage profile.

2.5 Conclusions

We have presented a two-step process for generating surface wettability gradients. The method involves 1) formation of a homogeneous SAM of organosilanes on silica surfaces and 2) a gradual degrafting of organosilanes from the surface with TBAF. This process improves upon previously developed techniques as the SAM number density gradient profile can be easily tuned by controlling the incubation time and temperature of the SAM in TBAF solution. A vapor or solution phase approach can be used initially to deposit the homogeneous silane layer, allowing for the use of a wider variety of silanes with different chemical functionalities. The subtractive approach used here can generate surfaces with more homogeneous coverage as the morphology is not controlled by the nucleation and growth during silane deposition processes. Using this approach, we can generate surface wettability gradients with tunable profiles over a desired length scale which has not been possible with previous approaches.

The degrafting process generates reactive hydroxyl groups on the surface as it removes the organosilanes, allowing for backfilling of these gradients with a second silane to generate both wettability and chemical gradients. The ability to precisely tune the grafting density of functional groups on the surface will allow for investigation into the effect of surface energy on protein adsorption, polymer wetting behavior, density dependent mechanics of polymer brushes, and directed self-assembly.

2.6 References

(1) Mansky, P.; Liu, Y.; Huang, E.; Russell, T. P.; Hawker, C. Controlling Polymer-Surface Interactions with Random Copolymer Brushes. *Science* **1997**, *275*, 1458–1460.

(2) Chaudhury, M. K.; Whitesides, G. M. How to Make Water Run Uphill. *Science* **2013**, *20*, 38–59.

(3) Bhat, R. R.; Fischer, D. A.; Genzer, J. Fabricating Planar Nanoparticle Assemblies with Number Density Gradients. *Langmuir* **2002**, *18*, 5640–5643.

(4) Kelley, E. G.; Albert, J. N. L.; Sullivan, M. O.; Epps, T. H. Stimuli-Responsive Copolymer Solution and Surface Assemblies for Biomedical Applications. *Chem. Soc. Rev.* **2013**, *42*, 7057–7071.

(5) Tesoro, G.; Wu, Y. Silane Coupling Agents: The Role of the Organofunctional Group. *J. Adhes. Sci. Technol.* **1991**, *5*, 771–784.

(6) Kumar, G.; Ho, C. C.; Co, C. C. Guiding Cell Migration Using One-Way Micropattern Arrays. *Adv. Mater.* **2007**, *19*, 1084–1090.

(7) Zaari, N.; Rajagopalan, P.; Kim, S. K.; Engler, A. J.; Wong, J. Y. Photopolymerization in Microfluidic Gradient Generators: Microscale Control of Substrate Compliance to Manipulate Cell Response. *Adv. Mater.* **2004**, *16*, 2133–2137.

(8) Bhat, R. R.; Chaney, B. N.; Rowley, J.; Liebmann-Vinson, A.; Genzer, J. Tailoring Cell Adhesion Using Surface-Grafted Polymer Gradient Assemblies. *Adv. Mater.* **2005**, *17*, 2802–2807.

(9) Kennedy, S. B.; Washburn, N. R.; Simon Jr., C. G.; Amis, E. J. Combinatorial Screen of the Effect of Surface Energy on Fibronectin-Mediated Osteoblast Adhesion, Spreading and Proliferation. *Biomaterials* **2006**, *27*, 3817–3824.

(10) Genzer, J.; Bhat, R. R. Surface-Bound Soft Matter Gradients. *Langmuir* **2008**, *24*, 2294–2317.

(11) Morgenthaler, S.; Zink, C.; Spencer, N. D. Surface-Chemical and -Morphological Gradients. *Soft Matter* **2008**, *4*, 419–434.

(12) Genzer, J. Surface-Bound Gradients for Studies of Soft Materials Behavior. *Annu. Rev. Mater. Res.* **2012**, *42*, 435–468.

(13) Morgenthaler, S.; Lee, S.; Zürcher, S.; Spencer, N. D. A Simple, Reproducible Approach to the Preparation of Surface-Chemical Gradients. *Langmuir* **2003**, *19*, 10459–10462.

(14) Albert, J. N. L.; Baney, M. J.; Epps, T. H. Generation of Monolayer Gradients in Surface Energy and Surface Chemistry for Block Copolymer Thin Film Studies. *ACS Nano* **2009**, *3*, 3977–3986.

(15) Ulman, A. Formation and Structure of Self-Assembled Monolayers. *Chem. Rev.* **1996**, *96*, 1533–1554.

(16) Bain, C. D.; Whitesides, G. M. Modeling Organic Surfaces with Self-Assembled Monolayers. *Adv. Mater.* **1989**, *1*, 110–116.

(17) Watson, S.; Nie, M.; Wang, L.; Stokes, K. Challenges and Developments of Self-Assembled Monolayers and Polymer Brushes as a Green Lubrication Solution for Tribological Applications. *RSC Adv.* **2015**, *5*, 89698–89730.

(18) Pujari, S. P.; Scheres, L.; Marcelis, A. T. M.; Zuilhof, H. Covalent Surface Modification of Oxide Surfaces. *Angew. Chemie - Int. Ed.* **2014**, *53*, 6322–6356.

(19) Smith, M. B.; Efimenko, K.; Fischer, D. A.; Lappi, S. E.; Kilpatrick, P. K.; Genzer, J. Study of the Packing Density and Molecular Orientation of Bimolecular Self-Assembled Monolayers of Aromatic and Aliphatic Organosilanes on Silica. *Langmuir* **2007**, *23*, 673–683.

(20) Booth, B. D.; Vilt, S. G.; Lewis, J. B.; Rivera, J. L.; Buehler, E. A.; McCabe, C.; Jennings, G. K. Tribological Durability of Silane Monolayers on Silicon. *Langmuir* **2011**, *27*, 5909–5917.

(21) Elwing, H.; Welin, S.; Askendal, A.; Nilsson, U.; Lundström, I. A Wettability Gradient Method for Studies of Macromolecular Interactions at the Liquid/Solid Interface. *J. Colloid Interface Sci.* **1987**, *119*, 203–210.

(22) Epps, T. H.; DeLongchamp, D. M.; Fasolka, M. J.; Fischer, D. A.; Jablonski, E. L. Substrate Surface Energy Dependent Morphology and Dewetting in an ABC Triblock Copolymer Film. *Langmuir* **2007**, *23*, 3355–3362.

(23) Giri, D.; Li, Z.; Ashraf, K. M.; Collinson, M. M.; Higgins, D. A. Molecular Combing of λ-DNA Using Self-Propelled Water Droplets on Wettability Gradient Surfaces. *ACS Appl. Mater. Interfaces* **2016**, *8*, 24265–24272.

(24) Albert, J. N. L.; Kim, J. D.; Stafford, C. M.; Epps, T. H. Controlled Vapor Deposition Approach to Generating Substrate Surface Energy/Chemistry Gradients. *Rev. Sci. Instrum.* **2011**, *82*, 065103.

(25) Patil, R. R.; Turgman-Cohen, S.; Šrogl, J.; Kiserow, D.; Genzer, J. On-Demand Degrafting and the Study of Molecular Weight and Grafting Density of Poly(Methyl Methacrylate) Brushes on Flat Silica Substrates. *Langmuir* **2015**, *31*, 2372–2381.

(26) Zuo, B.; Zhang, S.; Niu, C.; Zhou, H.; Sun, S.; Wang, X. Grafting Density Dominant Glass Transition of Dry Polystyrene Brushes. *Soft Matter* **2017**, *13*, 2426–2436.

(27) Lee, J. H.; Hon, M. H.; Chung, Y. W.; Leu, I. C. Microcontact Printing of Organic Self-Assembled Monolayers for Patterned Growth of Well-Aligned Zno Nanorod Arrays and Their Field-Emission Properties. *J. Am. Ceram. Soc.* **2009**, *92*, 2192–2196.

(28) Yanker, D. M.; Maurer, J. A. Direct Printing of Trichlorosilanes on Glass for Selective Protein Adsorption and Cell Growth. *Mol. Biosyst.* **2008**, *4*, 502–504.

(29) Roberson, S. V.; Fahey, A. J.; Sehgal, A.; Karim, A. Multifunctional ToF-SIMS: Combinatorial Mapping of Gradient Energy Substrates. *Appl. Surf. Sci.* **2002**, *200*, 150–164.

(30) Herzer, N.; Haensch, C.; Hoeppener, S.; Schubert, U. S. Orthogonal Functionalization of Silicon Substrates Using Self-Assembled Monolayers. *Langmuir* **2010**, *26*, 8358–8365.

(31) Patil, R.; Kiserow, D.; Genzer, J. Creating Surface Patterns of Polymer Brushes by Degrafting via Tetrabutyl Ammonium Fluoride. *RSC Adv.* **2015**, *5*, 86120–86125.

(32) Stevens, M. J. Thoughts on the Structure of Alkylsilane Monolayers. *Langmuir* **1999**, *15*, 2773–2778.

(33) Efimenko, K.; Crowe, J. A.; Manias, E.; Schwark, D. W.; Fischer, D. A.; Genzer, J. Rapid Formation of Soft Hydrophilic Silicone Elastomer Surfaces. *Polymer* **2005**, *46*, 9329–9341.

(34) Naik, V. V.; Crobu, M.; Venkataraman, N. V.; Spencer, N. D. Multiple Transmission-Reflection IR Spectroscopy Shows That Surface Hydroxyls Play Only a Minor Role in Alkylsilane Monolayer Formation on Silica. *J. Phys. Chem. Lett.* **2013**, *4*, 2745–2751.

(35) Naik, V. V.; Städler, R.; Spencer, N. D. Effect of Leaving Group on the Structures of Alkylsilane SAMs. *Langmuir* **2014**, *30*, 14824–14831.

(36) Jayaraman, K.; Shaw, L. H.; McCarthy, T. J. Versatile Multilayer Thin Film Preparation Using Hydrophobic Interactions, Crystallization, and Chemical Modification of Poly(Vinyl Alcohol). *Langmuir* **2007**, *23*, 3260–3264.

(37) Wasserman, S. R.; Tao, Y. T.; Whitesides, G. M. Structure and Reactivity of Alkylsiloxane Monolayers Formed by Reaction of Alkyltrichlorosilanes on Silicon Substrates. *Langmuir* **1989**, *5*, 1074–1087.

(38) Cassie, A. B. D.; Baxter, S. Wettability of Porous Surfaces. *Trans. Faraday Soc.* **1944**, *40*, 546–551.

Chapter 3: Dependence of Deposition Method on the Molecular Structure and Stability of Organosilanes Revealed from Degrafting by Tetrabutylammonium Fluoride

3.1 Abstract

We probe the structure of self-assembled monolayers (SAMs) comprising organosilanes deposited on flat silica-based surfaces prepared by liquid and vapor deposition by removing the organosilane molecules gradually from the underlying substrate via tetrabutylammonium fluoride (TBAF). Removal of organosilanes from the surface involves the cleavage of all pertinent Si-O bonds that anchor the organosilane molecules to the SAM, *i.e.*, direct organosilane-surface linkages and in-plane crosslinks between neighboring organosilanes. We gain insight into the organosilane structure and stability by monitoring the organosilane density as a function of exposure time to TBAF. Degrafting of trifunctional chloro- and methoxy-alkylsilanes deposited from solution yields similar degrafting kinetics. We observe fast degrafting for organosilane SAMs deposited from the vapor phase, indicating that SAMs prepared in this manner form more loosely packed arrays, with less in-plane connectivity, compared to their solution-deposited counterparts. Bulkier, fluorinated silanes form more stable SAMs due to their ability to readily align and form a network with few aggregates and a relatively high fraction of surface bonds. The addition of a polymer brush to an anchored organosilane molecule demonstrates that increased bond tension accelerates the degrafting process despite the increased diffusion resistance.

3.2 Introduction

Polymeric films or self-assembled monolayers (SAMs) have been employed routinely to tune the wettability and chemical reactivity of surfaces.[1–6] Varying the chemical composition and density of SAMs on the surface provides molecular control of surface properties. The assembly of thiols on gold (or other noble metal) surfaces and the attachment of organosilanes to hydroxyl-covered surfaces have been among the most popular methods to form SAMs. While the assembly of thiols is simple to implement and offers a wide variety of chemistries, the relatively low stability of the thiol-based SAMs may limit utilization in applications.[7] Organosilanes are available with a variety of chemistries and generate more robust SAMs than the thiol-based SAMs. However, the attachment of organosilanes to surfaces depends upon multiple deposition parameters, which complicates the formation of stable, and well-organized SAMs.[8]

Many studies have reported on the deposition of silane SAMs. However, only a few investigate the mechanical and chemical stability of organosilane SAMs. These studies do not typically consider the underlying binding structure that influences the stability of organosilane SAMs.[9–15] Organosilanes form SAMs on hydroxyl functionalized surfaces due to the formation of strong covalent linkages between the silicone head group and the substrate functionalities (primarily -OH).[16] The surface attachment occurs by the hydrolysis of the functional groups attached to silicon (chloride or alkoxy), alignment due to van der Waals forces, and condensation reaction with surface hydroxyls to form siloxane bonds. Due to the alignment of silanes on the surface by van der Waals forces before attachment, many silane SAMs form by a nucleation and growth process.[17–21] The alignment of silanes during this process dictates their density on the surface as the siloxane network develops. Monofunctional silanes form reproducible SAMs but result in lower surface coverage due to bulky methyl groups, thus causing steric hindrance around the siloxane head-group.[22] The hydrolysis of trifunctional silanes before attachment allows for more dense packing on the surface, thus resulting in higher surface coverage and the ability to form intramolecular crosslinks among neighboring silane molecules.[23] While these intramolecular crosslinks can improve the packing density and stability[24,25] of silane SAMs, they also allow for the formation of multilayers, disordered structures, and the deposition of aggregates onto the surface.

Previously, we presented a subtractive approach to tailor the grafting density of propyl- and octyl-based silanes on a surface based on the selective removal by tetrabutylammonium fluoride (TBAF) solutions.[26] TBAF is a fluoride ion source which cleaves the Si-O bonds at the head group of the silanes, thus liberating the silane molecules from the surface. Adjusting the incubation time, temperature, and TBAF concentration allows for fine-tuning of the grafting density of silanes on the surface while regenerating surface-bound hydroxyl functionalities for later modification.[27]

The kinetics of degrafting for silane monolayers by TBAF depends on the silane connectivity, the structure of the siloxane network, and the diffusion of TBAF to the surface. The connectivity of silanes to the surface and the resulting siloxane network depend, in turn, on the number of hydrolyzable groups, their reactivity, and the bulkiness of the silane. Evaluation of the degrafting profiles allows us to gain insight into the bonding structure at the surface and better understand the stability of silane SAMs. Mono-functional silanes, which can only form one siloxane bond with the surface, exhibit a simple exponential decay as a function of degrafting time. The degrafting profiles of tri-functional silanes are more complex and exhibit a delay in the degrafting due to their ability to form a siloxane network at the surface, consisting of surface bonds and an in-plane siloxane network. The rate of hydrolysis, bulkiness, and ability of silanes to align during their deposition impacts the structure of the siloxane network. Rapid decreases in grafting density during degrafting suggest the presence of aggregates on the surface formed mostly by in-plane siloxane linkages that lead to an overall instability of the SAM.

The medium, from which the SAMs are grown, *i.e.*, vapor or solution deposition, plays a crucial role in governing the density of the silane molecules in the SAMs. We are not aware of any previous study that has compared the two deposition methods concerning the compactness and bonding structure of the SAM. In this work, we evaluate the degrafting profiles for alkylsilanes concerning their reactivity and deposition method, fluorinated silanes to examine the effect of bulkiness, and a common polymerization initiator before and after growth of a polymer brush to determine how subsequent functionalization affects the stability of the SAM.

3.3 Experimental Section

All chemicals were purchased from Sigma-Aldrich and used without further purification unless otherwise specified. Deionized water was obtained using Millipore Elix 3. Silicon wafers (p-doped, orientation <100>) were purchased from Silicon Valley Microelectronics. *n*-octyltrichlorosilane (OTCS), *n*-octyltrimethoxysilane (OTMS), heptadecafluoro-1,1,2,2-tetrahydrodecyltrichlorosilane (FTCS), and (heptadecafluoro-1,1,2,2-tetrahydrodecyl)dimethylchlorosilane (FDMCS) were purchased from Gelest. The 3-aminopropyltriethoxysilane (APTES) was purchased from Fisher Scientific. The (11-(2-bromo-2-methyl)propionyloxyundecyltrichlorosilane (eBMPUS) was synthesized, as described in the literature.[28]

3.3.1 Silane Deposition

Silane monolayers were deposited on flat silicon substrates (45 mm x 30 mm). Silicon wafers were cleaned by rinsing with toluene followed by sonication in toluene for 1 min. Subsequently, the substrates were rinsed with methanol and acetone and dried under a stream of nitrogen gas. The silicon wafers were then placed in an ultraviolet-ozone (UVO, Model 42, Jelight Co.) chamber for 20 minutes to generate free hydroxyl (-OH) groups at the surface. The silane solution of OTMS was prepared by adding 150 μL of OTMS to 15 mL of hexanes (water content of 45 ppm). eBMPUS solutions (0.005% by volume) were prepared by adding eBMPUS to hexanes. UVO treated silicon wafers were placed in a glass jar containing the silane solutions, filled with nitrogen, and were sealed. Substrates were incubated in OTMS solutions and eBMPUS solution for 48 hours at room temperature. After deposition, the substrates were rinsed with hexanes and sonicated in chloroform for 30 seconds followed by rinsing with methanol and DI water before drying under a nitrogen stream. The silane solutions of APTES were prepared by adding 1.5 µL of APTES to 15 mL of anhydrous toluene (water content of <5 ppm). Substrates were incubated in APTES solutions for 5 minutes. After deposition, the substrates were rinsed with toluene and sonicated in methanol for 30 seconds, followed by annealing at 115 °C for 16 hours. Substrates to be functionalized with OTCS, FTCS, and FDMCS were placed in a desiccator containing a mixture of the desired silane and either mineral oil for OTCS or perfluoro(methyldecalin) for FTCS and FDMCS. The desiccator was evacuated by a vacuum pump for 30 seconds and then sealed. The deposition times for the OTCS, FTCS, and FDMCS were 20, 30, and 60 minutes, respectively. The substrates were divided into four segments (45 mm x 7.5 mm each) and rinsed with DI water before use in degrafting experiments.

3.3.2 Surface-initiated Atom Transfer Radical Polymerization (ATRP) of PMMA

ATRP solution was prepared as following; methyl methacrylate (MMA) (9.4 mL, 88 mmol), methanol (8.7 mL), and deionized water (1.9 mL) were added to a 50 mL round-bottom flask followed by purging with nitrogen gas for 15 mins. 2,2'-Bipyridine (555.5 mg, 3.60 mmol) and CuCl(I) (177.9 mg, 1.80 mmol) were sequentially added to the flask. After nitrogen purging for another 15 mins, the solution was transferred to a 20 mL scintillation vial. The eBMPUS functionalized substrates were immersed in the ATRP solution for 20 hours.

3.3.3 Degrafting the Attached Silane Layer

Silanes were degrafted from silicon wafers covered with silane SAMs by vertically dipping the substrates into a TBAF solution. We prepared solutions of 0.1 M TBAF by adding 3 mL of 1 M TBAF in tetrahydrofuran (THF) and 30 mL of dimethylacetamide (DMA) and heated them to 60°C for >3 hours to evaporate the THF. Before incubation of the silane functionalized substrates, we adjusted the temperature of the solution to 40, 45, 50, or 55°C. We employed a KSV NIMA Single Vessel Dip Coater to progressively immerse silane functionalized substrates into the TBAF solution in 5 mm steps at a rate of 10 cm/min between each step. After each dipping step, we held the sample at a given position to vary the degrafting time. The degrafting times for each region on the substrate were 180, 120, 60, 30, 10, 5, 1, and 0.5 min.

3.3.4 Characterization

We determined the thickness of the silane SAMs using variable angle spectroscopic ellipsometry (VASE, J.A. Woollam Co.) at 70° and 75° angles of incidence. The thickness of the silane was obtained by fitting the ellipsometry data using a 3-layer model with a 1 mm silicon layer, a 15 Å SiO_x layer, and a "Cauchy" layer with a refractive index of 1.45. We measured the static water contact angle under atmospheric conditions at 40-60% humidity using a contact angle goniometer (Model 100-00, Ramé Hart). We used deionized water (DIW) in all experiments as the probing liquid. We deposited drops of DIW (3-5 µL in volume) from a syringe; we recorded the water contact angle (WCA) within 5 seconds after the drop deposition.

3.4 Results and Discussion

The kinetics of degrafting can be described by using a series of first-order rate equations (*cf.* **Equations (1)-(3)**) as described elsewhere.[26] These rate equations correspond to the cleaving of Si-O bonds in the system with α, β, and γ representing the fractions of species attached with one, two, and three Si-O bonds, respectively. The rate constant, k, characterizes the rate of breaking a single Si-O bond (either at the substrate or in the silane network).

$$\frac{d\gamma}{dt} = -k\gamma \qquad (1)$$

$$\frac{d\beta}{dt} = k\gamma - k\beta \qquad (2)$$

$$\frac{d\alpha}{dt} = k\beta - k\alpha \qquad (3)$$

The model fits experimental data by setting the fractional coverage of silanes equal to the summation of α, β and γ. Initial values of α, β and γ depend on the structure and connectivity of the silanes at the surface and can vary significantly among silanes and deposition conditions. Previously, we have employed this model to capture the general trends of a silane degrafting process by performing Monte Carlo (MC) simulations using a simplified 2D lattice model.[26] While these simulations described many of the features of the process, they could not fully depict the effects of in-plane connectivity of silanes and the influence of aggregates or "moguls" of silanes on a surface. Here we present more complete MC simulations that account for both effects. A one-dimensional model was used for a planar substrate with integer grid sites ($x \in [1,100]$, $y = 1$) representing binding domains on the surface; similarly, the silane species occupy grid sites ($x \in [1,100]$, $y = 2$). The x and y coordinates denote the coordinates parallel and perpendicular to the substrate, respectively. Bonds can connect silanes occupying adjacent grid sites or connect a binding domain on the surface and an adjacent silane.

For each MC step a bond is randomly selected from the total set of bond possibilities; if the bond exists, it can break with a certain probability, p (here we set p = 0.0675). If the bond breaks, the algorithm removes the bond from the existing set of bonds, and this process continues until all bonds are broken. We monitor the total number of species with a series of bonds connecting them to the surface during the process and evaluate the fractional coverage. We repeat the MC procedure 100 times and then calculate the average values of the fractional coverage, the number of silanes removed per degrafting event, and the number of moguls present on the surface, and their corresponding standard deviations. We use **Equations (1)-(3)** to model the simulation data.

Figure A-2-1 shows the results from simulations of mono, di, and tri-functional species with one surface bond per species. The model captures well the degrafting of mono-, di-, and tri-functional species, with only slight deviations for di- and tri-functional molecules as a result of the bond connectivity. The in-plane connectivity of the molecules allows for the removal of multiple species (*i.e.*, a cluster of molecules) from the surface during a single degrafting event, breaking a surface bond or an in-plane bond if a resulting structure has no connectivity to the surface. Higher α values and lower β and γ values indicate the removal of clusters of molecules.

Tri-functional silanes are unlikely to form a SAM with a large fraction of all bonds attached to the surface, relative to the number of in-plane bonds in the silane network.[29,30] The bulkiness of the silanes alkyl backbone limits the number of surface attachments due to the van der Waals diameter of the hydrocarbon chain (4.4 - 4.9 Å) being larger than the space allowed by the Si-O bonds formed from the condensation of neighboring silanes (2.9 - 3.2 Å).[31,32] Proposed silane structure models account for this steric hindrance by describing a SAM made up of mogul-like clusters of silanes.[30,33] In these models, the silane network mostly consists of in-plane siloxane linkages with a low density of surface bonds. If present, such structures greatly increase the degrafting rate, thus reducing the apparent delay reported previously, as the probability of removing large numbers of molecules at the same time would increase.[26] In the degrafting computer simulations, we have maintained 100 molecules on the surface while varying the number of surface bonds and retaining the number of in-plane crosslinks (*cf.* **Figure 3-1**). To simulate the presence of aggregates, we considered a combination of low (20:1 molecules to surface bonds) and high (5:1 molecules to surface bonds) density of surface bonds.

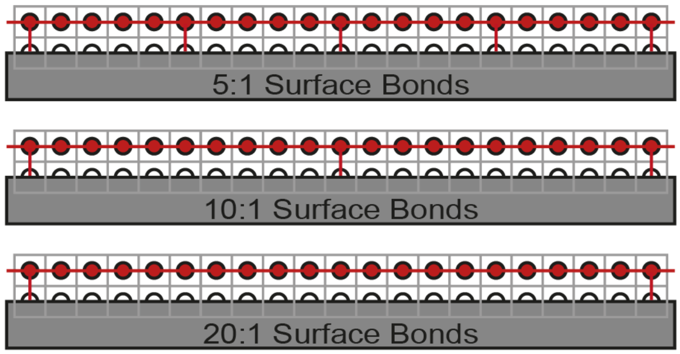

Figure 3-1. Schematic depicting the initial geometry of trifunctional molecules covalently attached to a substrate with varying ratios of molecules to surface bonds. The grey squares denote the lattice sites in the simulation box.

Figure 3-2 displays the results from the simulations of degrafting mogul-like clusters. The initial plateau in the degrafting profile shortens, and the rate, in which silanes degraft from the surface, increases as the number of surface attachments decreases. Every 250 Monte Carlo steps we bin the average number of silanes removed per degrafting event and calculate the number of distinct moguls present on the surface. Breaking of an in-plane bond leads to two possible scenarios. First, if the bond breaks between two surface attachments, the structure fragments into two distinct moguls. Second, if the bond breaks between a surface attachment and a dangling end, the silanes between the break and the dangling end are removed from the surface. Upon increasing the spacing between surface attachments, the maximum number of moguls present on the surface occurs at earlier times (*i.e.*, it shifts to a lower number of Monte Carlo steps), and this shift is mirrored in the number of silanes removed per degrafting event and with the size of the plateau region during the initial stages of degrafting. Consideration of the amount and length of dangling ends present on the surface at any step can explain the change in degrafting profiles. For small spacing between surface attachments, the length of the dangling ends formed will be small, and the probability of generating two distinct moguls will be high when compared to that of silane removal. However, for large spacing between surface attachments, the length of the dangling ends will be greater, and the probability of generating two distinct moguls will be lower when compared to that of silane removal. When examining a more realistic surface that may contain aggregates or disordered multilayers (*cf.* **Figure 3-2d**), we detect characteristics of both small and large spacing between surface attachments. These realistic surfaces initially exhibit a rapid decrease in the fractional coverage, due to large moguls favoring the removal of multiple silanes at once, followed by a plateau in degrafting caused by regions with a robust bonding network.

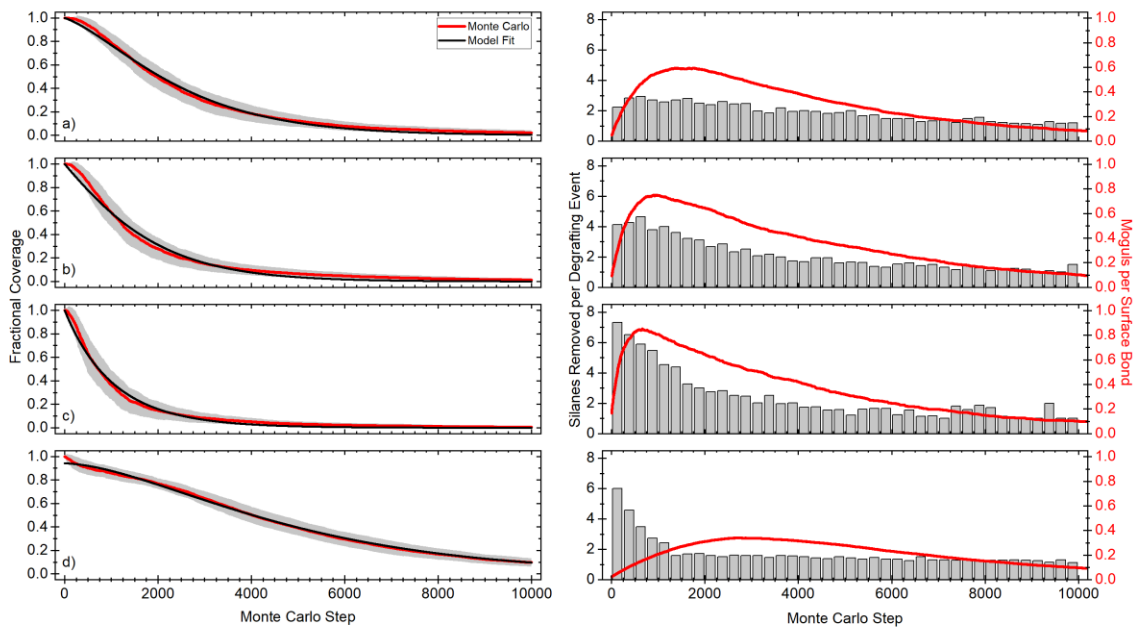

Figure 3-2. Fractional coverage of 100 molecules with a) 5:1, b) 10:1, c) 20:1 molecule to surface (M:S) bond ratio, and d) 80 molecules with a 1:1 M:S ratio and 20 molecules with an M:S 20:1 ratio as a function of the number of MC steps. The red line and the grey shaded area denote the average and standard deviation from the MC simulation, respectively. The black lines are best fits to Equations (1)-(3). The right panels show the number of silanes removed per degrafting event (left ordinate) and the number of moguls present on the surface (right ordinate) as a function of MC steps.

The silanes investigated in our study differ in the reactive head groups and the exposed chemical functionality (*cf.* **Figure 3-3**).

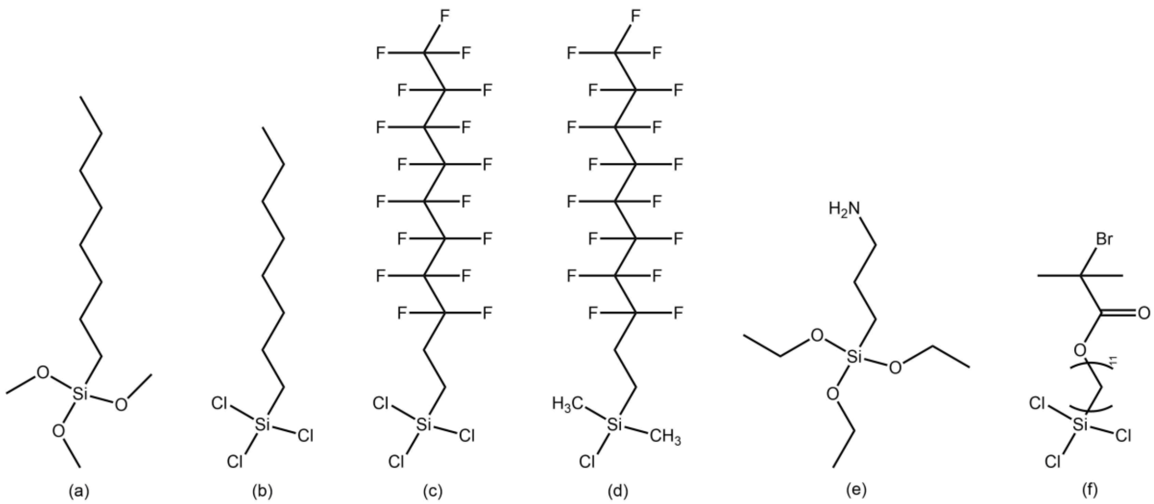

Figure 3-3. Self-assembled monolayers of a) *n*-octyltrimethoxysilane (OTMS), b) *n*-octyltrichlorosilane, c) heptadecafluoro-1,1,2,2-tetrahydrodecyltrichlorosilane (FTCS), d) heptadecafluoro-1,1,2,2-tetrahydrodecyldimethylchlorosilane (FDMCS), e) (3-aminopropyl)triethoxysilane, and f) (11-(2-bromo-2-methyl)propionyloxyundecyltrichlorosilane (eBMPUS) were deposited on UVO treated silicon substrates.

Table 3-1. Summary of the measured thicknesses, contact angles, and approximate roughness for the various silanes. See **Figure 3-3** for abbreviations.

Silane	**Thickness (nm)**	**Water contact angle (deg)**
OTMS	1.23 ± 0.06	106 ± 1
OTCS*	1.18 ± 0.28	106 ± 3
FTCS*	1.60 ± 0.06	112 ± 1
FDMCS*	0.95 ± 0.05	108 ± 1
APTES	1.10 ± 0.37	78 ± 2
eBMPUS	2.71 ± 0.33	83 ± 1

* Deposited from the vapor phase

The SAMs deposited for the OTMS, OTCS, FTCS, and FDMCS were all within 1 Å of the expected thickness; however, SAMs of APTES and eBMPUS were on average 4 Å thicker than expected, suggesting the presence of aggregates or multilayers on the surface. The water contact angles for all silanes studied were within reason for full coverage on a silica surface (*cf.* **Table 3-**

1). We calculated the initial fractional coverage (ϕ) of silanes on the silica surfaces for OTMS, OTCS, FTCS, FDMCS, and eBMPUS using the Cassie-Baxter equation (**Equation (4)**),[34] where the contact angles of the full coverage SAMs were approximated as 110 (for OTMS), 110 (OTCS), 115 (FTCS), 115 (FDMCS), and 83 (eBMPUS) degrees with a contact angle of bare silica taken as 5 degrees.

$$cos\,\theta = \phi_1\,cos\,\theta_1 + \phi_2\,cos\,\theta_2 \quad (4)$$

Variations in fractional coverage were achieved on the surface by degrafting silane SAMs in a 0.1 M TBAF solution as a function of time. The silane-coated substrates were lowered vertically into the solution in a stepwise fashion (5 mm increments, each for a different TBAF exposure time) to allow for measurements in uniform regions. This method produced eight 5.0 mm x 7.5 mm regions on the sample surface that had been exposed to the TBAF solution for varying times. Previously, we have investigated the degrafting kinetics of alkyltrichlorosilanes, including *n*-octyltrichlorosilane (OTCS).[26] The structure of OTCS and OTMS varies only in the chemistry of their binding domain. Alkoxysilanes hydrolyze less readily than chlorosilanes and typically pack less densely on the surface. However, with appropriate deposition conditions, SAMs with high coverage can be produced. **Figure 3-4** shows the comparison of the degrafting kinetics of OTCS and OTMS layers. The OTMS SAM starts at a slightly lower fractional coverage due to the bulkiness of the alkoxy groups present before hydrolysis. We observe a slight, initial decrease of ~5% in fractional coverage in both OTCS and OTMS. Following this initial decrease, the degrafting rate is similar for both SAMs (*cf.* **Table A-3-1**). The similarities in degrafting profiles suggest that the structure of OTCS and OTMS is analogous and that the kinetic of degrafting does not possess a strong dependence on the chemistry of the binding domain.

Silanes deposited from the solution tend to aggregate in the parent solution, which may result in non-uniform surface coverage and unstable SAMs. Duchet *et al.* have shown that the deposition of alkylsilanes on silica depends on the solvent used.[35] Lower grafting density of chlorosilanes results from deposition in toluene when compared to deposition in carbon tetrachloride. Lower coverage resulted likely from the presence of the more polar toluene displacing surface-bound water and leading to the decreased accessibility of surface hydroxyls while promoting condensation in the bulk solution. Carbon tetrachloride is less polar than water, thus leading to better solubility of the alkyl chain and less displacement of the surface-bound water.

By choosing the appropriate solvent deposition conditions, the grafting density of silanes on the surface can be comparable to or better than that of vapor phase deposition approaches.

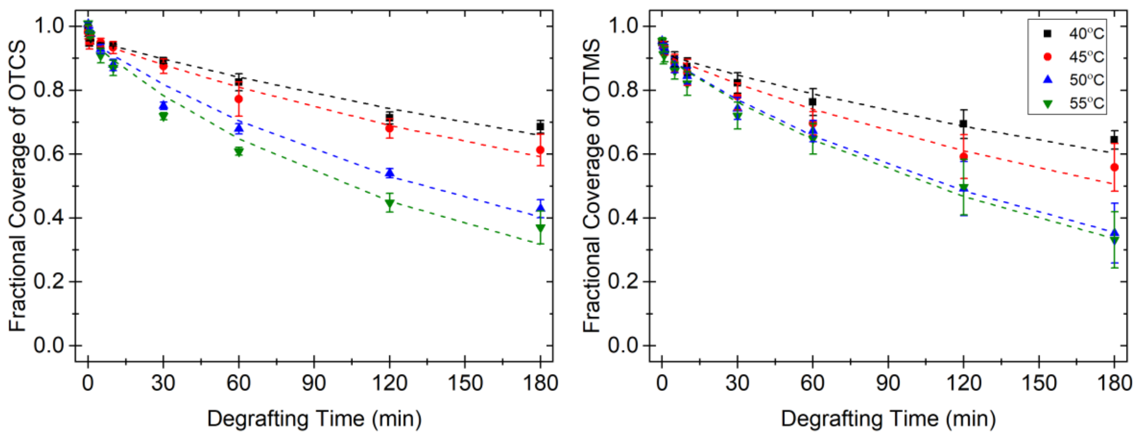

Figure 3-4. Fractional coverage profiles of OTCS[26] and OTMS (deposited from hexanes) from degrafting in 0.1 M TBAF in DMA as a function of temperature and incubation time. Dashed lines show best fits to Equations (1)-(3).

Little (if any) work has compared the silane SAM structure between the vapor and solution deposition approaches. By comparing degrafting profiles of alkylsilanes deposited from hexanes and the vapor phase, we provide insight into the effect of deposition medium of a given silane. The OTCS deposited from the vapor phase in this work exhibits a slightly lower WCA and thickness than our previous work when deposited from hexanes,[26] but are still within an acceptable range for a monolayer coverage. **Figure 3-5** shows the degrafting profiles of vapor-deposited OTCS. We observe a small, sharp initial decrease in fractional coverage, comparable to the hexane deposited OTCS. However, we detect no plateau region, even at low temperatures, and the overall degrafting rate is faster. These differences and fits from the model (*cf.* **Table A-3-2**) suggest that while the grafting density of silanes initially is similar, the network of siloxane bonds at the surface (on average fewer bonds per silane molecule) prepared from the vapor phase is less robust than that formed from hexane solutions.

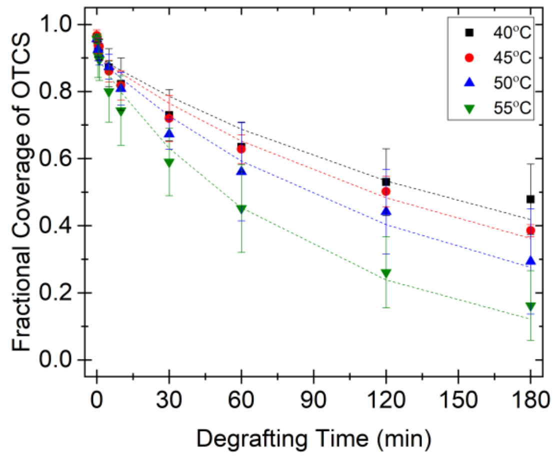

Figure 3-5. Fractional coverage profiles of OTCS (deposited from the vapor phase) from degrafting in 0.1 M TBAF in DMA as a function of temperature and incubation time. Dashed lines show best fits to Equations (1)-(3).

Fluorinated silanes are commonly used to generate non-wetting, low friction surfaces with high thermal stability. These silanes form well-ordered SAMs when deposited from the vapor phase.[36] This process limits the deposition of aggregates formed in the initial silane solution due to their lower volatility. Minimal multilayer formation occurs due to the larger van der Waals diameter of the fluorinated backbone (5.7 Å) compared to hydrocarbon backbones (4.4 Å). This larger van der Waals diameter is a result of the helical conformation of fluorocarbon chains [37] and strongly influences the packing density of the SAM. At this lower packing density, less condensation occurs between neighboring silanes, leading to fewer in-plane network bonds, thus favoring condensation with surface silanol groups. **Figure 3-6** plots the degrafting profiles for FTCS and FDMCS. We detect a distinct initial plateau in the degrafting profile of FTCS, with it being less distinguishable at higher temperatures as the degrafting rate increases. The degrafting model captures the kinetics of the FTCS well as there are few aggregates or multilayers on the surface that would lead to sharp decreases in fractional coverage. Degrafting of the FDMCS follows a single exponential decay as FDMCS attaches to the substrate via a single bond, leading to a less robust SAM, as compared to FTCS, which can form in-plane siloxane networks.

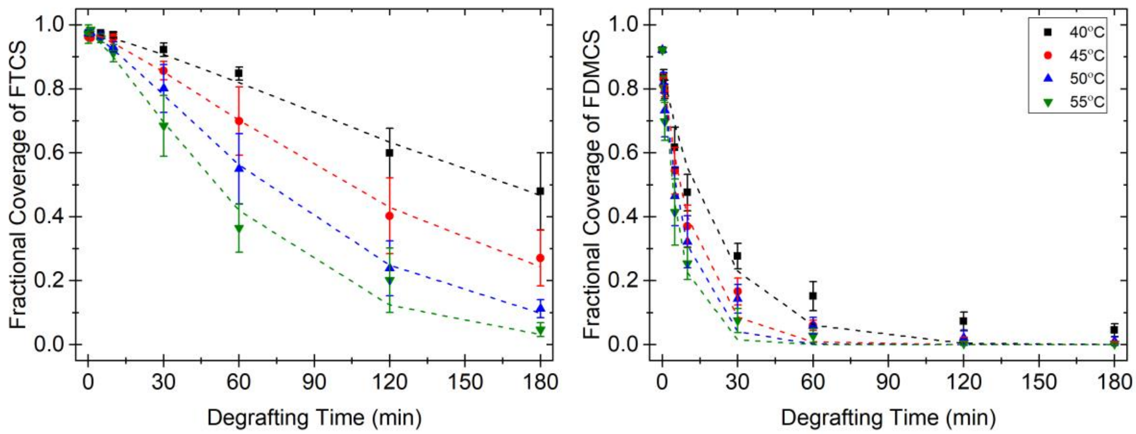

Figure 3-6. Fractional coverage profiles of FTCS and FDMCS from degrafting in 0.1 M TBAF in DMA as a function of temperature and incubation time. Dashed lines show best fits to Equations (1)-(3).

Amine-functionalized silanes are used frequently for biological applications and for attaching species to the surface covalently or by charge-charge interactions. Despite their heavy use during the past few decades, the best procedure leading to the controlled deposition of such molecules, to form a uniform and stable SAM, is still under debate.[38,39] The difficulty in depositing amine-functionalized silanes arises from their amphiphilic nature that allows for electrostatic interactions between the amine functionality and surface hydroxyls and often gives rise to the formation of aggregates in solution and multilayers on surfaces. One of the most commonly employed deposition methods of APTES uses anhydrous toluene as the solvent, followed by an annealing step in a closed container; this is the method we used for our investigation. The non-uniformity of the APTES SAMs resulted in the largest variance observed in the degrafting profiles (*cf.* **Figure 3-7**). We detect an initial, large decrease in surface coverage due to the removal of aggregated structures and potential catalysis of the Si-O bond cleavage by the amine functionality.[40,41]

Brominated silanes, such as eBMPUS, are commonly used as initiators to grow polymer brushes from the surface by atom transfer radical polymerization. Similar to OTCS and OTMS, the long alkyl backbone of eBMPUS allows for highly ordered SAMs to be deposited on the surface when aggregation in bulk solution is limited by having a low water content. As a result, the degrafting profiles for eBMPUS are comparable to alkyl silanes (*cf.* **Figure 3-8**) with only a small sharp decrease observed initially. The eBMPUS degrafts less during the period studied.

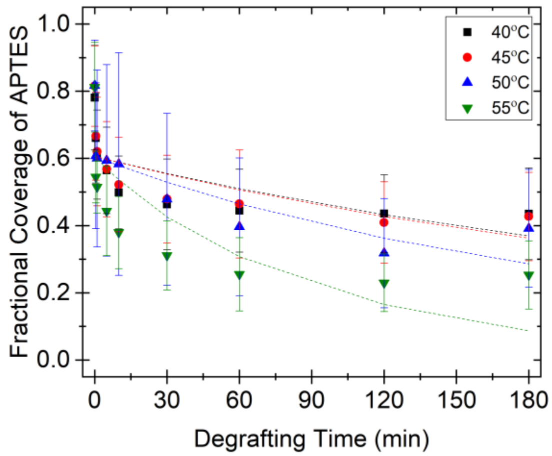

Figure 3-7. Fractional coverage profiles of APTES (deposited from anhydrous toluene) from degrafting in 0.1 M TBAF in DMA as a function of temperature and incubation time. Dashed lines show best fits to Equations (1)-(3).

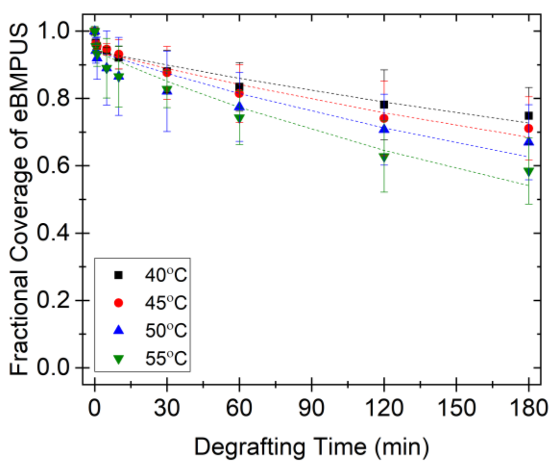

Figure 3-8. Fractional coverage profiles of eBMPUS from degrafting in 0.1 M TBAF in DMA as a function of temperature and incubation time. Dashed lines show best fits to Equations (1)-(3).

Previous work demonstrated that degrafting polymer brushes with TBAF can be used to determine the molecular weight of polymer brushes (in conjunction with size exclusion chromatography)[42] and can be used to pattern surfaces.[27] The rate of degrafting of the brushes from the surface is not critical for these applications. However, the stability of polymer brushes is more complex than that of small molecule SAMs due to their increased diffusion resistance and swelling behavior. As the thickness of the polymer brush layer increases, the diffusion of species to the surface occurs on a longer time scale. This increased diffusion time can result in more stable brush layers. For polymer brush layers, it is important to consider the effect of solvent quality. When placed in a good solvent, the swelling allows for faster diffusion of species through the layer and increases the tension on the bonds in the brush and at the surface. This increase in tension is more significant at high grafting densities and decreases the bond lifetime of the surface linkage,[43] making it more susceptible to cleavage.[44] To gain an insight into the role of these factors on brush stability, we have examined the grafting density of brushes grown after degrafting of eBMPUS initiator layers and compared this to the grafting density of degrafted PMMA brushes (*cf.* **Figure 3-9**).

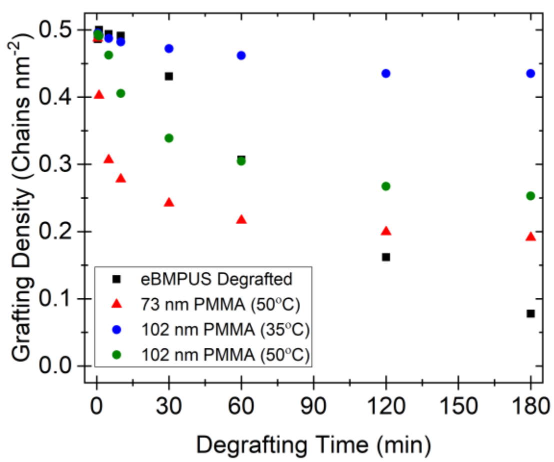

Figure 3-9. Grafting density of PMMA brushes grown from eBMPUS gradient substrates degrafted at 50°C (black squares) and homogeneous PMMA brushes degrafted at 35 and 50°C.

Similar to the degrafting profile eBMPUS SAMs, PMMA brushes grown from degrafted eBMPUS layers exhibit an initial distinguishable plateau in grafting density followed by a gradual decrease in the grafting density. In contrast, the degrafting of PMMA brushes, grown from a homogeneous initiator SAM, results in an initial sharp decrease in grafting density followed by a rapid decrease in degrafting rate when degrafted at 50°C. Similarly, PMMA brushes degrafted at 35°C do not exhibit an initial delay in degrafting. As the eBMPUS initiator layers were deposited by the same method for each of these cases, we conclude that the surface structure is similar to that of alkane-based silanes. Thus, the differences in profiles arise from the presence of the polymer brush layer. As the thickness of the brush layer increases the diffusion time of the TBAF to the surface increases, leading to an overall decrease in the degrafting rate. However, this does not account for the rapid removal of polymer brushes from the surface and the change in the degrafting rate. We propose that the rapid degrafting arises from the increased tension caused by the swelling of the polymer brush in a good solvent. This increased tension may result in more rapid cleavage of the Si-O bonds at the surface by TBAF but will have less of an effect as degrafting proceeds due to the decreased grafting density.

3.5 Conclusions

We have investigated the structure of silane SAMs on the surface by probing their degrafting kinetics in a solution of TBAF. We detect little difference in the kinetics of the degrafting of OTMS when compared to OTCS despite its slower rate of hydrolysis and condensation with the surface. This result implies that the siloxane networks formed with these silanes are similar, most likely due to their alignment on the surface by van der Waals forces between neighboring silane molecules before condensation. When deposited from the vapor phase, alkylsilanes degraft faster than those deposited from solution, suggesting a lower crosslink density among neighboring silanes due to the limited condensation of silanes before attachment. The degrafting profiles of the fluorinated silanes examined show a significant plateau at short degrafting times, with no sharp decrease initially for the FTCS as has been previously observed for tri-functional alkylsilanes. We propose that the lack of a sharp decrease in the degrafting profile is a result of the bulkiness of the fluorinated backbone preventing significant aggregation and limiting the size of the mogul-like structures formed on the surface.[23] Degrafting of a silane-based initiator for polymerization resulted in a similar degrafting profile to alkyl silanes and the subsequent growth of polymer brushes resulted in a comparable profile in grafting density. However, when polymer brushes were grown from a homogeneous initiator layer and then degrafted, the grafting density decreased sharply during the initial stages of degrafting due to the increased tension on the surface linkages caused by swelling of the brushes despite the increased diffusion barrier for the TBAF degrafting agent.

3.6 References

(1) Yanker, D. M.; Maurer, J. A. Direct Printing of Trichlorosilanes on Glass for Selective Protein Adsorption and Cell Growth. *Mol. Biosyst.* **2008**, *4*, 502–504.

(2) Genzer, J.; Bhat, R. R. Surface-Bound Soft Matter Gradients. *Langmuir* **2008**, *24*, 2294–2317.

(3) Ulman, A. Formation and Structure of Self-Assembled Monolayers. *Chem. Rev.* **1996**, *96*, 1533–1554.

(4) Takahara, A.; Kojio, K.; Ge, S.; Kajiyama, T. Scanning Force Microscopic Studies of Surface Structure and Protein Adsorption Behavior of Organosilane Monolayers. *J. Vac. Sci. Technol. A Vacuum, Surfaces, Film.* **2002**, *14*, 1747–1754.

(5) Roberson, S. V.; Fahey, A. J.; Sehgal, A.; Karim, A. Multifunctional ToF-SIMS: Combinatorial Mapping of Gradient Energy Substrates. *Appl. Surf. Sci.* **2002**, *200*, 150–164.

(6) Kennedy, S. B.; Washburn, N. R.; Simon Jr., C. G.; Amis, E. J. Combinatorial Screen of the Effect of Surface Energy on Fibronectin-Mediated Osteoblast Adhesion, Spreading and Proliferation. *Biomaterials* **2006**, *27*, 3817–3824.

(7) Vericat, C.; Vela, M. E.; Benitez, G.; Carro, P.; Salvarezza, R. C. Self-Assembled Monolayers of Thiols and Dithiols on Gold: New Challenges for a Well-Known System. *Chem. Soc. Rev.* **2010**, *39*, 1805–1834.

(8) Schreiber, F. Structure and Growth of Self-Assembling Monolayers. *Prog. Surf. Sci.* **2000**, *65*, 151–257.

(9) Iimura, K.; Nakajima, Y.; Kato, T. A Study on Structures and Formation Mechanisms of Self-Assembled Monolayers of n-Alkyltrichlorosilanes Using Infrared Spectroscopy and Atomic Force Microscopy. *Thin Solid Films* **2000**, *379*, 230–239.

(10) Popat, K. C.; Johnson, R. W.; Desai, T. A. Characterization of Vapor Deposited Thin Silane Films on Silicon Substrates for Biomedical Microdevices. *Surf. Coatings Technol.* **2002**, *154*, 253–261.

(11) Wang, A.; Tang, H.; Cao, T.; Salley, S. O.; Ng, K. Y. S. In Vitro Stability Study of Organosilane Self-Assemble Monolayers and Multilayers. *J. Colloid Interface Sci.* **2005**, *291*, 438–447.

(12) Wei, M.; Bowman, R. S.; Wilson, J. L.; Morrow, N. R. Wetting Properties and Stability of Silane-Treated Glass Exposed to Water, Air, and Oil. *J. Colloid Interface Sci.* **1993**, *157*, 154–159.

(13) Chandekar, A.; Sengupta, S. K.; Whitten, J. E. Thermal Stability of Thiol and Silane Monolayers: A Comparative Study. *Appl. Surf. Sci.* **2010**, *256*, 2742–2749.

(14) Zhang, F.; Sautter, K.; Larsen, A. M.; Findley, D. A.; Davis, R. C.; Samha, H.; Linford, M. R. Chemical Vapor Deposition of Three Aminosilanes on Silicon Dioxide: Surface Characterization, Stability, Effects of Silane Concentration, and Cyanine Dye Adsorption. *Langmuir* **2010**, *26*, 14648–14654.

(15) Marcinko, S.; Fadeev, A. Y. Hydrolytic Stability of Organic Monolayers Supported on TiO2 and ZrO2. *Langmuir* **2004**, *20*, 2270–2273.

(16) Pujari, S. P.; Scheres, L.; Marcelis, A. T. M.; Zuilhof, H. Covalent Surface Modification of Oxide Surfaces. *Angew. Chemie - Int. Ed.* **2014**, *53*, 6322–6356.

(17) Iwasa, J.; Kumazawa, K.; Aoyama, K.; Suzuki, H.; Norimoto, S.; Shimoaka, T.; Hasegawa, T. In Situ Observation of a Self-Assembled Monolayer Formation of Octadecyltrimethoxysilane on a Silicon Oxide Surface Using a High-Speed Atomic Force Microscope. *J. Phys. Chem. C* **2016**, *120*, 2807–2813.

(18) Choi, S. H.; Newby, B. M. Z. Micrometer-Scaled Gradient Surfaces Generated Using Contact Printing of Octadecyltrichlorosilane. *Langmuir* **2003**, *19*, 7427–7435.

(19) Li, S.; Zheng, Y.; Chen, C. AFM Investigation of Effect of Absorbed Water Layer Structure on Growth Mechanism of Octadecyltrichlorosilane Self-Assembled Monolayer on Oxidized Silicon. *J. Chem. Phys.* **2016**, *144*, 244709.

(20) Fang, J.; Knobler, C. M. Control of Density in Self-Assembled Organosilane Monolayers by Langmuir-Blodgett Deposition. *J. Phys. Chem.* **1995**, *99*, 10425–10429.

(21) Bierbaum, K.; Grunze, M.; Baski, A. A.; Chi, L. F.; Schrepp, W.; Fuchs, H. Growth of Self-Assembled n-Alkyltrichlorosilane Films on Si(100) Investigated by Atomic Force Microscopy. *Langmuir* **1995**, *11*, 2143–2150.

(22) Smith, M. B.; Efimenko, K.; Fischer, D. A.; Lappi, S. E.; Kilpatrick, P. K.; Genzer, J. Study of the Packing Density and Molecular Orientation of Bimolecular Self-Assembled Monolayers of Aromatic and Aliphatic Organosilanes on Silica. *Langmuir* **2007**, *23*, 673–683.

(23) Genzer, J.; Efimenko, K.; Fischer, D. A. Molecular Orientation and Grafting Density in Semifluorinated Self-Assembled Monolayers of Mono-, Di-, and Trichloro Silanes on Silica Substrates. *Langmuir* **2002**, *18*, 9307–9311.

(24) Booth, B. D.; Vilt, S. G.; Lewis, J. B.; Rivera, J. L.; Buehler, E. A.; McCabe, C.; Jennings, G. K. Tribological Durability of Silane Monolayers on Silicon. *Langmuir* **2011**, *27*, 5909–5917.

(25) Booth, B. D.; Martin, N. J.; Buehler, E. A.; McCabe, C.; Jennings, G. K. Tribological Characterization of Gradient Monolayer Films from Trichlorosilanes on Silicon. *Colloids Surfaces A Physicochem. Eng. Asp.* **2012**, *412*, 57–63.

(26) Miles, J.; Schlenker, S.; Ko, Y.; Patil, R.; Rao, B. M.; Genzer, J. Design and Fabrication of Wettability Gradients with Tunable Profiles through Degrafting Organosilane Layers from Silica Surfaces by Tetrabutylammonium Fluoride. *Langmuir* **2017**, *33*, 14556–14564.

(27) Patil, R.; Kiserow, D.; Genzer, J. Creating Surface Patterns of Polymer Brushes by Degrafting via Tetrabutyl Ammonium Fluoride. *RSC Adv.* **2015**, *5*, 86120–86125.

(28) Matyjaszewski, K.; Miller, P. J.; Shukla, N.; Immaraporn, B.; Gelman, A.; Luokala, B. B.; Siclovan, T. M.; Kickelbick, G.; Vallant, T.; Hoffmann, H.; Pakula, T. Polymers at Interfaces: Using Atom Transfer Radical Polymerization in the Controlled Growth of Homopolymers and Block Copolymers from Silicon Surfaces in the Absence of Untethered Sacrificial Initiator. *Macromolecules* **1999**, *32*, 8716–8724.

(29) Stevens, M. J. Thoughts on the Structure of Alkylsilane Monolayers. *Langmuir* **1999**, *15*, 2773–2778.

(30) Naik, V. V.; Crobu, M.; Venkataraman, N. V.; Spencer, N. D. Multiple Transmission-Reflection IR Spectroscopy Shows That Surface Hydroxyls Play Only a Minor Role in Alkylsilane Monolayer Formation on Silica. *J. Phys. Chem. Lett.* **2013**, *4*, 2745–2751.

(31) Onclin, S.; Ravoo, B. J.; Reinhoudt, D. N. Engineering Silicon Oxide Surfaces Using Self-Assembled Monolayers. *Angew. Chemie Int. Ed.* **2005**, *44*, 6282–6304.

(32) Naik, V. V.; Vasudevan, S. Effect of Alkyl Chain Arrangement on Conformation and Dynamics in a Surfactant Intercalated Layered Double Hydroxide: Spectroscopic Measurements and MD Simulations. *J. Phys. Chem. C* **2011**, *115*, 8221–8232.

(33) Naik, V. V.; Städler, R.; Spencer, N. D. Effect of Leaving Group on the Structures of Alkylsilane SAMs. *Langmuir* **2014**, *30*, 14824–14831.

(34) Cassie, A. B. D.; Baxter, S. Wettability of Porous Surfaces. *Trans. Faraday Soc.* **1944**, *40*, 546–551.

(35) Duchet, J.; Chabert, B.; Chapel, J. P.; Gérard, J. F.; Chovelon, J. M.; Jaffrezic-Renault, N. Influence of the Deposition Process on the Structure of Grafted Alkylsilane Layers. *Langmuir* **1997**, *13*, 2271–2278.

(36) Genzer, J.; Efimenko, K.; Fischer, D. A. Formation Mechanisms and Properties of Semifluorinated Molecular Gradients on Silica Surfaces. *Langmuir* **2006**, *22*, 8532–8541.

(37) Bunn, C. W.; Howells, E. R. Structures of Molecules and Crystals of Fluorocarbons. *Nature* **1954**, *174*, 549–551.

(38) Yadav, A. R.; Sriram, R.; Carter, J. A.; Miller, B. L. Comparative Study of Solution–Phase and Vapor–Phase Deposition of Aminosilanes on Silicon Dioxide Surfaces. *Mater. Sci. Eng. C* **2014**, *35*, 283–290.

(39) Pasternack, R. M.; Amy, S. R.; Chabal, Y. J. Attachment of 3-(Aminopropyl)Triethoxysilane on Silicon Oxide Surfaces: Dependence on Solution Temperature. *Langmuir* **2008**, *24*, 12963–12971.

(40) Smith, E. A.; Chen, W. How To Prevent the Loss of Surface Functionality Derived from Aminosilanes. *Langmuir* **2008**, *24*, 12405–12409.

(41) Aissaoui, N.; Bergaoui, L.; Landoulsi, J.; Lambert, J.-F.; Boujday, S. Silane Layers on Silicon Surfaces: Mechanism of Interaction, Stability, and Influence on Protein Adsorption. *Langmuir* **2012**, *28*, 656–665.

(42) Patil, R. R.; Turgman-Cohen, S.; Šrogl, J.; Kiserow, D.; Genzer, J. Direct Measurement of Molecular Weight and Grafting Density by Controlled and Quantitative Degrafting of Surface-Anchored Poly(Methyl Methacrylate). *ACS Macro Lett.* **2015**, *4*, 251–254.

(43) Sheiko, S. S.; Panyukov, S.; Rubinstein, M. Bond Tension in Tethered Macromolecules. *Macromolecules* **2011**, *44*, 4520–4529.

(44) Wang, J.; Klok, H.-A. Swelling-Induced Chain Stretching Enhances Hydrolytic Degrafting of Hydrophobic Polymer Brushes in Organic Media. *Angew. Chemie Int. Ed.* **2019**, *58*, 9989–9993.

Chapter 4: Covalent Attachment of Elastin-like Polypeptides to Silica Surfaces

4.1 Introduction

Non-specific protein adsorption is not a well-understood phenomenon, despite extensive research. Some of the factors that influence protein adsorption include solvent-protein interactions, solvent-surface interactions, and surface-protein interactions. Surface hydrophobicity plays a significant role in the adsorption of species.[1] Many surfaces possess a hydrophobic character which can lead to the simultaneous dehydration of the hydrophobic domains of a species in solution, resulting in energetically favorable adsorption. Further, when the protein contains a significant amount of hydrophobic amino acids (i.e., alanine, valine, leucine, isoleucine, phenylalanine, tryptophan, and methionine), the ability for it to adsorb onto hydrophobic surfaces increases. The driving force for adsorption is the decreased thermodynamic stability of the proteins in aqueous solutions accompanied by their tendency to populate surfaces. The stability of proteins on the surface after adsorption is not strongly affected by the hydrophobicity of the surface when a species with a more favorable surface interaction is present.[2] The hydrophobicity of the surface is not the only factor that has a large influence on surface-protein interactions. Other factors include van der Waals forces, electrostatic interactions, and hydrogen bonding.[3] However, adjusting temperature or ionic strength shields these factors to some extent.

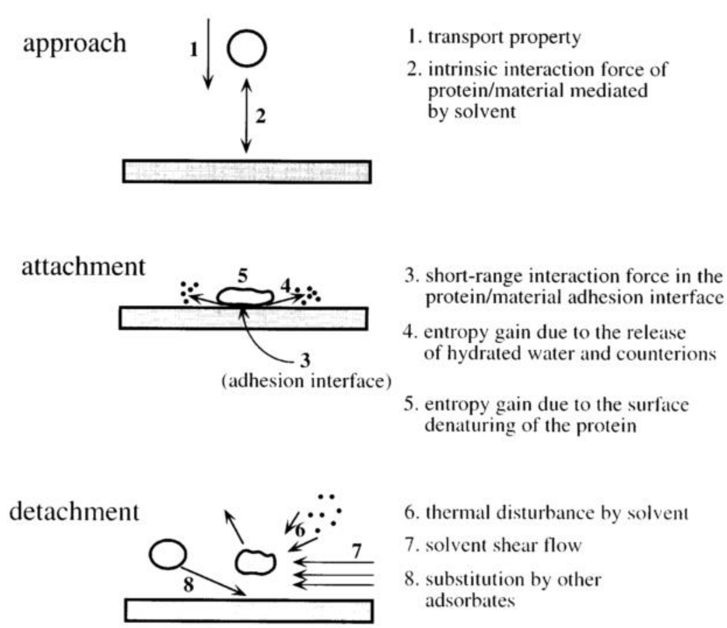

Figure 4-1. Typical factors important for protein adsorption.[3]

Covalent grafting of polymers onto surfaces is a relatively mature area. Studies examining the interactions of polypeptides and proteins with surfaces focus mainly on physical adsorption, however.[4,5] Modifying surfaces by employing physical adsorption alone suffers from many drawbacks such as low stability and non-uniform coverage of the coatings. However, covalent linking is not possible on all substrates, and the non-site specific interactions with the surface may still have significant, undesired effects on the assembly of proteins onto surfaces and their function.

Site-specific adsorption of proteins onto surfaces typically uses carbodiimide chemistry to bind primary amines to carboxyl groups on the surface. Often 1-ethyl-3-(3-dimethylaminopropyl)carbodiimide (EDC) reacts with the carboxyl groups to form an amine-reactive intermediate. The presence of n-hydroxysuccinimide (NHS) stabilizes the intermediate formed by EDC. This method is efficient for the binding of amine groups to the surface, but the chemistry may result in undesired effects on more reactive surfaces or proteins. Functionalizing a surface with anhydride groups may allow for site-specific adsorption of proteins onto the surface through cyclic anhydride reactions without the addition of other species. These reactions involve two steps. The first reversible step is the anhydride ring opening to form amic acid. The second step is the ring closure and water elimination. Anhydrides can undergo competing hydrolysis reactions which are fully reversible but result in a reduced reaction rate; typically the system can be driven to the closed anhydride by annealing at 120°C.[6]

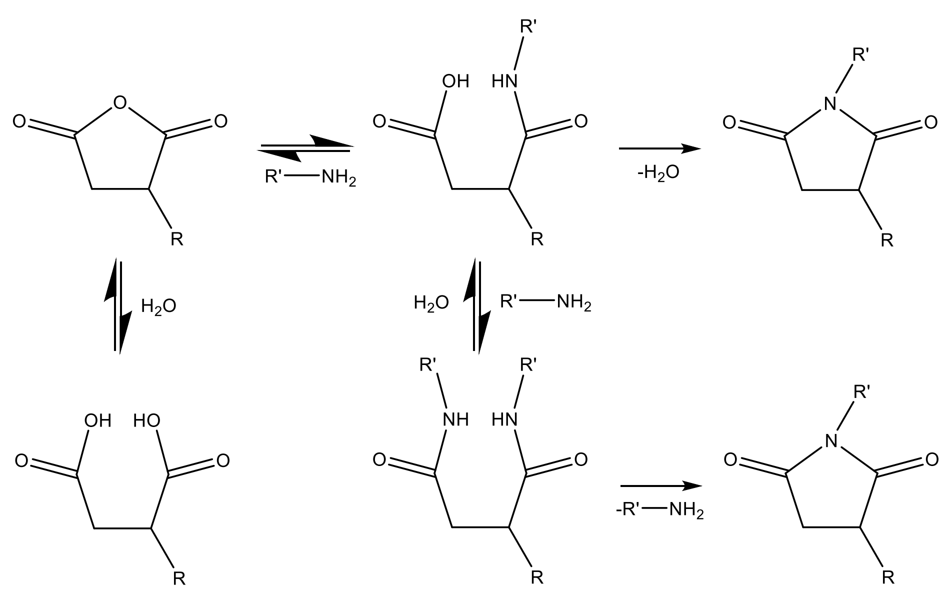

Figure 4-2. Reaction pathway of succinic anhydride with primary amines.

Additionally, functionalizing a surface with epoxides can allow for covalent attachment of amines. Epoxide ring-opening reactions with amines proceed by an S_N2 mechanism to generate β-amino alcohol.[7] These reactions are typically acid- or base-catalyzed, and these conditions can result in undesired modification of the surfaces' chemical and physical properties. Water is also able to react with epoxides via a nucleophilic addition, leading to competition for reactive sites between the desired amine and the solvent. However, an efficient reaction of epoxides with amines in water, at neutral pH values, is possible due to the high nucleophilic strength of amines relative to water.[8]

Recently, there has been a growing interest in the development of polymers for surface-mediated drug delivery or regenerative medicine in which the response of a "smart" material can trigger cellular adhesion and release from a surface.[9–11] Studies on stimuli-responsive surfaces have mostly employed copolymer brushes tethered to a substrate. Interactions with the substrate and free surfaces influence the film morphology and nanostructure orientation.[12] The proliferation of 'click' reactions, such as the anhydride-amine reaction, has provided highly efficient orthogonal coupling chemistries, which have allowed for the fabrication of well-defined copolymers and their attachment onto surfaces.[13] Of recent interest is the use of smart biopolymers for these applications to enhance biocompatibility and function, with one of the most promising candidates being an elastin-like polypeptide (ELP).

Elastin is a structural extracellular matrix protein that is present in all vertebrate connective tissue and provides elasticity and resilience to tissues. Recombinantly synthesized elastin-like polypeptides consist of the repeat unit of amino acids (Val-Pro-Gly-Xaa-Gly). The well-defined sequence of amino acids in the structure of ELPs results in high biocompatibility and their ability to undergo a temperature-dependent, reversible self-aggregation (an inverse phase transition).[14] When below the transition temperature (T_t), the ELPs are soluble in solution, and as the temperature increases past the transition temperature, they are no longer soluble and form aggregates.[15] The T_t is a function of the solvent composition, ionic strength, ELP concentration, chain length, and the guest residues present.[16–19] Further, the hydrophobicity of the amino acid in the Xaa position has a strong influence on the T_t of the ELP, with more hydrophobic amino acids exhibiting a lower T_t and its increase with increasing polarity.[15] The change in T_t is due to hydrophobic molecules forming assemblies which minimize the organic-water interface.[4]

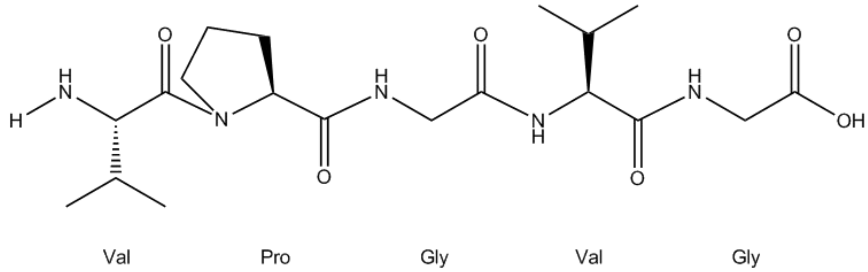

Figure 4-3. An elastin-like polypeptide repeat unit with a sequence of VPGVG.

The elastin blocks, which contain hydrophobic amino acids in the Xaa position, typically valine, have a propensity to adopt random coil, type II β-turn, or β-strand conformations. A conformational transition from random coils to repetitive type II β-turns and β-strands occurs at the T_t.[20–22] Conformational changes in ELPs are most likely a consequence of hydrophobic interactions that are driven by positive entropies of dehydration.[23] When a charged amino acid is in the Xaa position, the blocks maintain a random coil formation over a physiologic temperature range. ELPs with two distinct blocks (diblock ELPs) exhibit two transition temperatures. These varying transition temperatures are a result of the hydrophobicity of each block and cause the diblock ELP to pass through a micellar stage before completely collapsing.[24,25] Non-covalent interactions stabilize thermodynamically different morphologies through non-covalent interactions; however, varying the ELP sequence and solution properties can alter their reversible changes in morphology. The morphology changes are not known to be irreversible without the addition of a cross-linker or the use of cosolvents.[26]

Costa *et al.* have shown that adsorption of ELPs, featuring a cell adhesion sequence and with most guest residues being lysine, onto glass substrates (WCA of approximately 30 degrees) exhibits a large variation in wettability when measured below and above their T_t.[27] The T_t of the ELP when adsorbed onto the surface increased from a bulk value of 32 °C to close to 50 °C. The measured water contact angles at 25 °C and 50 °C were reported to be ~70 and ~5° respectively. Reordering of the ELPs on the surface, exposing hydrophilic amino acids to the solution, and an increase in surface roughness is believed to cause this significant change in wettability.

Di-block ELPs adsorbed on hydroxyl functionalized silica below their transition temperatures, with and without a silica binding domain, exhibit stimuli-responsive behavior upon heating.[28] Upon heating the contact angle of captive air bubbles on these ELP functionalized surfaces increased from 30° to 40 and 50° at the two distinct bulk transition temperatures of the diblock ELP. ELP di-blocks deposited above one of their transition temperatures, in a micellar state, exhibit no stimuli-responsive behavior.

Recently, Costa *et al.* has investigated the adsorption of hydrophobic and amphiphilic ELPs onto SAMs of alkanethiols on gold with terminal groups of -CH_3, -OH, -COOH, and -NH_2.[29] Hydrophobic ELPs adsorbed with a higher affinity to all surfaces studied than the amphiphilic ELP and showed little to no mass loss during rinsing of the substrate. Adsorption of the amphiphilic ELP in a micellar state was rapid, suggesting that it is a kinetically driven process when compared to that of the hydrophobic ELP adsorbing by a thermodynamically controlled process involving rearrangement on the surface. Importantly, the desorption of these ELPs upon rinsing showed large differences, such that the hydrophobic ELP had relatively no change in the adsorbed amount and the amphiphilic ELP showed significant desorption. However, this desorption of the micellar amphiphilic ELPs was limited to the outer layer of micelles which weakly bonds to the more strongly bound aggregate layer that is dictated by ELP-SAM interactions.

In this work, we investigate the possibility of covalently attaching ELPs with various sequences to substrates using anhydride or epoxide coupling reactions. The non-site specific adsorption of ELPs to surfaces competes with covalent attachment and results in undesired morphology and inhibits the stimuli-responsive behavior of the ELP. Surfaces with both homogeneous and heterogeneous coverages of hydrophobic domains result in strong adsorption of ELPs with varying morphologies. Further, we discuss how the deposition of ELPs onto silane functionalized surfaces terminated by anhydride or epoxide groups results in similar film thicknesses as those of inert hydrophobic surfaces and show no stimuli-responsive behavior.

4.2 Methods

All chemicals were purchased from Sigma-Aldrich and used without further purification unless otherwise specified. Deionized water was obtained using Millipore Elix 3. Silicon wafers (p-doped, orientation <100>) were purchased from Silicon Valley Microelectronics. *n*-octyltrichlorosilane, *n*-octadecyltrichlorosilane, (3-triethoxysilyl)propylsuccinic anhydride, and (3-glycidoxypropyl)trimethoxysilane were purchased from Gelest. All elastin-like peptides were fabricated by recombinant synthesis and purified by inverse transition cycling by the Chilkoti group at Duke University.[30]

4.2.1 Elastin-like Polypeptide Depositions

Elastin-like polypeptide solutions were prepared by suspending ELPs in either phosphate-buffered saline (PBS), pH 7.4, or dimethylacetamide (DMA). An appropriate amount of the desired ELP was dissolved in 5 mL of filtered PBS or DMA. This solution was this stirred with a vortex mixer for 1 min and centrifuged at 13,000 rpm. This mixing procedure was repeated three times before the solution being divided into 1 mL aliquots. The aliquots were then frozen until required for use, where they were thawed at room temperature and diluted to a total solution volume of 10 mL with the appropriate solvent to achieve a final concentration of 25 µM. ELPs were deposited onto substrates by first equilibrating the ELP solution at the desired temperature in an oil bath with light stirring followed by incubation of the substrate for 12 hours. The substrate was then removed, sonicated in DI water for 30 minutes, and dried under a stream of nitrogen to remove any unbound ELPs from the surface.

4.2.2 Wettability Gradients

A monolayer of *n*-octyltrichlorosilane (OTCS) was deposited on a flat silicon substrate (45 mm x 10mm). The substrates were cleaned by rinsing with toluene followed by sonication in toluene for 1 min. Subsequently, the substrates were rinsed with methanol and acetone and dried under a stream of nitrogen gas. The silicon wafers were then placed in an ultraviolet-ozone (UVO, Model 42, Jelight Co.) chamber for 20 minutes to generate free hydroxyl (-OH) groups at the surface. The silane solutions were prepared by adding 200 µL of OTCS to 20 mL of anhydrous toluene in a scintillation vial. UVO treated silicon wafers were placed into the vial, backfilled with nitrogen, and were sealed. Substrates were incubated in OTCS solutions for 33 minutes. After the deposition was complete, the substrates were rinsed with toluene and sonicated in toluene for 30 seconds followed by rinsing with methanol and DI water before drying under a nitrogen stream.

Wettability gradients were fabricated by progressively dipping OTCS functionalized substrates into a tetrabutylammonium fluoride (TBAF) solution. Solutions of 0.1M TBAF were made by adding 3 mL of 1 M TBAF in tetrahydrofuran (THF) to 27 mL of THF in a glass jar to reach a final solution concentration of 0.1 M in TBAF. The solutions were heated to 50 °C in an oil bath. OTCS-functionalized substrates were progressively dipped into the TBAF solution using a KSV NIMA Single Vessel Dip Coater. The substrates were dipped in 5 mm steps at a rate of 100 mm/min. After each 5 mm step the sample was held at that position to vary the degrafting time; the degrafting times for each region on the substrate were in increments of 25 min to a maximum time of 200 min.

4.2.3 Non-uniform Silane Deposition

Non-uniform layers of OTCS were deposited onto flat silicon substrates by spin coating. The substrates were cleaned and UVO-treated, as mentioned previously. The OTCS solution was prepared by adding OTCS to trichloroethylene to achieve a final concentration of 3 mM. The UVO treaded silicon was placed on the spin coater, and enough of the OTCS solution was placed on the substrate to completely cover the surface and allowed to sit for 20 seconds. The spin coating was then performed at 3,000 rpm for 20 seconds, followed by rinsing the substrate with methanol and drying with a stream of nitrogen. This procedure was repeated three times to achieve high coverage of OTCS before curing the substrate at 135°C for 1 hour.

4.2.4 Characterization

The thicknesses of thin films were determined using variable angle spectroscopic ellipsometry (VASE, J.A. Woollam Co.) at a 70° angle of incidence. The layer thickness was obtained by fitting the ellipsometry data using a 3-layer model with a 1 mm silicon layer, a 15 Å SiO_x layer, and a "Cauchy" layer with a refractive index of 1.45. The static water contact angle was measured using a contact angle goniometer (Model 100-00, Ramé Hart). All measurements were made using DI water as the probing liquid (3-5 μL in volume) deposited as drops from a syringe. For each WCA measurement, the drop was lowered onto the substrate, and the angle recorded within 5 seconds. The water contact angle measurements were performed under atmospheric conditions at 40-60% humidity. Advancing and receding contact angle measurements were measured by adding and removing water from the drop, contact angles were determined by when the base area first increased or decreased, respectively (Model 1000B, First Ten Angstroms). AFM measurements were performed on an Asylum Research MFP-3D AFM with an Asylum Research AC160TS-R3 cantilever in tapping mode.

4.3 Results and Discussion

Covalent attachment of elastin-like polypeptides onto surfaces can be employed to generate biocompatible and stimuli-responsive coatings. Tailoring of surface chemistry is necessary to bind the terminal group of the ELP, while non-specific interactions between the protein backbone and the surface must be controlled to limit non-specific adsorption of the ELP. Significant protein adsorption on short-time scales can limit protein adsorption due to steric hindrance; whereas, adsorption after covalent attachment can inhibit the coating's response to stimuli. In this study, silane functionalized surfaces are being used to investigate the influence of wettability and morphology on the non-specific adsorption of ELPs. **Table 4-1** summarizes the sequences and transition temperatures of ELPs used in this study, and notations of the di-blocks are such that either the N terminus or C terminus collapse at the lower of the two transition temperatures.

Table 4-1. Summary of ELP sequences and transition temperatures. All values reported as measured with an ELP concentration of 25 µM in PBS buffer (pH 7.4).

Surface	**Sequence**	**T_t (°C)**
Homopolymer	$(VPGVG)_{80}$	32
N-Diblock	$N-(VPGVG)_{40}-(VPGSG)_{40}-C$	50, 65
C-Diblock	$N-(VPGSG)_{40}-(VPGVG)_{40}-C$	53, 62
Alternating	$N-(VPGSGVPGVG)_{40}-C$	50
Blocky-10	$N-[(VPGSG)_{10}-(VPGVG)_{10}]_4-C$	48

Wettability gradients were fabricated by the degrafting of OTCS as described previously. These substrates were then incubated in 25 µM ELP solutions in PBS (pH 7.4) for 12 hours. After incubation, the substrates were rinsed thoroughly and sonicated in DI water. The WCA of these surfaces after incubation varied from 70º to 80º while the thickness of the film, silane, and ELP, varied from 2.2 to 3.9 nm in the direction of increasing hydrophobicity as can be seen in **Figure 4-4**. Incubation of these substrates in a 1.57 M solution of guanidine hydrochloride (GuHCl) in DI water under light agitation resulted in further removal of ELPs from the surface. The removal may have resulted from the disruption of weak protein-protein and protein-surface interactions for more favorable protein-GuHCl interactions (due to hydrogen bonding). More ELP desorbed from the surface during the GuHCl incubation on the hydrophilic regions of the substrate; this suggests either weaker or less numerous interactions between the ELP and the substrate.

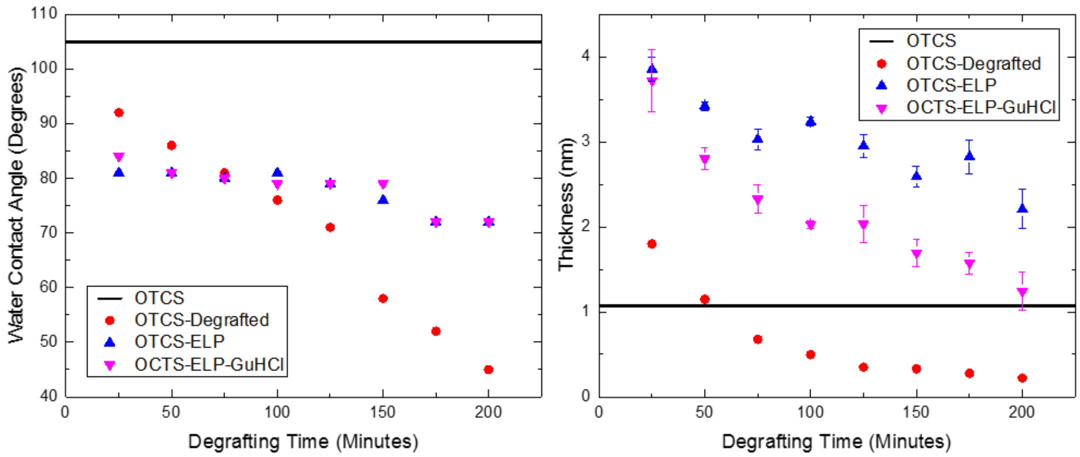

Figure 4-4. Adsorption of ELPs on gradients of OTCS results in wettability and thickness changes.

Figure 4-5 depicts AFM micrographs demonstrating morphology changes after ELP adsorption. OTCS-functionalized substrates with adsorbed ELPs exhibit small aggregates and holes. Incubation in GuHCl results in smoothing of the morphology. However, a similar distribution of holes and aggregates exists both before and after this incubation, implying that these features result, at least partially, from the structure of the underlying silane monolayer. The frequency of these features increases as the area coverage of the silane increases. This similarity is more apparent in the phase images (**Figure 4-6**). The phase shift and feature size observed are similar for both the hole and aggregates seen on these surfaces, suggesting that the source of these features is the same. As discussed previously these features may be areas with a high density of silane or large silane aggregates on the surface.

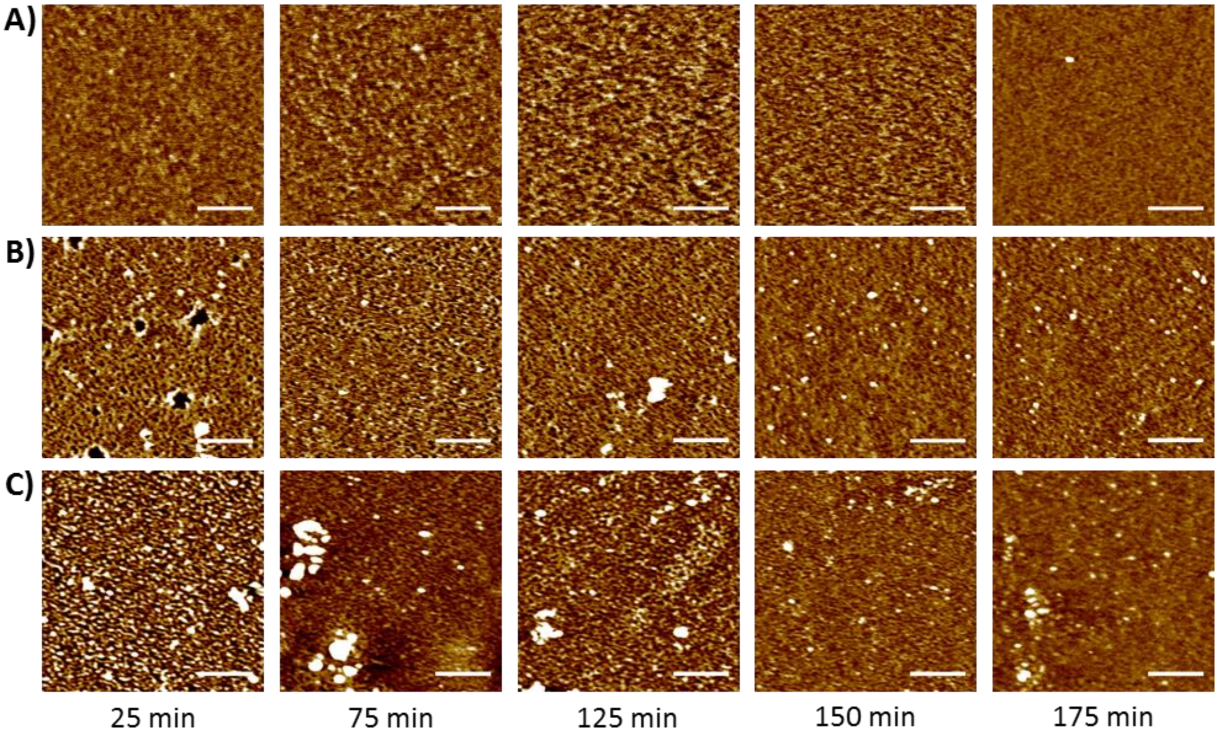

Figure 4-5. AFM height images of adsorption of ELP on OTCS functionalized substrate after degrafting for 25, 75, 125, 150, and 175 minutes. A) OTCS degrafting B) ELP deposition C) Incubation in GuHCl solution. All scale bars are 500 nm.

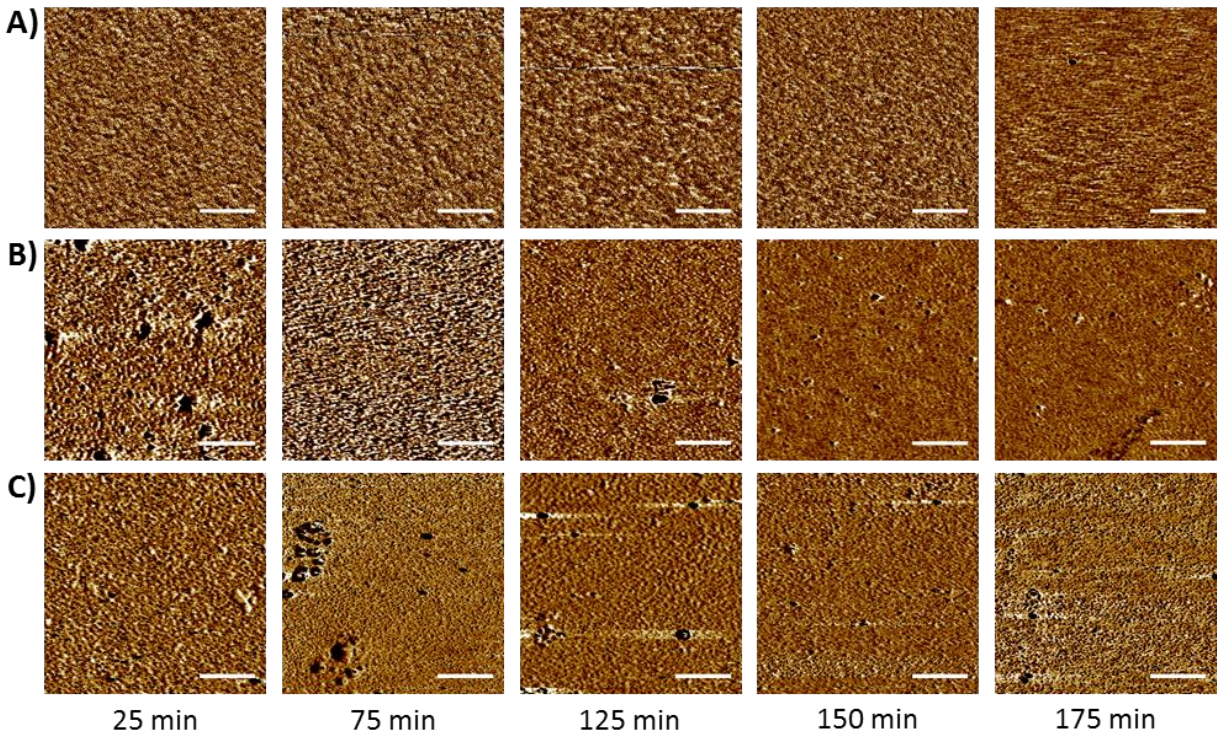

Figure 4-6. AFM phase images of adsorption of ELP on OTCS functionalized substrate after degrafting for 25, 75, 125, 150, and 175 minutes. A) OTCS degrafting B) ELP deposition C) Incubation in GuHCl solution. All scale bars are 500 nm.

Non-homogeneous silane SAMs were formed by spin coating *n*-octadecyltrichlorosilane (ODTCS) from trichloroethylene to investigate the effects of SAM morphology on ELP adsorption. Relatively high surface coverage of ODTCS with little multilayer formation was achieved by this method as determined by a WCA of 96º and thickness of 2.9 nm as measured by ellipsometry. Examination of the surface by AFM reveals large island morphologies on the surface; these consist of smaller ODTCS features with a lateral size of ~40 nm as can be seen in **Figure 4-7**. ELP adsorption onto these surfaces results in relative preservation of these morphologies; however, there are some significant differences.

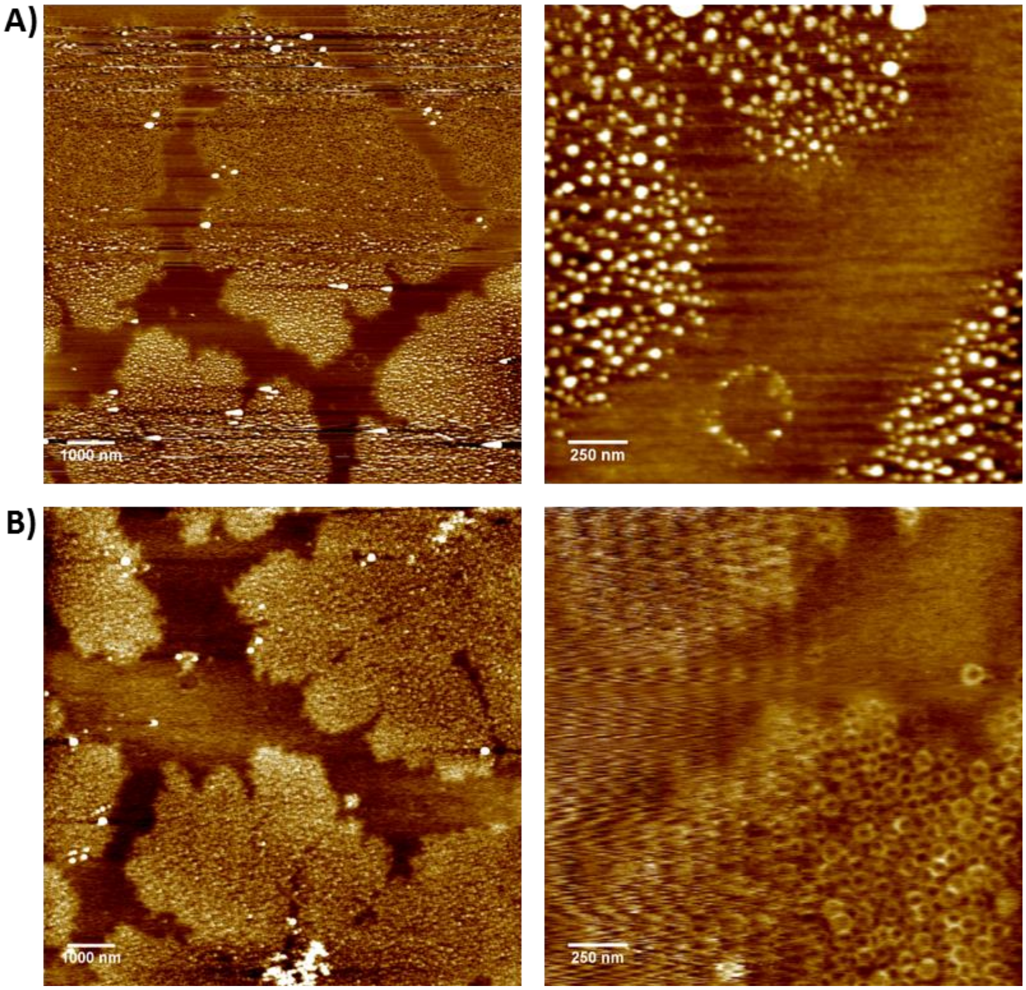

Figure 4-7. AFM height images of partial ODTCS layers formed by spin coating A) before and B) after ELP adsorption.

The thickness of the film on the surface increased to 8.5 nm, which corresponds to ~5.6 nm of protein adsorbed. Typically, ELP adsorption thicknesses have been ~3 nm. The slight increase in thickness here may be a result of the non-uniformity of the substrate and the increased hydrophobic character of the ODTCS. Ring structures appear on the surface with an inner diameter of ~40 nm, consistent with the ODTCS features seen before ELP adsorption. These structures may be forming due to the stabilization of ELPs by hydrophobic interactions with the long alkyl chains of ODTCS. The height of these ring structures is found to be 2-3 nm which is consistent with the thickness of adsorbed ELP layers found previously.

Functionalization of hydroxylated silicon wafers with 3-(triethoxysilyl) propylsuccinic anhydride (TESPSA) resulted in anhydride functionality exhibiting a WCA of ~55º. Some variance exists in this measurement due to the hydrolysis of the anhydride when exposed to atmospheric water. This functionalization with anhydrides allows for the covalent attachment of species containing primary amines to the surface. TESPSA-functionalized surfaces were incubated in a cysteamine solution to demonstrate their reactivity. **Figure 4-8** displays the XPS spectra of these surfaces both before and after incubation. Before incubation the C 1s region shows a distinct peak at ~289 eV corresponding to –COO; after incubation, a peak appears at ~288 eV depicting the presence of imides. After incubation, nitrogen is present in the samples.

A)

B)

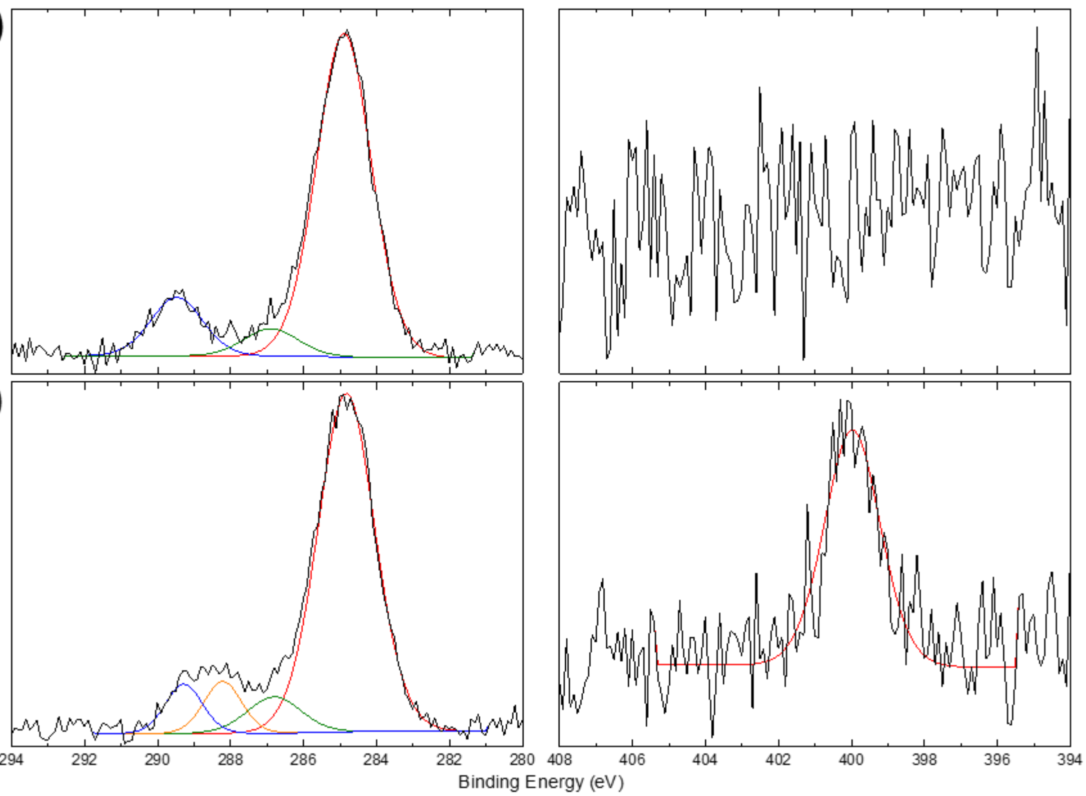

Figure 4-8. XPS spectra of TESPSA functionalized silicon wafers in the C 1s and N 1s regions A) after deposition and B) after reaction with cysteamine.

Reactivity of the surface toward primary amines can allow for the covalent attachment of ELPs. Incubation in a 25 µM ELP solution in PBS resulted in the surfaces shown in **Figure 4-9**. Circular structures are visible in the phase images, and the dimensions are similar to those seen for

ELP adsorption on OTCS functionalized surfaces. The thickness of the ELPs on these surfaces was measured to be between 2-4 nm, which is consistent with that seen for the adsorption studies.

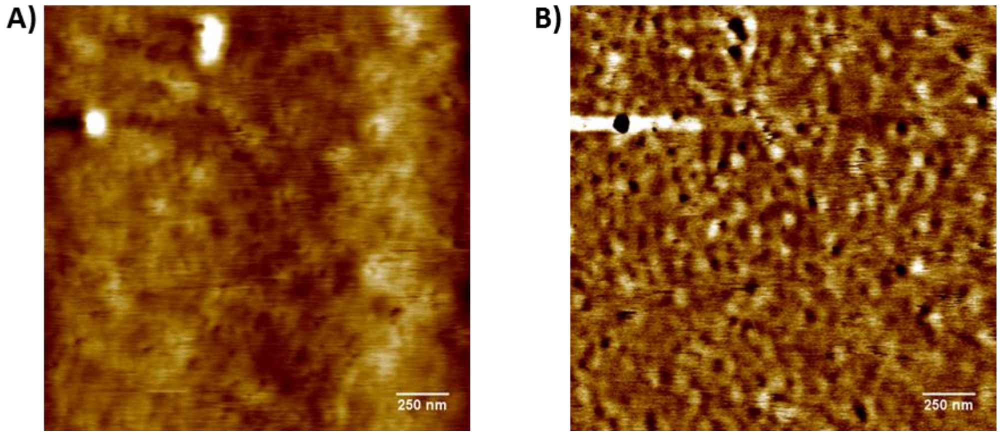

Figure 4-9. AFM A) height and B) phase images of TESPSA functionalized surfaces after incubation in the ELP solution.

Similar morphologies and thicknesses of the ELP layers on anhydride functionalized surfaces indicate that there may be a significant amount of physical adsorption occurring. As ELPs adsorb onto the surface, they prevent covalent attachment due to steric hindrance. The WCA should decrease when measured above the transition temperature due to a collapse of the ELPs on the surface. We have measured the contact angle both above and below the transition temperature and detect no decrease in the WCA, implying that there are significant interactions between the ELP and the substrate. The morphology of the surface would need to be examined in liquid cell AFM both below and above the transition temperature to verify if there is a morphology change.

The sequence of the ELP was varied to be alternating or to have various degrees of blockiness by introducing a second ELP sequence with the guest residue being serine. Changing the residue from valine to a serine increases the hydrophilicity of the ELP, increasing transition temperature. Incubation of anhydride functionalized surfaces in solutions of ELPs at 55°C resulted in the morphologies depicted in **Figure 4-10**.

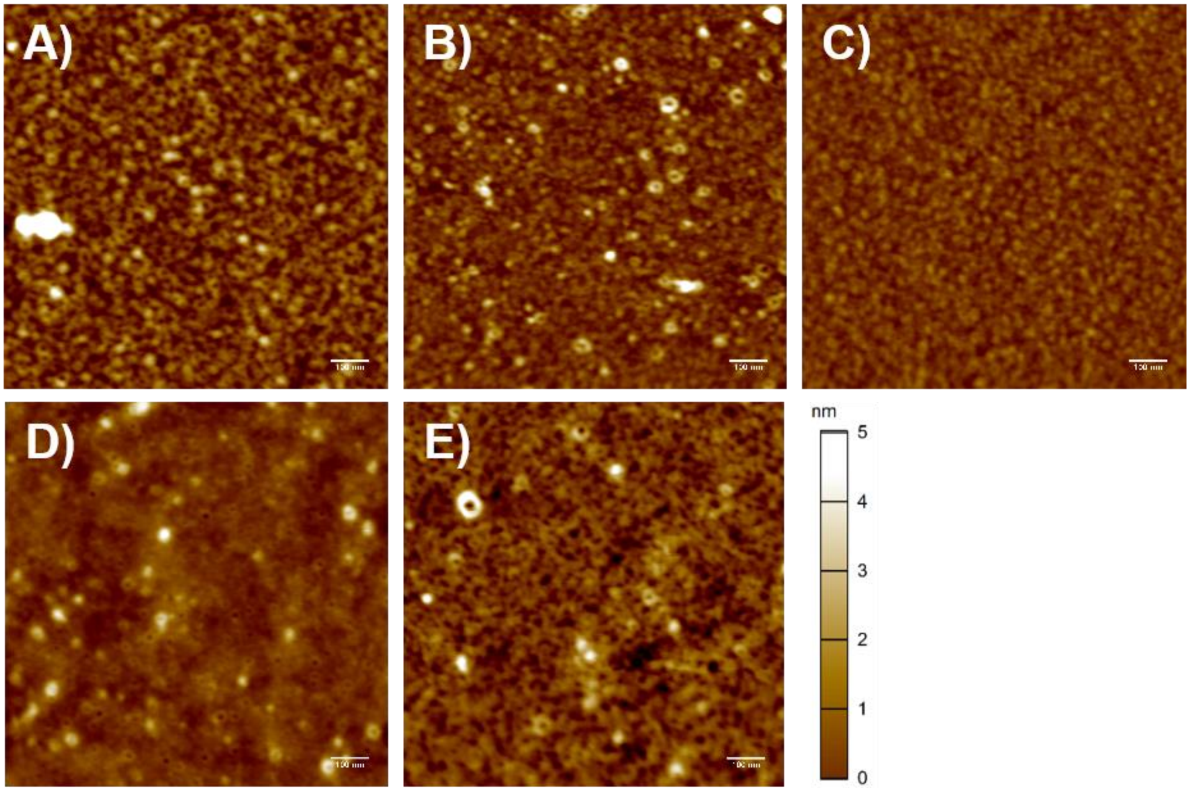

Figure 4-10. AFM micrographs of anhydride functionalized surfaces incubated in A) homopolymer, B) N-diblock, C) C-diblock, D) alternating, or E) blocky-10 ELP solutions in PBS at 55 °C.

When comparing the morphologies of the hydrophobic ELP homopolymer to that of the two diblock ELPs the feature size is slightly larger for the homopolymer ELP, leading to an increase in roughness of the surface. The formation of ring structures on the N-diblock ELP functionalized surface is more pronounced than on the C-diblock ELP functionalized surface. The C-diblock ELP exhibiting the N-terminus on its soluble block can explain this difference, allowing it to more easily react with the surface epoxide groups; whereas, the N-diblock ELP would favor physically adsorbing as the rate of reaction with the surface would be lower due to the hindrance around the N-terminus.

To overcome the rapid hydrolysis of anhydrides, which can limit their reactivity and lead to hydrogen bonding between the surface and the ELP, we have investigated the attachment of ELPs to layers of GPTMS. GPTMS features a glycidyl ether which can readily react with primary amines in water to form β-amino alcohols (*cf.* **Figure 4-11**).[31]

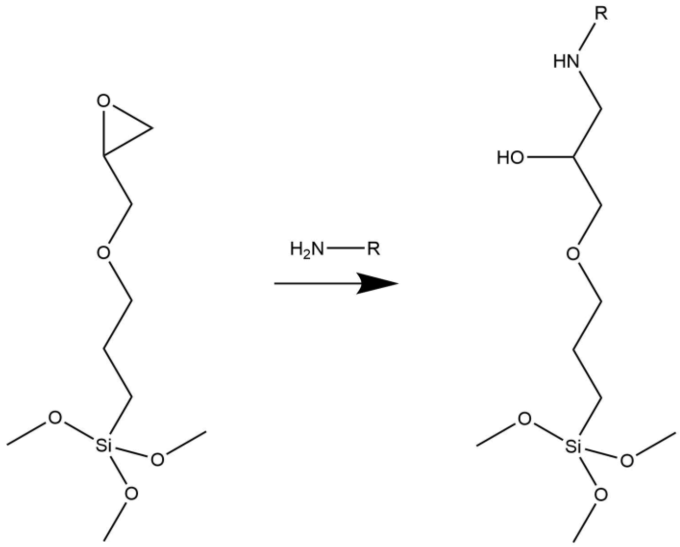

Figure 4-11. The reaction of GPTMS with a primary amine to form β-amino alcohol.

For this system, the formation of β-amino alcohols is complicated by the hydrolysis of the epoxide to form a diol product. Hydrolysis of epoxides undergoes an acid-catalyzed mechanism at low pH[32] and a base-catalyzed mechanism at high pH.[33] Thus, it is important to control the pH of the reaction medium as the nucleophilic strength of amines is much higher than that of water; however, the nucleophilic strength of protonated amines ($pH < pK_a$) is negligible, and the reaction will not occur to a significant extent.[8]

Table 4-2. Water contact angle and thickness of modified GPTMS layers.

Surface Treatment	**pK_a**	**WCA (deg)**	**Thickness (nm)**
GPTMS		53	0.75
PBS (RT)		29	0.99
PBS (75°C)		20	0.79
Propylamine (RT)	10.7	13	0.62
Propylamine (75°C)	10.7	46	*
Aniline (RT)	4.6	63	1.60
Aniline (75°C)	4.6	51	1.50
ELP (RT)	8	62	2.03
ELP (55°C)	8	71	3.24

We examined the change in water contact angle and thickness of GPTMS layers after exposure to PBS buffer (pH 7.4), propylamine, aniline, and ELP solutions at ambient and elevated temperatures (*cf.* **Table 4-2**). Initially, AFM height scans of the GPTMS monolayer show a relatively uniform morphology with few aggregates on the surface (*cf.* **Figure 4-12**). When exposed to PBS buffer the contact angle of the surface decreased, and the thickness remained relatively unchanged, with a slight increase under ambient conditions most likely due to salt crashing out of solution onto the surface. When the layers were exposed to propylamine the contact angle and thickness decreased dramatically. As propylamine has a pK_a of 10.7 it is protonated when dissolved in the PBS buffer, so little reaction with epoxide is expected. The change in contact angle and thickness mostly results from etching of the GPTMS and underlying silica layer. Upon exposure to an aniline solution the water contact angle and thickness increase as the aniline is not protonated in PBS buffer, favoring reaction of the amine with the epoxide.

Incubating the GPTMS films in ELP solutions at ambient conditions and 55°C resulted in increased contact angles and thicknesses as would be expected for the addition of the peptide layer. When exposed to ambient conditions, the changes were less dramatic, suggesting a smaller amount of peptide attached to the surface. AFM scans of these surfaces depict features with a lateral dimension of approximately 40 nm for both deposition conditions when measured in the dry state (*cf.* **Figure 12**). However, the density of these features is greater when the ELP is deposited at 55°C. This increased surface density is most likely a result of the ELPs being collapsed above their LCST allowing for more efficient packing on the surface.

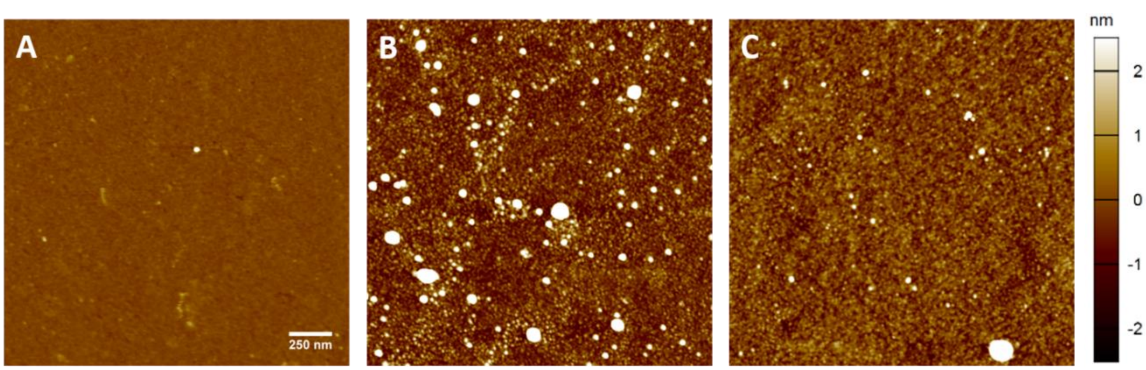

Figure 4-12. AFM micrographs of A) GPTMS functionalized surface, B) surface after deposition of homopolymer ELP at 23°C, and C) surface after deposition of homopolymer ELP at 55°C.

Attachment of ELPs to GPTMS functionalized surfaces resulted in more uniform coverage when compared to that of anhydride functionalized surfaces; however, it is difficult to determine why this is the case. No ring structures are observed on GPTMS-ELP functionalized surfaces, suggesting that the initial silane layers are more uniform with few aggregates present. The similar feature sizes observed between the two deposition conditions may be a result of ELP collapse after adsorption, in the case of room temperature deposition, due to an increase in local concentration significantly decreasing the T_t. This potentially irreversible collapse of ELPs during deposition is detrimental for generating a stimuli-responsive surface. Incubation and sonication of these samples in cold water and DMA resulted in an insignificant change in the thickness and morphology of the ELP layer when compared to that of after the initial rinsing.

Table 4-3. The thickness of GPTMS-ELP modified surfaces.

Surface	Deposition pH	Thickness (nm)
Homopolymer	7.2	3.1
Homopolymer	9.2	2.6
N-Diblock	7.2	2.9
C-Diblock	7.2	1.0

We have examined the change in the wettability of our ELP functionalized surfaces to check for their stimuli-responsive behavior upon heating. The surface contact angles were measured at saturation humidity to minimize drop evaporation, and a PNIPAM brush functionalized surface was measured as a control (*cf.* **Figure 4-13**). The deposition occurred below the transition temperatures of each ELP (thickness values reported in **Table 4-3**), and a wide temperature range was examined to attempt to account for an increase in T_t due to surface affinity effects. The control PNIPAM brush exhibited a strong response when heated above its LCST (32°C), with the surface becoming more hydrophobic. The diblock ELP functionalized surfaces showed no change in wettability upon heating past their transition temperatures, suggesting little to no morphological change of the adsorbed diblock ELPs. Multiple factors, such as the ELPs high affinity to the underlying SAM or due to an irreversible collapse of the ELP, can explain the lack of response. In comparison, the homopolymer ELPs show a decrease in wettability upon heating, but no sharp shift in wettability occurs. The lack of a sharp transition could result from hydrophobic interactions between the ELP and the SAM.

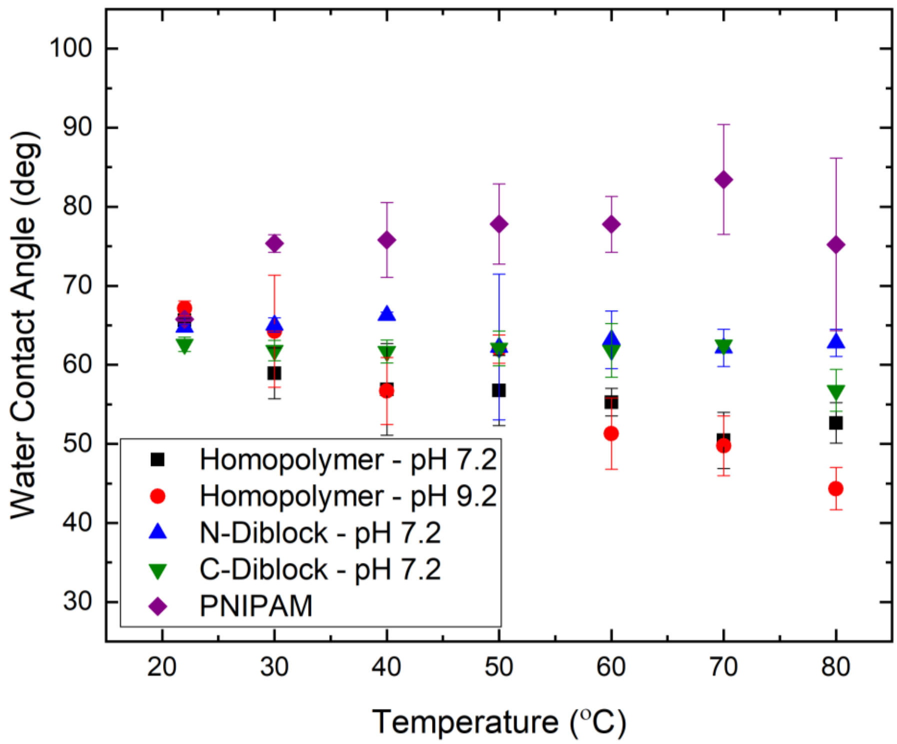

Figure 4-13. Water contact angles of GPTMS-ELP and PNIPAM modified surfaces as a function of temperature.

4.4 Conclusions

It is important to control both the availability of binding domains and the non-site-specific interactions to successfully achieve chemical grafting onto a surface. Wettability gradients were used to examine the adsorption of ELPs on the surface. The ELPs readily adsorb and form stable films on hydrophobic surfaces. Incubation of these films in the presence of a strong denaturant, GuHCl, allowed for partial removal of proteins from the surface. This removal was observed to a greater extent when the underlying substrate was less hydrophobic. We attempted to graft ELPs onto hard substrates covalently using anhydride-amine coupling chemistry. The reaction of TESPSA with cysteamine confirmed the reactivity of anhydrides on the surface with primary amines. TESPSA functionalized surfaces incubated in ELP solutions exhibited similar thickness increases and morphology as that of adsorption on hydrophobic surfaces. The morphology of these ELP layers contained ring structures that were prevalent when ELPs adsorbed onto heterogeneous silane SAMs.

To overcome the non-uniformity in the ELP layers, we investigated the use of a silane featuring a glycidyl ether to attach ELPs to the surface. These epoxide groups are reactive with non-protonated amines and have the potential to covalently attach the peptides to the surface while also resulting in more uniform coverage of the ELP layer and the underlying SAM. The GPTMS functionalized surfaces exhibited more uniform surface coverage with similar feature sizes observed for homopolymer ELPs deposited below and above their T_t. The density of distinct features observed was higher for ELPs deposited above their T_t. Diblock ELP functionalized surfaces exhibit no stimuli-responsive behavior, possibly due to the high surface affinity of the ELP or an irreversible collapse of the structure. Homopolymer functionalized ELP surfaces exhibit a gradual increase in wettability when heated above their T_t.

4.5 References

(1) Xu, L.-C.; Siedlecki, C. A. Effects of Surface Wettability and Contact Time on Protein Adhesion to Biomaterial Surfaces. *Biomaterials* **2007**, *28*, 3273–3283.

(2) Sigal, G. B.; Mrksich, M.; Whitesides, G. M. Effect of Surface Wettability on the Adsorption of Proteins and Detergents. *J. Am. Chem. Soc.* **1998**, *120*, 3464–3473.

(3) Kidoaki, S.; Matsuda, T. Mechanistic Aspects of Protein/Material Interactions Probed by Atomic Force Microscopy. *Colloids Surfaces B Biointerfaces* **2002**, *23*, 153–163.

(4) Castle, J. E.; Salvi, A. M.; Flamia, R.; Satriano, G. Surface Science Aspects of Supramolecular Conformation in Elastin-like Polypeptides. *Surf. Interface Anal.* **2012**, *44*, 246–257.

(5) Rodriguez-Hernandez, J.; Ibarboure, E.; Papon, E. Surface Segregation of Polypeptide-Based Block Copolymer Micelles: An Approach to Engineer Nanostructured and Stimuli Responsive Surfaces. *Eur. Polym. J.* **2011**, *47*, 2063–2068.

(6) Schmidt, U.; Zschoche, S.; Werner, C. Modification of Poly(Octadecene-Alt-Maleic Anhydride) Films by Reaction with Functional Amines. *J. Appl. Polym. Sci.* **2003**, *87*, 1255–1266.

(7) Bonollo, S.; Lanari, D.; Vaccaro, L. Ring-Opening of Epoxides in Water. *European J. Org. Chem.* **2011**, No. 14, 2587–2598.

(8) Stropoli, S. J.; Elrod, M. J. Assessing the Potential for the Reactions of Epoxides with Amines on Secondary Organic Aerosol Particles. *J. Phys. Chem. A* **2015**, *119*, 10181–10189.

(9) Chen, T.; Ferris, R.; Zhang, J.; Ducker, R.; Zauscher, S. Stimulus-Responsive Polymer Brushes on Surfaces: Transduction Mechanisms and Applications. *Prog. Polym. Sci.* **2010**, *35*, 94–112.

(10) Minko, S. Responsive Polymer Brushes. *J. Macromol. Sci. Part C Polym. Rev.* **2006**, *46*, 397–420.

(11) Blit, P. H.; Battiston, K. G.; Woodhouse, K. a.; Santerre, J. P. Surface Immobilization of Elastin-like Polypeptides Using Fluorinated Surface Modifying Additives. *J. Biomed. Mater. Res. Part A* **2011**, *96A*, 648–662.

(12) Eloi, J.-C.; Jones, S. E. W.; Poór, V.; Okuda, M.; Gwyther, J.; Schwarzacher, W. Electrochemically Triggered Selective Adsorption of Biotemplated Nanoparticles on Self-

Assembled Organometallic Diblock Copolymer Thin Films. *Adv. Funct. Mater.* **2012**, *22*, 3273–3278.

(13) Iha, R. K.; Wooley, K. L.; Nyström, A. M.; Burke, D. J.; Kade, M. J.; Hawker, C. J. Applications of Orthogonal “Click” Chemistries in the Synthesis of Functional Soft Materials. *Chem. Rev.* **2009**, *109*, 5620–5686.

(14) Floss, D. M.; Schallau, K.; Rose-John, S.; Conrad, U.; Scheller, J. Elastin-like Polypeptides Revolutionize Recombinant Protein Expression and Their Biomedical Application. *Trends Biotechnol.* **2010**, *28*, 37–45.

(15) Urry, D. W. Physical Chemistry of Biological Free Energy Transduction As Demonstrated by Elastic Protein-Based Polymers. *J. Phys. Chem. B* **1997**, *101*, 11007–11028.

(16) Girotti, A.; Reguera, J.; Arias, F. J.; Alonso, M.; Testera, A. M.; Rodríguez-Cabello, J. C. Influence of the Molecular Weight on the Inverse Temperature Transition of a Model Genetically Engineered Elastin-like PH-Responsive Polymer. *Macromolecules* **2004**, *37*, 3396–3400.

(17) Meyer, D. E.; Chilkoti, A. Quantification of the Effects of Chain Length and Concentration on the Thermal Behavior of Elastin-like Polypeptides. *Biomacromolecules* **2004**, *5*, 846–851.

(18) Urry, D. W.; Luan, C. H.; Parker, T. M.; Gowda, D. C.; Prasad, K. U.; Reid, M. C.; Safavy, A. Temperature of Polypeptide Inverse Temperature Transition Depends on Mean Residue Hydrophobicity. *J. Am. Chem. Soc.* **1991**, *113*, 4346–4348.

(19) Ribeiro, A.; Arias, F. J.; Reguera, J.; Alonso, M.; Rodríguez-Cabello, J. C. Influence of the Amino-Acid Sequence on the Inverse Temperature Transition of Elastin-Like Polymers. *Biophys. J.* **2009**, *97*, 312–320.

(20) Reiersen, H.; Clarke, A. R.; Rees, A. R. Short Elastin-like Peptides Exhibit the Same Temperature-Induced Structural Transitions as Elastin Polymers: Implications for Protein Engineering. *J. Mol. Biol.* **1998**, *283*, 255–264.

(21) Yao, X. L.; Hong, M. Structure Distribution in an Elastin-Mimetic Peptide (VPGVG)3 Investigated by Solid-State NMR. *J. Am. Chem. Soc.* **2004**, *126*, 4199–4210.

(22) Sallach, R. E.; Wei, M.; Biswas, N.; Conticello, V. P.; Lecommandoux, S.; Dluhy, R. A.; Chaikof, E. L. Micelle Density Regulated by a Reversible Switch of Protein Secondary Structure. *J. Am. Chem. Soc.* **2006**, *128*, 12014–12019.

(23) Privalov, P. L.; Makhatadze, G. I. Contribution of Hydration to Protein Folding Thermodynamics. *J. Mol. Biol.* **1993**, *232*, 660–679.

(24) Kim, W.; Thévenot, J.; Ibarboure, E.; Lecommandoux, S.; Chaikof, E. L. Self-Assembly of Thermally Responsive Amphiphilic Diblock Copolypeptides into Spherical Micellar Nanoparticles. *Angew. Chemie Int. Ed.* **2010**, *49*, 4257–4260.

(25) Carlsen, A.; Lecommandoux, S. Self-Assembly of Polypeptide-Based Block Copolymer Amphiphiles. *Curr. Opin. Colloid Interface Sci.* **2009**, *14*, 329–339.

(26) Osborne, J. L.; Farmer, R.; Woodhouse, K. a. Self-Assembled Elastin-like Polypeptide Particles. *Acta Biomater.* **2008**, *4*, 49–57.

(27) Costa, R. R.; Custódio, C. a.; Testera, A. M.; Arias, F. J.; Rodríguez-Cabello, J. C.; Alves, N. M.; Mano, J. F. Stimuli-Responsive Thin Coatings Using Elastin-Like Polymers for Biomedical Applications. *Adv. Funct. Mater.* **2009**, *19*, 3210–3218.

(28) Li, L.; Li, N. K.; Tu, Q.; Im, O.; Mo, C.-K.; Han, W.; Fuss, W. H.; Carroll, N. J.; Chilkoti, A.; Yingling, Y. G.; Zauscher, S.; López, G. P. Functional Modification of Silica through Enhanced Adsorption of Elastin-Like Polypeptide Block Copolymers. *Biomacromolecules* **2018**, *19*, 298–306.

(29) Costa, R. R.; González-Pérez, M.; Herrero-Gutiérrez, M.; Pires, R. A.; Alonso, M.; Rodriguez-Cabello, J. C.; Reis, R. L.; Pashkuleva, I. Tuning the Stiffness of Surfaces by Assembling Genetically Engineered Polypeptides with Tailored Amino Acid Sequence. *Biomacromolecules* **2018**, *19*, 3401–3411.

(30) Dreher, M. R.; Simnick, A. J.; Fischer, K.; Smith, R. J.; Patel, A.; Schmidt, M.; Chilkoti, A. Temperature Triggered Self-Assembly of Polypeptides into Multivalent Spherical Micelles. *J. Am. Chem. Soc.* **2008**, *130*, 687–694.

(31) Azizi, N.; Saidi, M. R. Highly Chemoselective Addition of Amines to Epoxides in Water. *Org. Lett.* **2005**, *7*, 3649–3651.

(32) Minerath, E. C.; Elrod, M. J. Assessing the Potential for Diol and Hydroxy Sulfate Ester Formation from the Reaction of Epoxides in Tropospheric Aerosols. *Environ. Sci. Technol.* **2009**, *43*, 1386–1392.

(33) Whalen, D. L. Mechanisms of Hydrolysis and Rearrangements of Epoxides. In *Advances in Physical Organic Chemistry*; 2005; Vol. 40, pp 247–298.

Chapter 5: Summary & Outlook

5.1 Summary

This Ph.D. dissertation investigated the self-assembly of silane SAMs on hydroxyl functionalized surfaces to produce finely tuned, robust, and functional surfaces. We demonstrated a degrafting approach for the tuning of the silanes fractional coverage using TBAF as a degrafting agent. The TBAF degrafting approach described allows for the formation of gradient surfaces with tunable profiles and for the elucidation of the binding structure of the silane SAM to provide information concerning stability. Additionally, we demonstrated the importance of proper surface functionalization for the use in biological applications where it is important to control adhesion while maintaining functionality. This degrafting technique can be used to fabricate surfaces with properties tailored to specific applications. The following sections describe potential opportunities that extend this work.

5.2 Determining the Stability of Silane SAMs

The degrafting of silane SAMs by TBAF provides a quick and easily accessible method to gain insight into the bonding structure of silane SAMs by the evaluation of the degrafting kinetics of various silanes and deposition conditions. However, additional experiments should be performed to validate this approach. Tribometry experiments on silane SAMs are useful for the determination of friction properties and wear resistance.[1,2] However, little has been done to relate the mechanical stability to the bonding structure. Experiments can be designed to modulate the degree of in-plane silane connectivity at the surface by varying the silane binding functionality, deposition solvent, and age of the silane solution. Generally accepted is the idea that the in-plane connectivity of tri-functional silanes increases their mechanical stability due to the dissipation of stresses. However, forces applied to silane networks with a low fraction of surface-silane linkages can result in a large area of silanes removed from the surface at once. Thus, an expected increase in the applied force required to degrade the silane SAM occurs in the order of mono-functional, aggregated tri-functional, and ordered tri-functional silanes but the rate of degradation may be highest for that of the aggregated SAM.

A natural extension of this work would be to perform tribological experiments comparing the stability of silane layers on surfaces with tuned coverages formed by direct deposition of silanes and from degrafting. As silanes deposit by a nucleation and growth process, direct deposition approaches to tune coverage result in heterogeneous surfaces with domains of high and low coverage. The sudden change in surface morphology and chemistry can result in increased wear when under shear. The degrafting with TBAF results in a more uniform surface.[3] The more uniform surface will exhibit a higher degree of mechanical stability; however, partial cleavage of the silane network by TBAF can result in a less stable layer if these bonds do not regenerate after the degrafting process.

5.3 Investigation of Density Induced Effects

Degrafting of polymer brush systems by TBAF has shown application for patterning of the surface and accurate determination of molecular weight, dispersity, and grafting density.[4,5] Further studies can be performed to investigate the effect of grafting density on the growth and modification of polymer brushes. Little work has investigated the effect of the initiator density on the kinetics of growth and dispersity of polymer brushes. Common theories state that higher initiator grafting densities result in greater molecular weight dispersity due to steric effects. TBAF degrafting of initiators provides an ideal system to study this behavior as the degrafting process, with little diffusion resistance, provides uniform surface coverage and allows for easy modulation of initiator grafting density. However, difficulties arise when attempting to study the effects of grafting density as a large, flat substrate must be used to collect a measurable amount of polymer. The degrafting of initiators from silica nanoparticles by TBAF and measurement of their grafting density by micro thermogravimetric analysis can overcome these limitations.

The high grafting density of polymer brushes grown from silane initiator functionalized surfaces may limit the efficiency of post-polymerization modifications. Due to geometric constraints, polymer brushes are more sterically hindered at the grafting point than they are at the free interface when placed in a good solvent. This difference in steric hindrance results in diffusion constraints when attempting to perform reactions along the polymer backbone, leading to non-uniform functionalization and often lower conversion than can be achieved in bulk solutions. The degrafting of polymer brushes by TBAF can allow for small changes in grafting density on the surface that have little influence on areal surface coverage of the polymer but can improve the diffusion of small molecule modifiers to the base of the brushes. Gradients in grafting density can be used to rapidly evaluate the dependence of modification extent on the grafting density and compared to the modification efficiency of bulk polymer to tune functionalization while maintaining coverage.

Another possible application for TBAF degrafting of polymer and macromolecule grafted systems is for the evaluation of concentration-dependent stimuli-responsive behavior. The stimuli-responsive behavior of these systems can be affected by surface interactions and local increases in concentration that can shift the temperature or pH at which the response occurs. The density of grafts is also important when designing anti-biofouling surfaces, as these surfaces typically depend on favorable interactions with water and steric repulsion to resist protein adsorption.[6,7] Thus, the density must be tailored to achieve complete surface coverage while not excluding water from the film. Commonly used grafts for anti-biofouling applications involve oligo(ethylene glycol) (OEG) or zwitterionic polymers, and both of these systems have decreased efficacy at high grafting densities. The conformation of OEG on surfaces has been shown to have a significant impact on the ability of the film to resist protein adsorption, with OEG chains oriented in an all-trans orientation not forming a sufficient hydration layer[7–9] and decreased steric repulsion. Zwitterionic polymer brushes exhibit a high degree of swelling in aqueous environments, which decreases the hydrolytic stability of these films due to increased tension on the surface linkages.[10] The degrafting with TBAF allows for the precise tuning of grafting density required to minimize these effects while maintaining a high areal surface coverage.

5.4 Fabrication of Multi-component SAMs

Multi-component SAMs are useful for finely tuning surface reactivity and wettability. The TBAF degrafting approach regenerates hydroxyl groups on the surface, which allows for the deposition of a second silane.[5] We have demonstrated this approach to form a multi-component system by the degrafting of a fluorinated silane and backfilling with a polymerization initiator. The growth of a PMMA brush from this surface resulted in a gradient in brush thickness that mirrored the initial coverage gradient of the fluorinated silane (*cf.* **Figure 5-1**). Generation of multi-component systems by this backfilling approach also allows for the tuning of fractional coverage of silanes which are not suitable for TBAF degrafting. Fractional coverage is difficult to tune by TBAF degrafting for silanes which form disordered structures or aggregates on the surface, and TBAF degrafting does not work for silanes which have adverse interactions with the fluorine ion, such as anhydrides, epoxides, or charged silanes. Fractional coverage of these silanes can be tuned by passivating the surface with a sacrificial silane, and its degrafting to form a guide with hydroxyl functionalized vacancies. The fractional coverage of these vacancies can be tuned by adjusting the degrafting parameters. The coverage of the desired silane is then tuned by backfilling of these vacancies. The backfilling procedure allows for varying the availability of chemical groups on the surface but would have limitations in controlling the surface energy due to the sacrificial silane remaining on the surface.

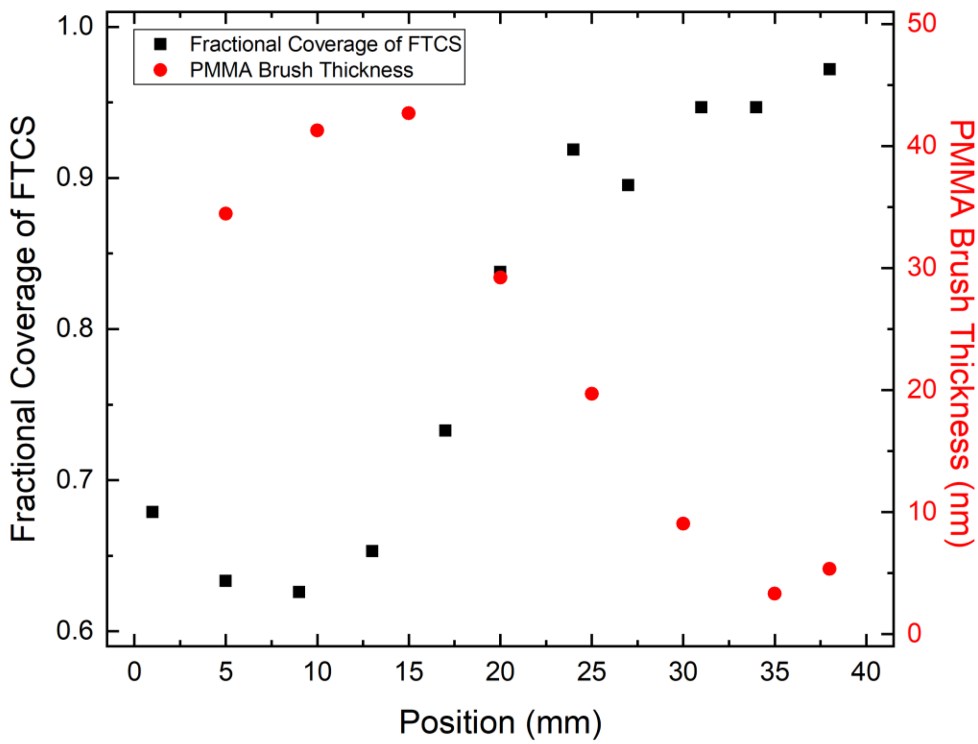

Figure 5-1. The thickness of a PMMA brush grown from an initiator gradient formed by the backfilling of an FTCS gradient substrate.

The use of multi-component SAMs for controlling the adsorption of macromolecules and for sensor applications has been of increasing interest. Sensor applications require surface chemistry to be finely tuned to target the species of interest while minimizing unfavorable non-specific interactions. Control over these interactions is even more important when considering biosensors which require the correct orientation of the antibody. Thus, it is important to generate a passivated surface that contains enough functionality to elicit a detectable response. Biosensors often employ oligo(ethylene glycol) to passivate the surface co-deposited with another species with the desired conjugation chemistry. The co-deposition approach often involves a trial and error approach to vary the relative coverage of the two species as the rate of surface attachment is generally not the same for the two species, and phase separation may occur due to miscibility. Using a degrafting approach to control the coverage of one of these species before backfilling with the other allows for precise control of the surface composition and does not result in phase separation. Furthermore, a single substrate can support numerous devices, and a step or continuous gradient approach can be used to tune these properties to achieve the desired response rapidly.

Another potential application of multi-component SAMs involves the investigation of the wetting behavior of polymer blends on surfaces. Studies have investigated these behaviors on homogeneous and microscopically patterned surfaces; however, multi-component SAMs, with a random distribution of the minor component, have the potential for the development of nanoscale variations in surface morphology. If the minor silane component is hydrophilic, the dewetting of a polymer blend, dilute in the more hydrophilic polymer, may result in the formation of nanoscale polymer droplets/features on the surface. This technique could provide a versatile method for generating nanoscale roughness on surfaces and could be used as a mold to transfer these features to other surfaces.

5.5 Covalent Functionalization of Surfaces with ELPs

The covalent functionalization of surfaces with ELPs facilitates the formation of stable, biocompatible films with stimuli-responsive behavior. Due to the hydrophobic nature of the grafting chemistry and the high density of ELPs on the surface, little change in surface energy occurs upon heating above the T_t, and the transition is not sharp, possibly due to favorable interactions between the surface and the ELP. To overcome these limitations, further investigations can be performed on this system by using a multi-component surface featuring OEG as a passivating agent and GPTMS for the subsequent covalent attachment of ELPs. Degrafting of an OEG functionalized silane followed by backfilling with GPTMS can produce multi-component surfaces without side reactions occurring between the epoxide functionality and TBAF. Alternatively, ELPs can be attached to a GPTMS SAM followed by degrafting by TBAF to vary the density of ELPs on the surface (*cf.* **Figure 5-2**). However, this approach can result in the adsorption of previously degrafted ELPs back onto the surface as stable ELP films are known to form on silica surfaces and stabilized by interactions with the alkyl backbone of the remaining silanes; these effects can be shielded using OEG.

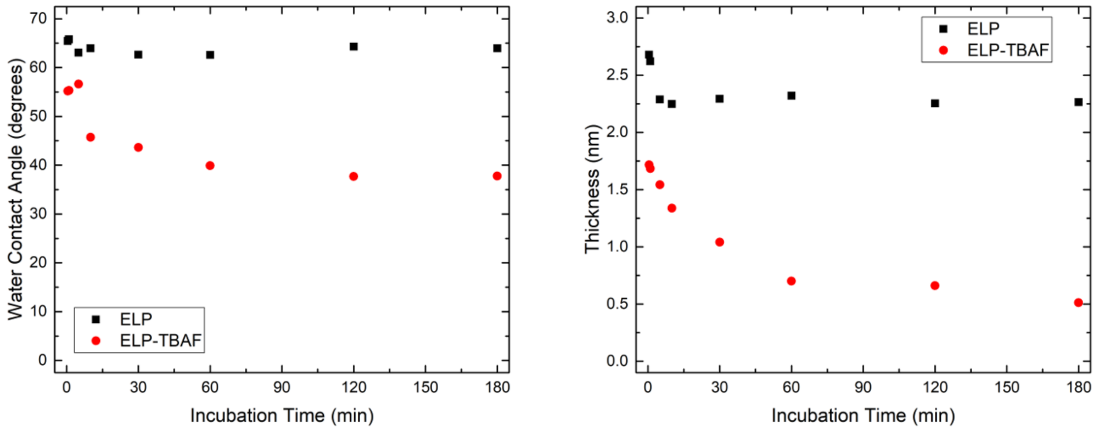

Figure 5-2. Water contact angle and thickness of GPTMS-ELP functionalized surfaces degrafted by TBAF.

ELPs are used for protein purification by inverse transition cycling (ITC). The ITC process involves the tagging of a protein of interest with an ELP, and the collapse of the ELP domains allows for the separation of the target protein by centrifugation or filtration. Removal of the supernatant and solubilization of the target protein in new solution results in a purified product. The covalent attachment of ELPs to surfaces has the potential for adapting this technique to a continuous flow-through process. The functionalization of microfluidic chambers or particles with ELPs allows for aggregation of ELP tagged proteins in solution with the surface-bound ELPs. Flowing a protein solution, with ELP tagged affinity-binding partners, through a heated packed bed of ELP functionalized particles may result in selective protein adsorption. Following the adsorption of ELPs to the bed, the flow can be switched to a fresh buffer solution of a different pH to shift the T_t of the ELP in such a manner as to resolubilize the ELP tagged proteins and remove them for collection. Alternation of these flows can allow for a high-throughput protein purification process.

5.6 References

(1) Booth, B. D.; Vilt, S. G.; Lewis, J. B.; Rivera, J. L.; Buehler, E. A.; McCabe, C.; Jennings, G. K. Tribological Durability of Silane Monolayers on Silicon. *Langmuir* **2011**, *27*, 5909–5917.

(2) Bhushan, B.; Kwak, K. J.; Gupta, S.; Lee, S. C. Nanoscale Adhesion, Friction and Wear Studies of Biomolecules on Silane Polymer-Coated Silica and Alumina-Based Surfaces. *J. R. Soc. Interface* **2009**, *6*, 719–733.

(3) Miles, J.; Schlenker, S.; Ko, Y.; Patil, R.; Rao, B. M.; Genzer, J. Design and Fabrication of Wettability Gradients with Tunable Profiles through Degrafting Organosilane Layers from Silica Surfaces by Tetrabutylammonium Fluoride. *Langmuir* **2017**, *33*, 14556–14564.

(4) Patil, R. R.; Turgman-Cohen, S.; Šrogl, J.; Kiserow, D.; Genzer, J. Direct Measurement of Molecular Weight and Grafting Density by Controlled and Quantitative Degrafting of Surface-Anchored Poly(Methyl Methacrylate). *ACS Macro Lett.* **2015**, *4*, 251–254.

(5) Patil, R.; Kiserow, D.; Genzer, J. Creating Surface Patterns of Polymer Brushes by Degrafting via Tetrabutyl Ammonium Fluoride. *RSC Adv.* **2015**, *5*, 86120–86125.

(6) Vanderah, D. J.; La, H.; Naff, J.; Silin, V.; Rubinsont, K. A. Control of Protein Adsorption: Molecular Level Structural and Spatial Variables. *J. Am. Chem. Soc.* **2004**, *126*, 13639–13641.

(7) Wang, R. L. C.; Kreuzer, H. J.; Grunze, M. Molecular Conformation and Solvation of Oligo(Ethylene Glycol)-Terminated Self-Assembled Monolayers and Their Resistance to Protein Adsorption. *J. Phys. Chem. B* **1997**, *101*, 9767–9773.

(8) Harder, P.; Grunze, M.; Dahint, R.; Whitesides, G. M.; Laibinis, P. E. Molecular Conformation in Oligo(Ethylene Glycol)-Terminated Self-Assembled Monolayers on Gold and Silver Surfaces Determines Their Ability To Resist Protein Adsorption. *J. Phys. Chem. B* **1998**, *102*, 426–436.

(9) Prime, K. L.; Whitesides, G. M. Adsorption of Proteins onto Surfaces Containing End-Attached Oligo(Ethylene Oxide): A Model System Using Self-Assembled Monolayers. *J. Am. Chem. Soc.* **1993**, *115*, 10714–10721.

(10) Wang, J.; Klok, H.-A. Swelling-Induced Chain Stretching Enhances Hydrolytic Degrafting of Hydrophobic Polymer Brushes in Organic Media. *Angew. Chemie Int. Ed.* **2019**, *58*, 9989–9993.

APPENDICES

Appendix A-1: Supplemental Information for Chapter 2

A-1.1 Degrafting Model

Silanes attach to the surface and to their neighbors (the latter for di- and tri-functional silanes) via covalent Si-O-Si linkages. Mono-functional silanes are only able to form one bond with the surface; whereas, di- and tri-functional silanes are able to form two and three bonds, respectively. We model the silane degrafting process as a series of three first order rate equations based on the current binding state of the silanes (*i.e.* one, two, or three bonds present for a single silane).

$$\frac{d\gamma}{dt} = -k_3\gamma \tag{A1}$$

$$\frac{d\beta}{dt} = k_3\gamma - k_2\beta \tag{A2}$$

$$\frac{d\alpha}{dt} = k_2\beta - k_1\alpha \tag{A3}$$

The variables α, β, and γ denote the fraction of silanes on the surface with one, two, or three bonds, respectively, with respect to the total number of silanes for a complete monolayer. The summation of α, β, and γ is taken to equal the fractional coverage of silanes on the surface. Further, α_0, β_0, and γ_0 denote the initial fraction of silanes on the surface with their respective binding states. The rate constants, k_i, characterize the breaking of a single bond from a species; the subscript denotes the number of bonds present for a species prior to the bond breaking. By using a series of first order rate equations we attempt to capture the breaking of bonds during the degrafting process which do not result in the removal of a silane from the surface. For example, if a bond is cleaved from a silane which was attached by two bonds it will not be detached from the surface as there is still one bond present. This event would result in a decrease in β and an increase in α. This model can be solved to yield:

$$\gamma = \gamma_0 e^{-k_3 t} \tag{A4}$$

$$\beta = \beta_0 e^{-k_2 t} - \gamma_0 \frac{k_3}{k_3 - k_2}\left(e^{-k_3 t} - e^{-k_2 t}\right) \tag{A5}$$

$$\alpha = \alpha_0 e^{-k_1 t} - \beta_0 \frac{k_2}{k_2 - k_1}\left(e^{-k_2 t} - e^{-k_1 t}\right) \tag{A6}$$

$$+\gamma_0 \frac{k_2 k_3}{(k_3 - k_2)(k_3 - k_1)(k_2 - k_1)}\left((k_3 - k_2)e^{-k_1 t} + (k_1 - k_3)e^{-k_2 t} + (k_2 - k_1)e^{-k_3 t}\right)$$

By assuming that a single rate constant can be used to describe the breakage of the Si-O bond regardless of its binding state (*i.e.*, the rate constant for breaking the Si-O bond for a species with one remaining bond is the same as breaking the Si-O bond for species with two or three remaining bonds) the model can be simplified and solved to yield:

$$\gamma = \gamma_0 e^{-kt} \tag{A7}$$

$$\beta = k\gamma_0 t e^{-kt} + \beta_0 e^{-kt} \tag{A8}$$

$$\alpha = \tfrac{1}{2}k^2\gamma_0 t^2 e^{-kt} + k\beta_0 t e^{-kt} + \alpha_0 e^{-kt} \tag{A9}$$

It is important to note that this model does not account for connectivity of the silane to the surface; as such, it assumes that all bonds for a single silane must be broken for it to be removed from the surface which is not the case, realistically. This may result in the model over estimating the value of α and the rate constant (substantial amounts of silane can be removed with few bond breaking events) and may be shown in experimental data by a sharp decrease at low degrafting times. The predicted degrafting behavior of an ideal surface with only tri-functional silanes present initially and a rate constant of 0.01 min^{-1} is shown below as an example.

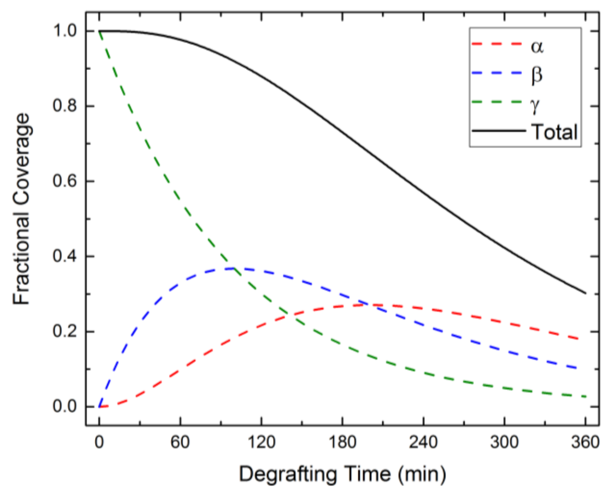

Figure A-1-1. Fractional coverage of tri-functional molecules attached covalently to the surface as a function of degrafting time. Dashed lines show the contribution of mono-, di-, and tri-functional molecules to the total fractional coverage.

It can be seen that as the fraction of triply bound silanes decreases over time there is an increase in doubly and singly bound silanes as a result. Due to the delayed degrafting of the silanes from the surface, a slight plateau is observed at short degrafting times which is not present for systems of only mono-functional silanes. This delay in degrafting is also observed for systems of di-functional silanes but it is less pronounced.

A-1.2 Silane SAM Morphology

Figure A-1-2 shows the morphology of as deposited silane SAMs. OTCS forms a smooth SAM on the surface due to their efficient packing. The monofunctional silanes (ODMCS and PDMCS) exhibit more surface roughness due to less efficient packing of the silane molecules due to the methyl groups. PTCS forms the roughest surface due to the deposition of multilayer/aggregate structures.

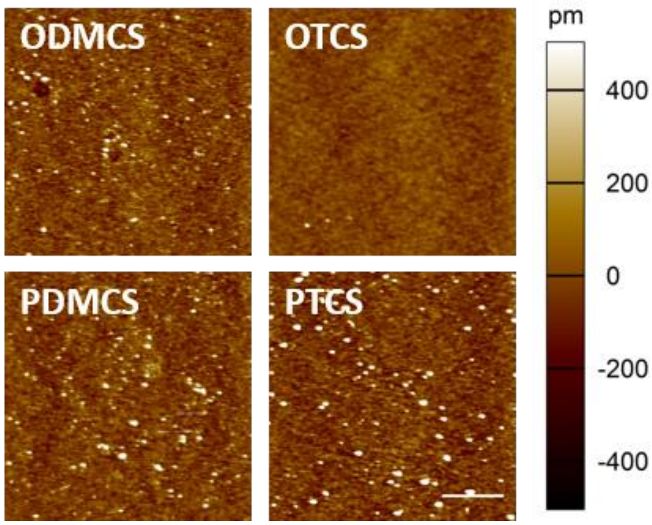

Figure A-1-2. AFM micrographs of as deposited silane SAMs (500 nm scale bar).

A-1.3 Advancing and Receding Water Contact Angle

Figure A-1-3 shows the advancing and receding water contact angles of fractional coverage gradients as a function of position. Degrafting time increases as the distance along the sample increases. Generally, an increase in contact angle hysteresis is observed as degrafting time increases. The observed profile of the advancing and receding contact angle match well with the profile of the static contact angle which was used for our analysis. **Figure A-1-4** shows the change in contact angle hysteresis along the length of the surface. Generally, an increase in hysteresis is observed as degrafting time increases. In the case of PTCS there is a decrease observed in the hysteresis initially which may be a result of silane aggregates being removed from the surface and is consistent with the sharp decrease observed in the wettability profile.

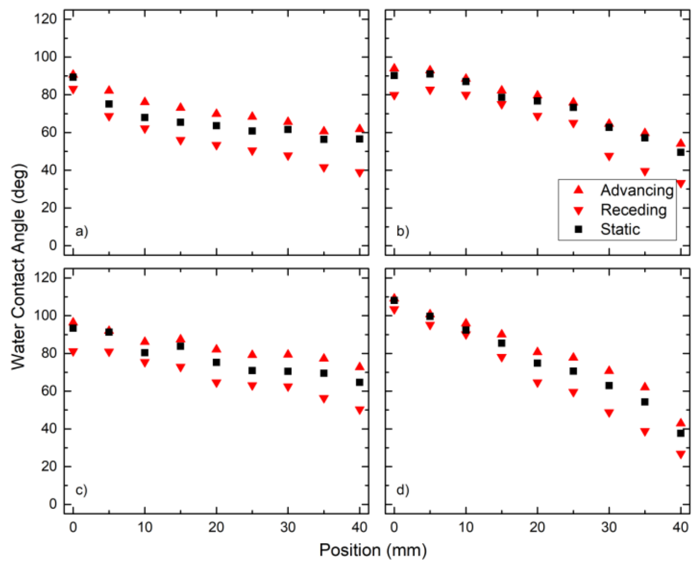

Figure A-1-3. Wettability profiles in a) PDMCS, b) PTCS, c) ODMCS, and d) OTCS generated by degrafting silane layers in 0.1 M TBAF in DMA at 50°C as a function of position.

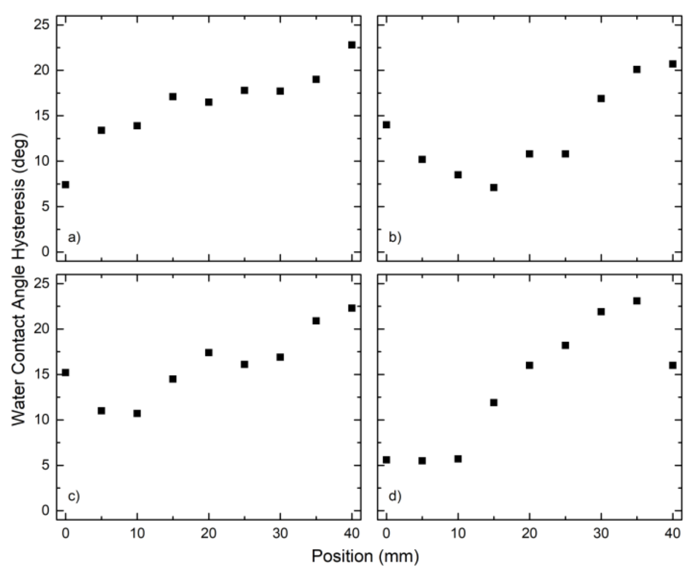

Figure A-1-4. Contact angle hysteresis of wettability profiles in a) PDMCS, b) PTCS, c) ODMCS, and d) OTCS generated by degrafting silane layers in 0.1 TBAF in DMA at 50°C as a function of position.

A-1.4 Arrhenius Fitting

Table A-1-1. Summary of the fitting parameters, activation energies (E_a), and Arrhenius pre-factors (A) for the various silane degrafting processes.

Silane	α_0	β_0	γ_0	E_a (kJ/mol)	A (min^{-1})	R^2
ODMCS	0.933	0.000	0.000	44.20	2.12×10^5	0.914
PDMCS	0.887	0.000	0.000	53.48	2.36×10^7	0.906
OTCS	0.660	0.000	0.306	54.75	5.45×10^6	0.951
PTCS	0.608	0.000	0.161	92.59	1.05×10^{14}	0.886

We used the Arrhenius equation, $k = Ae^{-E_a/(RT)}$, to calculate the activation energy, E_a, and pre-exponential factor, A, for the degrafting process of each of the silanes studied (*cf.* **Figure A-1-4**). The activation energy for the degrafting process was similar for the silanes studied; however, the activation energy was found to be higher for the PTCS degrafting (*cf.* **Table A-1-1**). This deviation in calculated activation energy is likely due to the presence of multilayer and aggregate structures in the initially formed PTCS SAM.

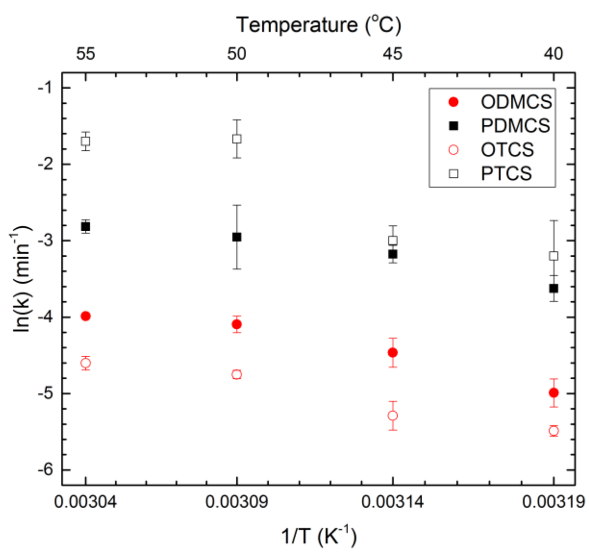

Figure A-1-5. Arrhenius plot for the various silane degrafting processes.

A-1.5 Linear Wettability Gradients

Figure A-1-6 shows linear wettability gradients for each of the silanes generated by degrafting in a 0.1 M solution of TBAF in DMA at 50°C for times predicted by the degrafting model.

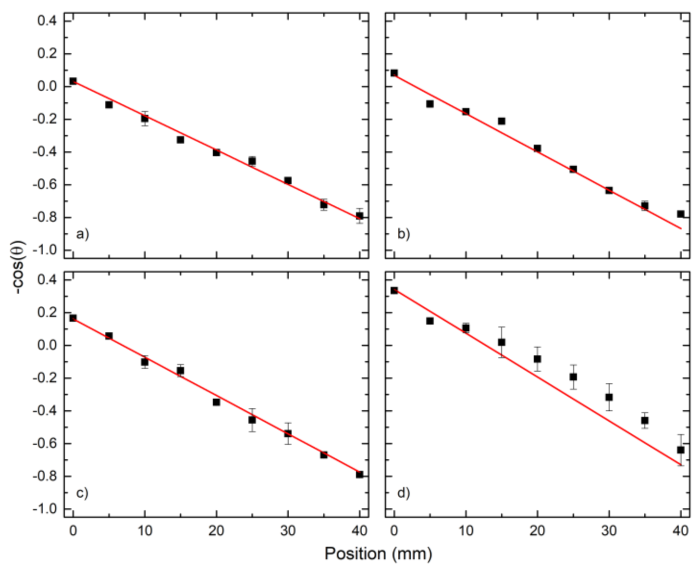

Figure A-1-6. Linear wettability gradients in a) PDMCS, b) PTCS, c) ODMCS, and d) OTCS. Solid red line represents target wettability profile.

Appendix A-2: Supplemental Information for Chapter 3

A-2.1 Monte Carlo Model Fitting

Figure A-2-1 shows the Monte Carlo fitting for the idealized structures of mono-, di-, and tri-functional silane SAMs with a high density of surface and in-plane linkages. We record an exponential decay for mono-functional silanes as expected. Variations from the model behavior are observed for di- and tri-functional silanes due to the in-plane connectivity.

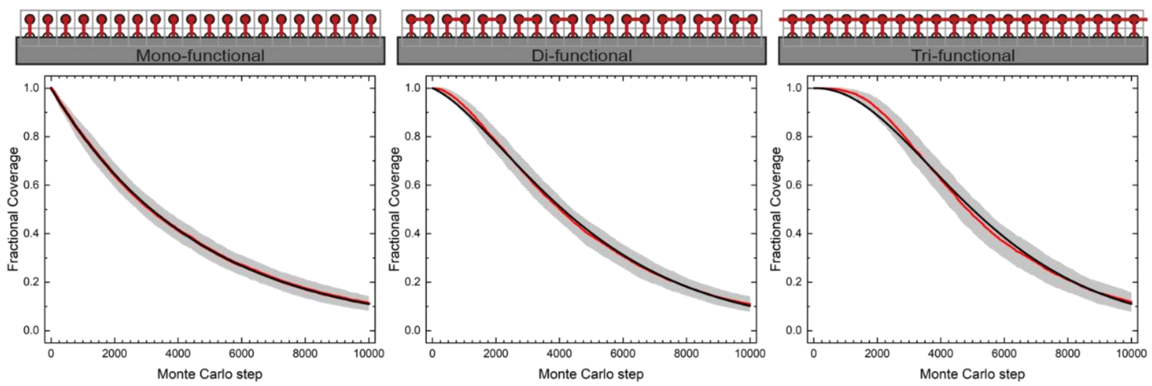

Figure A-2-1. Fractional coverage of 100 molecules with a) mono-, b) di-, c) tri-functional molecules attached covalently to the surface as a function of the number of Monte Carlo (MC) steps. The red line and the grey shaded area denote the average and standard deviation from the MC simulation, respectively. The black lines are the best fits to Equations (1)-(3) in the main text.

A-2.2 Model Fitting of Experimental Data

Table A-2-1. Summary of the rate constants (k in min-1) for the various silane degrafting processes.

Silane	Degrafting temperature (°C)			
	40	**45**	**50**	**55**
OTMS	0.004	0.006	0.010	0.011
OTCS*	0.007	0.008	0.011	0.018
FTCS*	0.008	0.014	0.020	0.028
FDMCS*	0.044	0.077	0.102	0.134
APTES	0.004	0.004	0.006	0.017
eBMPUS	0.003	0.004	0.005	0.006

Table A-2-1 lists the rate constants for the degrafting of the silanes studied resulting from the model fit. OTMS shows a nearly identical degrafting rate to what was previously observed for OTCS deposited from hexanes. OTCS deposited from the vapor phase shows a comparable rate to OTCS deposited from hexanes. The fluorinated silanes (FTCS and FDMCS) exhibit higher rate constants due to the lower density of silanes on the surface for a complete monolayer as a result of their bulkiness. eBMPUS has a lower reaction rate constant than the alkylsilanes most likely due to the longer backbone chain.

Table A-2-2. Summary of the fitting parameters, activation energies (Ea), and Arrhenius pre-factors (A) for the various silane degrafting processes.

Silane	α_0	β_0	γ_0	E_a (kJ/mol)	A (min^{-1})	R^2
OTMS	0.542	0.000	0.373	54.76	6.22×10^6	0.936
OTCS*	0.644	0.000	0.261	54.74	8.44×10^6	0.938
FTCS*	0.235	0.743	0.001	68.36	2.19×10^9	0.994
FDMCS*	0.858	0.000	0.000	62.12	1.09×10^9	0.971
APTES	0.449	0.000	0.157	79.88	6.47×10^{10}	0.818
eBMPUS	0.527	0.000	0.415	45.80	1.19×10^5	0.991

The Arrhenius equation, $k = Ae^{-E_a/(RT)}$, was used to calculate the activation energy, E_a, and pre-exponential factor, A, for the degrafting process of each of the silanes studied.

Appendix A-3: Fabrication of an Anhydride Functionalized p(MHS-co-DMS) Elastomer Network

A-3.1 Introduction

Originally developed for use as insulating and binding materials,[1] silicone elastomers have recently been applied to a variety of new processes to create complex surfaces and microfluidic devices.[2–4] Silicone elastomers are inherently elastic and are useful as flexible substrates due to their ability to deform without irreversibly degrading the material properties. Poly(dimethylsiloxane) (PDMS) is the most commonly used silicone elastomer. Due to its low thermal and electric conductivity and high fracture toughness over a wide temperature range PDMS has been a very useful material for insulation, anticorrosion, and antifouling coatings. PDMS is chemically inert and must undergo harsh chemical or physical treatments to add functionality to the surface which can lead to degradation of the material.[5,6]

Poly(methylhydrosiloxane) (PMHS) can be used to form reactive polymer networks with mechanical properties similar to that of PDMS. Chemical modification of PMHS can be achieved by hydrosilylation reactions, which allow for the addition of silicon hydrides across unsaturated carbon-carbon bonds in the presence of a transition metal catalyst, typically platinum. This mechanism is highly efficient and occurs by the oxidative addition of silicon hydrides to the transition metal catalyst, insertion of the alkene/alkyne into the metal-hydride bond and reductive elimination by Si-C bond formation.[7] Hydrosilylation allows for the addition of various chemical functionalities to a PMHS network which can be used for further modification or to control surface properties.

Due to the limitations of the cyclic ring-opening polymerization used to generate these functional silicones, the molecular weight of PMHS is severely limited. The low molecular weight of PMHS results in a less elastic network when using a small molecule crosslinking agent. Crosslinking of the network with vinyl terminated PDMS of increasing molecular weight to add elasticity to the network overcomes this problem. However, the crosslinking may decrease greatly the reactivity of the network as the major constituent quickly switches from methylhydrosiloxane to dimethylsiloxane units. Additionally, due to the greater hydrophilicity of the unreacted PMHS, and potentially reacted PMHS depending on the added functionality, there can be significant phase separation in this two-component system.[8] Using a copolymer of PMHS and PDMS (p(MHS-co-

DMS)), adding solvent, adjusting the crosslinking ratio, and tuning curing temperature and time minimizes phase separation.

A-3.2 Materials and Methods

Allylsuccinic anhydride was purchased from Tokyo Chemical Industry. Vinyl terminated polydimethylsiloxane (DMS-V21), and (25-35% methylhydrosiloxane)-dimethylsiloxane copolymer (HMS-301) were purchased from Gelest. *Cis*-dichlorobis(diethyl sulfide)platinum(II) was purchased from Sigma-Aldrich.

A-3.2.1 Hydrosilylation of p(MHS-co-DMS)

Allylsuccinic anhydride (ASA) was added to 0.28 g of (25-35% methylhydrosiloxane)-dimethylsiloxane copolymer (HMS-301, 25-35 cSt) in anhydrous toluene. A total of 28.9, 57.8, 86.7, 115.6, or 144.5 µL of ASA were added to achieve theoretical conversions of 20, 40, 60, 80, and 100%, respectively. Following the addition of ASA, 0.1 mg of the Pt(II) catalyst was added. The solution was then heated to 70°C and stirred at 800 rpm for 16 hours.

A-3.2.2 Network Formation

Elastomer networks were formed by the crosslinking of ASA-functionalized p(MHS-co-DMS) with vinyl terminated PDMS. 1.892 g of vinyl terminated PDMS (DMS-V21, 100 cSt) was added to the solution of ASA functionalized p(MHS-co-DMS) in anhydrous toluene. Following the addition of the vinyl terminated PDMS, 0.1 mg of the Pt(II) catalyst was added, the solution lightly stirred and was cast into a polypropylene Petri dish. The solution was heated to 35°C and left for 16 hours for the crosslinking reaction to proceed and the toluene to evaporate. The removal of the unreacted sol fraction of the network was accomplished by Soxhlet extraction. Soxhlet extraction was performed in toluene for 24 hours, followed by drying in a fume hood overnight and subsequent drying under vacuum for 24 hours before the mass of the network was measured to determine the gel fraction.

A-3.2.3 Reactions with Anhydride Functionality

Attempts to revert the anhydride functionality from the open ring di-acid form to the closed ring involved the incubation of the anhydride functionalized networks in xylenes at 130°C and heating under vacuum at 135°C for three days. Extracted networks were reacted with ethanolamine to determine the reactivity of the anhydride functionalities towards primary amines. Ethanolamine solutions were made by the dissolution of 0.5 mL of ethanolamine into 5 mL of DI water. Squares of the elastomer (1 cm x 1 cm) were cut to be used for these studies and were incubated in the ethanolamine solutions for up to 3 hours before rinsing with toluene and incubation in 20 mL toluene overnight to remove unreacted ethanolamine.

A-3.2.4 Characterization

Dynamic mechanical experiments were performed with an RSA-G2 Solids Analyzer (TA Instruments). The extracted networks were cut into rectangles (approximately 1 mm thick by 10 mm wide by 20 mm long) and loaded onto the instrument using the Tension Fixture attachment. The samples were subjected to angular frequency sweeps from 0.1 to 100 rad/s. The tests were performed at room temperature (22°C) with a constant 1% strain applied at each frequency. The samples were equilibrated by applying 0.05 – 0.1 N of axial force for 30 s before the frequency sweeps were performed to minimize error due to sample loading. The tensile storage (E'), tensile loss (E''), and the loss tangent ($\tan(\delta)=E''/E'$) were recorded at each frequency.

Chemical modification of the p(MHS-co-DMS) was measured with a Nicolet 6700 FT-IR equipped with a Ge ATR crystal and scanning between 400 and 4000 cm^{-1}. Samples were prepared by placing a drop of the p(MHS-co-DMS) solution onto the crystal face and allowing the toluene to evaporate, leaving a polymer film, to investigate the attachment of allylsuccinic anhydride to the polymer. The reactivity of anhydride functionalized polymer networks was performed by placing the network into contact with the ATR crystal and backing the elastomer with a glass slide to uniformly apply pressure.

A-3.3 Results and Discussion

We fabricated a silicon elastomer bearing an anhydride functionality for subsequent reactions with primary amines. Allylsuccinic anhydride functionalization of a copolymer comprising ~70% dimethylsiloxane and ~30% methylhydro-siloxane units (p(MHS-co-DMS)) proceeded by a hydrosilylation reaction which inserts the Si-H of the MHS units into the unsaturated C-C bond of the ASA in the presence of a transition metal catalyst.

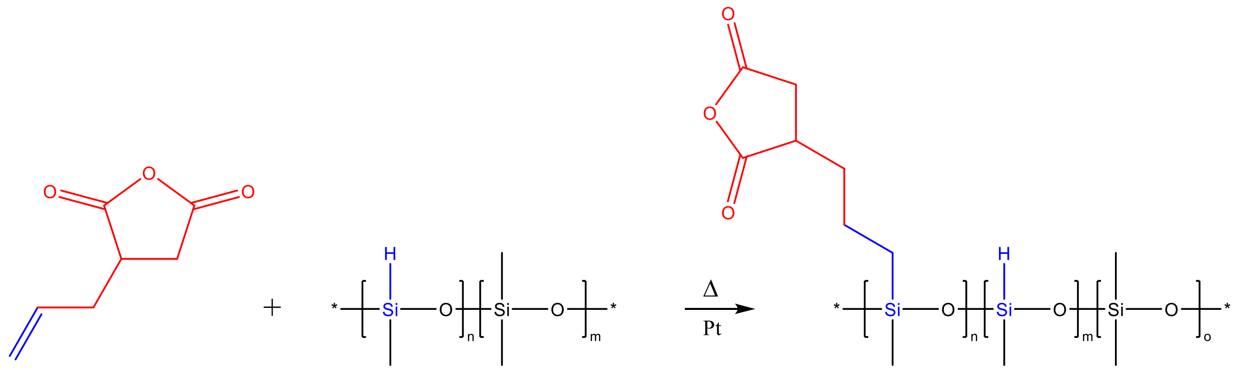

Figure A-3-1. The reaction of allylsuccinic anhydride with p(MHS-co-DMS) to form anhydride functionalized polymer.

An MHS homopolymer was not used to form this network because it is difficult to achieve high molecular weight PMHS due to side reactions during the cyclic ring-opening polymerization; the use of low molecular weight polymer would result in a relatively hard (and brittle) network. Using a second elastomer as a crosslinker, such as a vinyl terminated PDMS, can alleviate this limitation. However, due to the hydrophilic characteristics of the anhydride functionalized PMHS, phase separation can occur when crosslinking PHMS with a hydrophobic PDMS. Using a copolymer allows for higher molecular weight polymers to be used for both the backbone and crosslinker due to better miscibility of the two polymers. The random distribution of MHS units in the p(MHS-co-DMS) copolymer helps to ensure a more uniform distribution of anhydride functionalization.

The functionalization of p(MHS-co-DMS) with ASA using a *cis*-dichlorobis(diethyl sulfide)platinum(II) as a catalyst was tested by adding molar equivalents of ASA to achieve theoretical conversions of hydride groups ranging from 20 to 100%. All reactions were performed overnight in 10 mL of anhydrous toluene at 75 ºC. **Figure A-3-2** shows the conversion of hydride groups as measured by FTIR. Increasing the theoretical conversion results in a decrease in the Si-H peak intensity. When normalized against the backbone Si-CH_3 signal, the decrease in the Si-H signal is linear with respect to theoretical conversion. However, we are unable to determine the degree of modification due to a sharp increase in the Si-H peak intensity after the reaction at ~10% theoretical conversion. This linear decrease implies that there are few undesired side reactions taking place in the system. The anhydride functionalized p(MHS-co-DMS) starts to form gel-like aggregates at conversions above 40%, possibly due to ring-opening of the anhydride by water in the system.

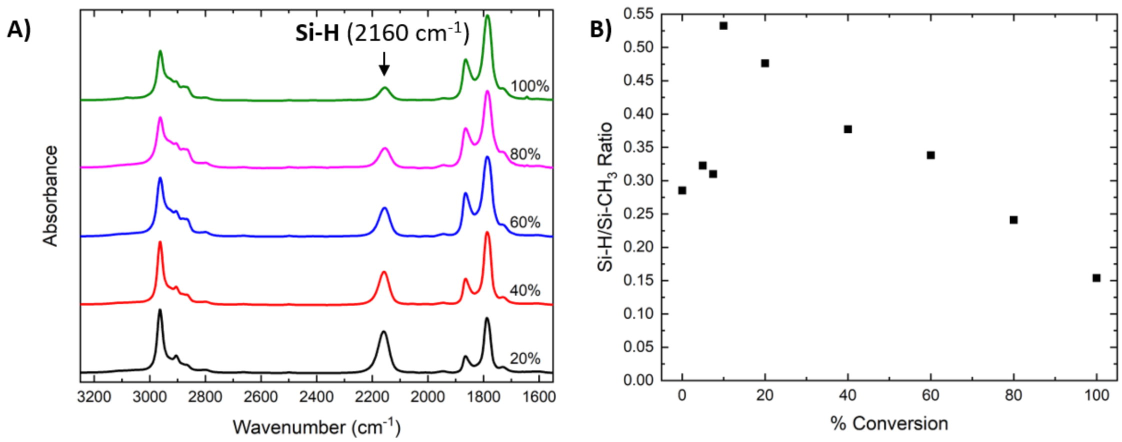

Figure A-3-2. A) FTIR spectra of functionalized p(MHS-co-DMS) with ASA for theoretical hydride unit conversion B) Ratio of Si-H to Si-CH_3 peak height as a function of theoretical hydride unit conversion.

Due to gelation and phase separation, anhydride functionalized networks were made with a theoretical conversion of 40% and crosslinked with a vinyl terminated PDMS (MW ~ 6 kDa). The molar ratio of available hydride functional groups on the polymer backbone relative to the number of vinyl end groups on the PDMS crosslinker, denoted by the r-value, defines the amount of crosslinker added. Crosslinking and casting of the elastomer network from solution required tuning of the curing parameters to prevent phase separation from occurring. The crosslinking reaction with a Pt(II) catalyst requires mild heating to proceed; however, minimizing the solvent evaporation rate is important to ensure polymer miscibility. Performing the crosslinking reaction at 75ºC leads to phase separation as a result of rapid solvent evaporation concerning the rate of crosslinking. Phase separation occurs in networks cast from 2 or 5 mL of toluene at 35ºC, with larger domains present at the interface and smaller domains persistent throughout the elastomer network (*cf*. **Figure A-3-3**). No significant phase separation occurs when casting the network from 10 mL of toluene at 35ºC.

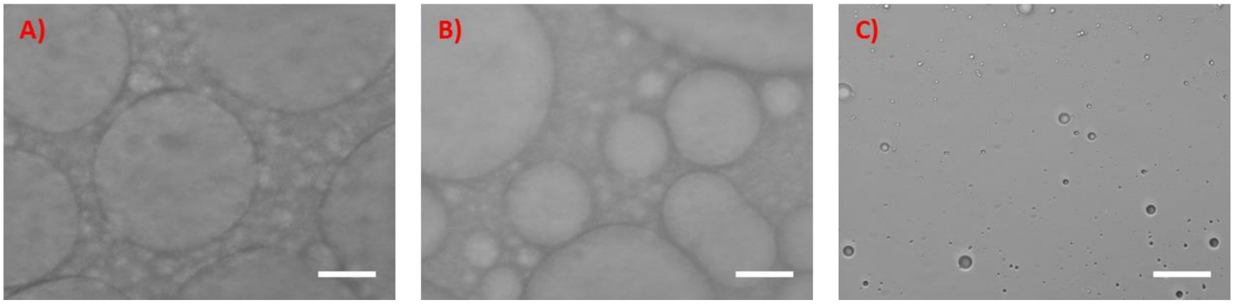

Figure A-3-3. Optical microscopy images of cured ASA functionalized p(MHS-co-DMS) networks at a 40% theoretical conversion of hydride units and an r-value of 2 in A) 2 mL, B) 5 mL and C) 10 mL of toluene. All scale bars are 100 µm.

We performed dynamic mechanical analysis of the anhydride functionalized polymer network to investigate mechanical properties (*cf*. **Table A-3-1**). The tensile storage modulus (E') of a material is a measure of the elastic and solid characteristics of the material. The tensile loss modulus (E") of a material is a measure of the material's ability to dissipate energy. The phase angle, δ, is the time delay between the applied force (stress) and resulting deformation (strain) of the material. When the phase angle nears zero, the material exhibits solid, elastic-like behavior as it has no viscous component to dissipate forces; when the phase angle approaches 90° the material behaves like a liquid. The viscous component of the network increases with increasing the r-value due to crosslinkers only reacting one of their functional groups, resulting in dangling chains. The low gel fraction of the network with an r-value of 10 reflects this behavior.

Table A-3-1. Gel fraction and dynamic mechanical properties at a frequency of 0.1 rad/sec as a function of the stoichiometric ratio, r-value.

r-value	Gel Fraction	E' (kPa)	E'' (kPa)	tan(δ)
1	0.94	$6.8x10^2$	$1.5x10^1$	0.02
2	0.86	$1.4x10^3$	$1.5x10^1$	0.01
3	0.77	$2.5x10^2$	$1.2x10^1$	0.05
4	0.90	$6.0x10^2$	$2.6x10^1$	0.04
5	0.91	$6.4x10^2$	$5.0x10^1$	0.08
10	0.60	$1.9x10^2$	$2.7x10^1$	0.14

During the processing of the anhydride functionalized elastomers, the anhydride ring opens to the acid form due to the absorption of atmospheric water, as seen by a shift in the anhydride IR peak from 1788 to 1730 cm^{-1}. When the anhydride species is present in bulk or in a thin film it is possible to close the anhydride by heating to drive off the water. However, after heating these networks at 135ºC under vacuum for three days, only a small fraction was converted back to the closed ring form detected by FTIR-ATR. Heating the network in xylenes at 130°C for three days did not result in conversion back to the closed ring form of the anhydride. The incubation of these networks in an ethanolamine solution in DI demonstrates the reactivity towards primary amines. The open ring conformation of the anhydride limits the reactivity, and the reaction does not proceed to a significant extent in the first hour. However, after 2-3 hours the presence of amide bands can be seen in **Figure A-3-4** following the incubation and subsequent rinsing in toluene.

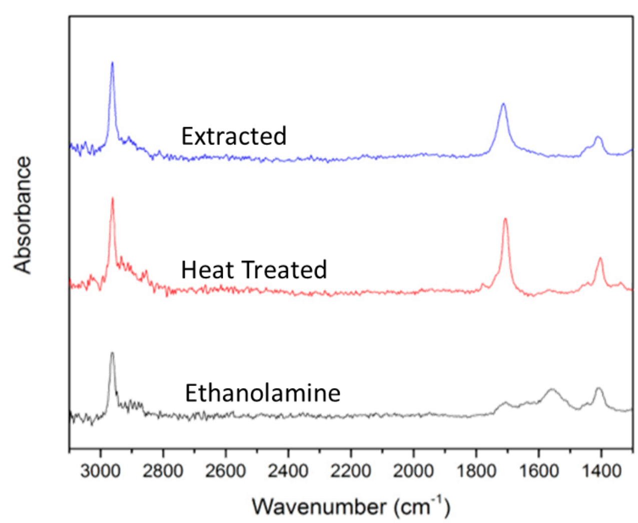

Figure A-3-4. FTIR spectra of ASA functionalized p(MHS-co-DMS) network after extraction, heating, and reaction with ethanolamine.

A-3.4 Conclusions

The reaction of p(MHS-co-DMS) with ASA and subsequent crosslinking with vinyl terminated PDMS allows for the generation of functional and reactive silicone elastomers. A copolymer consisting of ~30% HMS was used to increase miscibility with the PDMS crosslinker. Varying the crosslinking ratio and the MW of the crosslinker allows for tuning of the network properties. During the curing and extraction of the network, the anhydride units tend to hydrolyze to the diacid conformation, and it is difficult to regenerate the closed anhydride form. However, the network can still react with primary amines.

A-3.5 References

(1) Hillborg, H.; Gedde, U. W. Hydrophobicity Changes in Silicone Rubbers. *IEEE Trans. Dielectr. Electr. Insul.* **1999**, *6*, 703–717.

(2) Cortese, B.; D'Amone, S.; Manca, M.; Viola, I.; Cingolani, R.; Gigli, G. Superhydrophobicity Due to the Hierarchical Scale Roughness of PDMS Surfaces. *Langmuir* **2008**, *24*, 2712–2718.

(3) Patrito, N.; McCague, C.; Norton, P. R.; Petersen, N. O. Spatially Controlled Cell Adhesion via Micropatterned Surface Modification of Poly(Dimethylsiloxane). *Langmuir* **2007**, *23*, 715–719.

(4) Zhou, J.; Ellis, A. V.; Voelcker, N. H. Recent Developments in PDMS Surface Modification for Microfluidic Devices. *Electrophoresis* **2010**, *31*, 2–16.

(5) Özçam, A. E.; Efimenko, K.; Genzer, J. Effect of Ultraviolet/Ozone Treatment on the Surface and Bulk Properties of Poly(Dimethyl Siloxane) and Poly(Vinylmethyl Siloxane) Networks. *Polymer* **2014**, *55*, 3107–3119.

(6) Efimenko, K.; Wallace, W. E.; Genzer, J. Surface Modification of Sylgard-184 Poly(Dimethyl Siloxane) Networks by Ultraviolet and Ultraviolet/Ozone Treatment. *J. Colloid Interface Sci.* **2002**, *254*, 306–315.

(7) Maciejewski, H.; Pietraszuk, C. *Hydrosilylation*; Marciniec, B., Ed.; Advances In Silicon Science; Springer Netherlands: Dordrecht, **2009**; Vol. 1.

(8) Willoughby, J. A.-C. Design & Synthesis of Silicone Elastomer Networks with Tunable Physico-Chemical Characteristics, North Carolina State University, **2007**.